Journal of High Energy Astrophysics 1–2 (2014) 1–30

Contents lists available at ScienceDirect

Journal of High Energy Astrophysics

www.elsevier.com/locate/jheap

Review

Cosmic neutrino pevatrons: A brand new pathway to astronomy, astrophysics, and particle physics

Luis A. Anchordoqui [a,*], Vernon Barger [b], Ilias Cholis [c], Haim Goldberg [d], Dan Hooper [c,e], Alexander Kusenko [f,g], John G. Learned [h], Danny Marfatia [h], Sandip Pakvasa [h], Thomas C. Paul [a,d], Thomas J. Weiler [i]

[a] Department of Physics, University of Wisconsin–Milwaukee, Milwaukee, WI 53201, USA
[b] Department of Physics, University of Wisconsin, Madison, WI 53706, USA
[c] Center for Particle Astrophysics, Fermi National Accelerator Laboratory, Batavia, IL 60510, USA
[d] Department of Physics, Northeastern University, Boston, MA 02115, USA
[e] Department of Astronomy and Astrophysics, Enrico Fermi Institute, University of Chicago, Chicago, IL 60637, USA
[f] Department of Physics and Astronomy, University of California, Los Angeles, CA 90095-1547, USA
[g] Kavli IPMU (WPI), University of Tokyo, Kashiwa, Chiba 277-8568, Japan
[h] Department of Physics and Astronomy, University of Hawaii, Honolulu, HI 96822, USA
[i] Department of Physics and Astronomy, Vanderbilt University, Nashville, TN 37235, USA

ARTICLE INFO

Article history:
Received 25 December 2013
Accepted 30 January 2014

ABSTRACT

The announcement by the IceCube Collaboration of the observation of 28 cosmic neutrino candidates has been greeted with a great deal of justified excitement. The data reported so far depart by 4.3σ from the expected atmospheric neutrino background, which raises the obvious question: "Where in the Cosmos are these neutrinos coming from?" We review the many possibilities which have been explored in the literature to address this question, including origins at either Galactic or extragalactic celestial objects. For completeness, we also briefly discuss new physical processes which may either explain or be constrained by IceCube data.

Contents

* Corresponding author.

http://dx.doi.org/10.1016/j.jheap.2014.01.001
2214-4048/

1. Introduction

Neutrinos will serve as unique astronomical messengers. Except for oscillations induced by transit in a vacuum Higgs field, neutrinos propagate without interactions between source and Earth, providing powerful probes of high energy astrophysics. The neutrino's direction and energy (modulo the usual red-shifting due to expansion of the universe) are preserved, and the neutrino's flavor is altered in a calculable way. The potential power of neutrino astrophysics has been discussed in a number of review articles (Gaisser et al., 1995; Learned and Mannheim, 2000; Halzen and Hooper, 2002; Becker, 2008; Anchordoqui and Montaruli, 2010). In addition, the flavor composition of neutrinos originating at astrophysical sources can serve as a probe of new physics in the electroweak sector (Learned and Pakvasa, 1995; Beacom et al., 2003a, 2003b, 2004a, 2004b; Hooper et al., 2005a; Anchordoqui et al., 2005a). Furthermore, decays and annihilations of hypothetical dark matter particles accumulated in Sun are expected to produce a large flux of secondary neutrinos at energies far above the 1–20 MeV energies of neutrinos produced in solar burning (Silk et al., 1985; Srednicki et al., 1987; Halzen et al., 1992; Barger et al., 2002, 2010, 2011; Halzen and Hooper, 2006). Observation of such high energy neutrinos coming from the direction of the Sun would provide "smoking ice" for dark matter hunters (Aartsen et al., 2013a). However, neutrinos constitute something of a double-edged sword: they are excellent probes of astrophysics and particle physics because of their feeble interactions, but also extremely difficult to detect for the same reason.

Neutrino (antineutrino) interactions with matter can be reduced to two categories: (i) in charged current (CC) interactions the neutrino becomes a charged lepton through the exchange of a $W^{\pm}$ with some particle X, $\nu_\alpha(\bar{\nu}_\alpha) + X \to l^{\pm}_\alpha +$ anything; (ii) in neutral current (NC) interactions the neutrino interacts via a Z transferring momentum to jets of hadrons, but producing a neutrino rather than an $l^{\pm}$ in the final state: $\nu_\alpha(\bar{\nu}_\alpha) + X \to \nu_\alpha(\bar{\nu}_\alpha) +$ anything. Lepton flavor is labeled as $\alpha = e, \mu, \tau$ from here on. The neutrino–nucleon cross section rises roughly linearly with energy (Quigg et al., 1986; Reno and Quigg, 1988; Gandhi et al., 1996, 1998; Anchordoqui et al., 2006a; Cooper-Sarkar and Sarkar, 2008; Jeong and Reno, 2010; Block et al., 2010; Connolly et al., 2011; Illarionov et al., 2011; Cooper-Sarkar et al., 2011). For neutrino telescopes located on Earth, the detection probability is modulated by a combination of the neutrino energy E_ν and the arrival zenith angle θ. For $E_\nu \lesssim 10^5$ GeV, most neutrinos pass through the Earth unscattered, and thus in this energy range the detection probability rises with energy. At about 10^5 GeV, the interaction length of neutrinos is roughly equal to the Earth's diameter, and hence about 80% (40%) of ν_μ and ν_e with $\cos\theta = -1$ (-0.7) are absorbed (L'Abbate et al., 2005). For the case of the tau neutrino, there is a subtlety in its propagation through matter due to the short τ lifetime. A ν_τ propagating through the Earth can interact to generate a τ lepton which subsequently decays, producing a ν_τ of lower energy, a process referred to as the "regeneration effect" (Halzen and Saltzberg, 1998) (though this will generally have negligible consequence for steeply falling spectra).

The rate of interaction of ν_e, ν_μ, ν_τ, $\bar{\nu}_\mu$, $\bar{\nu}_\tau$, with electrons is mostly negligible compared to interactions with nucleons. However, the case of $\bar{\nu}_e$ is unique because of resonant scattering, $\bar{\nu}_e e^- \to W^- \to$ anything, at $E_\nu \simeq 6.3$ PeV. The W^- resonance in this process is commonly referred to as the Glashow resonance (Glashow, 1960). The signal for $\bar{\nu}_e$ at the Glashow resonance, when normalized to the total $\nu + \bar{\nu}$ flux, can be used to differentiate between the two primary candidates ($p\gamma$ and pp collisions) for neutrino-producing interactions in optically thin sources of cosmic rays (Anchordoqui et al., 2005b). In pp collisions the nearly isotopically neutral mix of pions will create on decay a neutrino population with the ratio $N_{\nu_\mu} = N_{\bar{\nu}_\mu} = 2N_{\nu_e} = 2N_{\bar{\nu}_e}$. On the other hand, in photopion interactions the isotopically asymmetric process $p\gamma \to \Delta^+ \to \pi^+ n$, $\pi^+ \to \mu^+ \nu_\mu \to e^+ \nu_e \bar{\nu}_\mu \nu_\mu$, is the dominant source of neutrinos so that at production, $N_{\nu_\mu} = N_{\bar{\nu}_\mu} = N_{\nu_e} \gg N_{\bar{\nu}_e}$.[1] Note that events at the Glashow resonance provide the only known physics calibration of neutrino detectors in this high energy range, always a worrisome problem (witness the difficulties with the highest energy air showers, as in the Piere Auger Observatory and Telescope Array (Anchordoqui et al., 2013a)).

At PeV energies neutrinos interact with nucleons with a cross section of about 1 nb (1 b $= 10^{-24}$ cm^2). Hence, for a detector medium with a density of about $N_A \simeq 6 \times 10^{23}$ nucleons per cm^3 we expect only a fraction $\mathcal{O}(10^{-5})$ of PeV neutrinos to interact within 1 km of the medium. If the medium is transparent, like water or ice, the fast-moving secondary charged particles created in these interactions can be observed via the resulting Cherenkov light emission. Assuming cosmic ray (CR) sources are optically thin, one can estimate the diffuse flux of extragalactic neutrinos from the observed cosmic ray flux, since the relevant particle physics is well-known. The only wiggle room is the efficiency of the energy transfer from protons to pions, ϵ_π. An upper bound on the flux ($\epsilon_\pi = 1$) was first obtained by Waxman and Bahcall (1999), Bahcall and Waxman (2001). For an estimate of ϵ_π based on our best current knowledge, the diffuse flux of extragalactic neutrinos would provide $\mathcal{O}(10^5)$ PeV neutrinos per year and km^2. Thus, observation of a few extragalactic PeV neutrinos per year requires neutrino telescopes with active detector volumes on the scale of cubic-kilometers. IceCube is the first observatory on this scale and we can hope that the European KM3-NET will soon join the club.

1.1. Historical background

The long road to developing the IceCube experiment has been thoroughly described in Halzen (2007), Spiering (2012). Here we recount some of the highlights. Early efforts concentrated on instrumenting large pre-existing volumes of water to produce giant Cherenkov detectors. The first major step from conceptual ideas to large-scale experimental efforts was taken by the Deep Underwater Muon and Neutrino Detector (DUMAND) project (Bosetti et al., 1980). In November 1987, the DUMAND Collaboration measured the muon vertical intensity at depths ranging between 2–4 km (in intervals of 500 m), with a prototype string of optical detectors deployed about 30 km off-shore the island of

[1] It has been noted that advanced civilizations across the Galaxy could use a monochromatic signal at the Glashow resonance for purposes of communication (Learned et al., 2009).

Hawaii (Babson et al., 1990), and set a limit on high energy showers (Bolesta, 1997). DUMAND paved the way for later efforts by pioneering many of the detector technologies in use today. This project inspired both the independent development and deployment of an instrument in the Siberian Lake Baikal (Belolaptikov et al., 1997), as well as later efforts to commission neutrino telescopes in the Mediterranean, NESTOR, NEMO and ANTARES.

The most developed of the Mediterranean efforts, the ANTARES detector is deployed at depth of about 2.5 km and has been operating in its complete configuration since 2008, with 885 photomultiplier tubes (PMTs) enclosed in Optical Modules (OMs) and distributed in triplets on 12 detection lines (Ageron et al., 2011). The Collaboration has published some physics results, but the apparatus is not large enough to compete with or complement the IceCube results, which are the focus of this review (the geometric volume of ANTARES is $\lesssim 1/1000$ that of IceCube). The KM3-NET Collaboration is aiming at cubic kilometer scale detector(s) to be placed in the Mediterranean within the next few years.

In addition to activity in deep underwater neutrino experiments pursued in the late 1980s, a variety of smaller underground detectors were active, starting in the early 1960s, but greatly ramping up in the 1980s largely motivated by the hunt for nucleon decay. The first large underground water-based Cherenkov detector was the 10 kiloton IMB (Irvine–Michigan–Brookhaven) water Cherenkov detector, which began operation in 1982 in a Morton salt mine near Cleveland, Ohio. It dispatched the $SU(5)$ grand unification prediction for proton decay and went on to make the first significant observations of contained neutrino interactions, including the first hints of muon neutrino oscillations, via the suggestion of a deficit in GeV atmospheric neutrino fluxes.

Several other experiments were deployed in the 1980s, including the Baksan (Russian), Frejus (France), LSD (Mont Blanc tunnel), LVD (Gran Sasso), Homestake Mine (South Dakota, water detector), Soudan (Minnesota), Kolar Gold Fields (India), and Kamioka (Japan). All detected mostly cosmic ray muons and a few neutrinos of typically 100 MeV to 1 GeV.

Most spectacular and unexpected, were the neutrino fireworks (in the 10 MeV range) from Supernova 1987A, which revealed the first neutrino source ever observed beyond our solar system (Hirata et al., 1987; Bionta et al., 1987) (and until now, the last!). These cosmic neutrinos (19 in all) were detected by the IMB and the smaller but more sensitive Kamiokande detector, as well as by the Baksan detector. Not only did this event confirm theoretical ideas about the mechanism of supernova explosion, but it provided a bound on the neutrino mass and many other neutrino properties. This event put much energy into the drive towards neutrino astronomy. Unfortunately in order to view a substantial rate of SN one would need to be sensitive out to the Virgo Cluster scale (20 Mpc) which requires a gigaton scale detector with 10 MeV sensitivity (a thousand times lower than IceCube threshold energy).

In 1998 Super-Kamiokande went on to confirm the long-suspected neutrino oscillation phenomenon via muon neutrinos produced in the atmosphere (Fukuda et al., 1998).

The first telescope on the scale envisaged by the DUMAND Collaboration was realized by transforming a large volume of the extremely transparent, deep Antarctic ice into a particle detector, called the Antarctic Muon and Neutrino Detector Array (AMANDA) (Halzen and Learned, 1988; Lowder et al., 1991). During 1993 and 1994, in an exploratory phase, the four-string AMANDA-A array was deployed and instrumented with 80 PMTs spaced at 10 m intervals from 810 to 1000 m. (The scattering length at that depth turned out to be too short to allow useful detection volume.) A deeper array of 10 strings, referred to as AMANDA-B10, was deployed during the austral summers between 1995 and 1997, to depths between 1500 and 2000 m. The instrumented volume formed a cylinder with diameter 120 m, viewed by

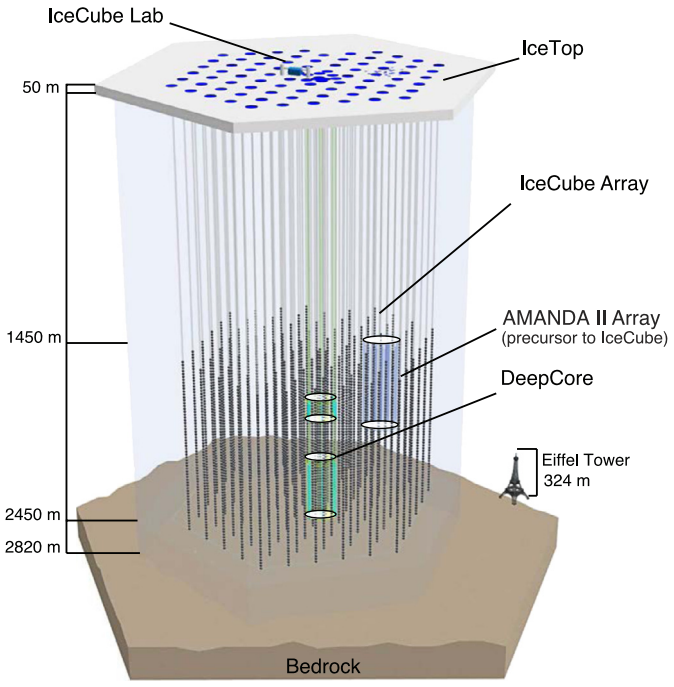

Fig. 1. Schematic of the IceCube instrument, which covers a cubic kilometer of Antarctic glacial ice. It detects neutrinos by observing Cherenkov light from secondary charged particles produced in neutrino–nucleon interactions. This light is detected by an array of 5160 DOMs, each of which contains a photomultiplier and readout electronics housed in a clear glass pressure resistant sphere. The DOMs are arranged into an array of 86 vertical strings, with 60 DOMs per string at depths between 1450 m and 2450 m. Outside of the DeepCore low-energy sub-array, these DOMs are vertically spaced at 17-meter intervals and the strings are on average 125 m apart horizontally. The DeepCore sub-array fills in the center of the detector with a denser array of photomultipliers and provides a lower energy threshold of 10 GeV over a fraction of the IceCube volume. Figure courtesy of the IceCube Collaboration.

302 OMs (Andres et al., 2000, 2001). During December 1997 and January 2000, the detector was expanded with an additional nine outer strings of OMs. The composite AMANDA-II array of 19 strings and 677 OMs comprising two concentric cylinders with larger diameter of 200 m became operational in 2000 and continued taking data up to 2009.

The follow-up to AMANDA-II, IceCube, finally realized the objective of instrumenting one cubic kilometer. IceCube is located near the Amundsen–Scott station below the surface of the Antarctic ice sheet at the geographic South Pole, sharing the location of its precursor observatory (Achterberg et al., 2006). A sketch of the IceCube facility is shown in Fig. 1. The main part of the detector is the "InIce" array of digital optical modules (DOMs) which detect Cherenkov light (Abbasi et al., 2009a). The DOMs are attached to km-long supply and read-out cables – so-called "strings" – and deployed deep (more than 1.5 km) in the Antarctic ice. Each string carries 60 DOMs spaced evenly along 1 km. The full baseline design of 86 strings was completed in December 2010. There is a region of dusty ice at about 2000 m, which is not useful. A region of particularly clear ice is equipped with a denser array of DOMs attached to six additional strings (Abbasi et al., 2012a). This "DeepCore" infill provides a low energy (to 10 GeV) extension of IceCube and increases the sensitivity of indirect dark matter searches and neutrino oscillations. In addition to the InIce array, IceCube also possesses an air shower array called "IceTop" which comprises 80 stations, each of which consists of two tanks of water–ice instrumented with 2 DOMs to detect Cherenkov light (Abbasi et al., 2013a). The hybrid observations of air showers in the InIce and IceTop arrays have mutual benefits, namely significant air shower background rejection (for neutrino studies) and an improved air shower muon detection (for CR studies).

1.2. The IceCube detector and neutrino detection

The IceCube event topologies are classified as cascades, tracks, or combinations of these. This leads to a zoo of possible signatures and the possibility to fully disentangle the neutrino flavor composition. The energy and angular resolution achievable for each event depends on the details of its topology. Here we pause to discuss in more detail the various event topologies.

In a CC event a ν_μ produces a muon traveling in nearly the same direction as the neutrino. Secondary muons range out over kilometers at $E_\mu \sim 10^3$ GeV, to tens of kilometers at $E_\mu \sim 10^9$ GeV, generating showers along their track by bremsstrahlung, pair production and photonuclear interactions. All of these are sources of Cherenkov light. As the energy of the muon degrades along its track, the energy of the secondary showers diminishes and the distance from the track over which the associated Cherenkov light can trigger a PMT becomes smaller. The geometry of the lightpool surrounding the muon track over which single photo-electron are produced, for muon of initial energy more than 200 GeV, is about a kilometer or more long cone with gradually decreasing radius. Energy is thus determined from range and energy loss rate. For such a muon observed over a 1 km path length in the IceCube detector, the energy resolution is $\Delta(\log_{10} E_\mu) \approx 0.22$ (Abbasi et al., 2013b). At energies $E_\mu > 100$ TeV or so, muons produced inside the instrumented volume will always leave the detector, allowing a strong lower bound on the neutrino energy, and depending upon circumstances some energy measurement of muon. The orientation of the Cherenkov cone reveals the neutrino direction, with an angular resolution of about 0.7° (Ahrens et al., 2003). Muons created by cosmic ray interactions in the atmosphere constitute the main background, up to ∼100 TeV energies. (Muons with energies of PeV shower strongly in the upper ice and cannot penetrate it to IceCube with substantial energy. A PeV energy muon from any direction must be due to neutrinos, or something even more interesting.)

Cascades (or showers of elementary particles) are generated by neutrino collisions – ν_e or ν_τ CC interactions, and all NC interactions – inside of or near the detector, and by unseen-muon-generated showers near the detector. These external showers most frequently will originate from muon induced pair production, bremsstrahlung or nuclear interactions. Normally, a reduction of the muon produced shower background is effected by placing a cut of $10^{4.6}$ GeV on the minimum reconstructed energy (Ackermann et al., 2004). Electron neutrinos deposit 50% to 80% of their energy into an electromagnetic shower initiated by the leading final state electron. The rest of the energy goes into the fragments of the target that produce a second (and nearly co-linear) subdominant shower.

The length of the shower is of orders of meters in ice, which is small compared to the PMT spacing. As a consequence, the shower results in roughly a point source of Cherenkov photons projected in some direction. The optical scattering length in ice (20 m or less) leads to diffusion of the radiation over a nearly spherical volume, rather than a conical projection. Still enough directionality is retained to reconstruct the shower direction to 15°–20° (as compared to <1° for muons). (We note that this provides an opportunity for KM3 as compared to IceCube, since in the ocean the shower directionality can be presumably much better.)

These events trigger the PMTs at the single photo-electron level over a spherical volume whose radius scales linearly with the logarithm of shower energy. For ice, the radius is 130 m at 10^4 GeV and 460 m at 10^{10} GeV, *i.e.* the shower radius grows by just over 50 m per decade in energy. The measurement of the radius of the sphere in the lattice of PMTs determines the energy and renders neutrino-detection-experiments as total energy calorimeters. The energy resolution is $\Delta(\log_{10} E_\nu) \approx 0.26$ (Abbasi et al., 2011a).

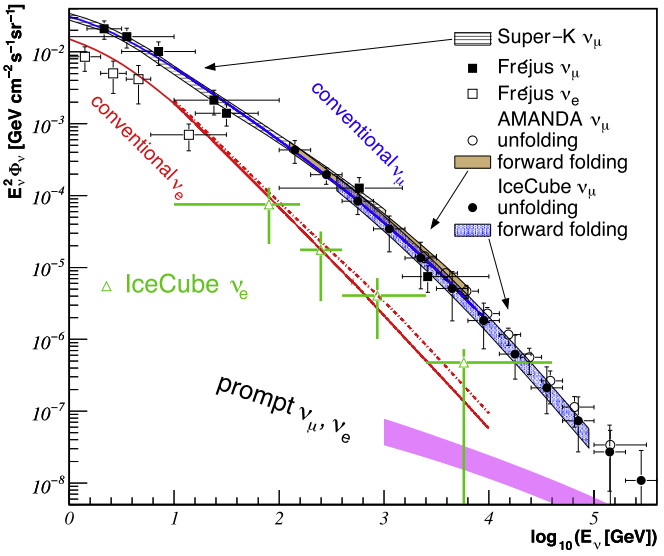

Fig. 2. Atmospheric muon and electron neutrino spectrum as function of energy. The open and filled symbols represent measurements of various detectors (Super-Kamiokande (Gonzalez-Garcia et al., 2006; Fréjus 1995), AMANDA forward folding analysis (Abbasi et al., 2009b) and unfolding analysis (Abbasi et al., 2010), IceCube (40 strings) forward folding ν_μ analysis (Abbasi et al., 2011b), unfolding ν_μ analysis (Abbasi et al., 2011c), and ν_e (Aartsen et al., 2013b)). Curved lines are theoretical predictions of atmospheric fluxes. The conventional ν_e (red solid line) and ν_μ (blue solid line) from Sanuki et al. (2007), and ν_e (red dotted line) from Barr et al. (2006). The (magenta) band for the prompt flux indicates the theoretical uncertainty of charm-induced neutrinos (Enberg et al., 2008). From Aartsen et al. (2013b). It should be noted that this figure contains deceptive spectra which do not consist of measured data points at given energies, but spectra fitted as a whole, and hence the individual "error bars" are misleading at best. The IceCube ν_e data is an exception. Super-Kamiokande has contained events for muons up to about 10 GeV and electrons up to about 100 GeV. (Frejus had no events in the highest energies in which they report a flux measurement with error bars, for example.) One should note that folding techniques can obscure any unexpected distortions of the tested spectra, which are typically simple power law distributions.

(Note that due to this non-linearity in response, even the unlikely contained interaction by a 10^{10} GeV neutrino will not saturate a km^3 detector volume, a redeeming virtue of the otherwise annoying optical scattering.)

For ν_τ's, CC current interactions produce different signals depending on the energy. For τ leptons less energetic than 10^6 GeV, the shower (hadronic or electromagnetic) from the τ decay cannot be separated from the hadronic shower of the initial ν_τ interaction. At $E_\tau \approx 10^6$ GeV, the τ range becomes a few hundred meters and the two showers produced may be easily separated and be identify as a double bang event (Learned and Pakvasa, 1995). At energies $10^7 \lesssim E_\tau/\text{GeV} < 10^{7.5}$, the τ decay length is comparable to the instrumented volume. In such cases, one may observe a τ track followed by the τ-decay shower ("lollipop topology"), or a hadronic shower followed by a τ track which leaves the detector ("popillol topology"). At energies $E_\tau > 10^{7.5}$ GeV, the decay length $\gg$1 km and τ's leave only a track like muons. However, a τ going through the detector at high energies without decaying will not deposit as much energy in the detector as a comparable-energy muon, due to the mass difference. (The direct-pair production process scales inversely with mass, so it dominates tau-lepton energy loss (Becattini and Bottai, 2001) resulting in 1/20th the light produced by a muon.) Such a τ might then be indistinguishable from a low energy muon track, and thus might not be flagged as an interesting event. In summary, the energy range from $10^{6.5} \lesssim E_\nu/\text{GeV} \lesssim 10^{7.5}$ is the "sweet spot" for τ detection in IceCube, since here one can observe all the distinctive topologies.

When protons and nuclei enter the atmosphere, they collide with the air molecules and produce all kinds of secondary particles, which in turn interact, decay or propagate to the ground,

depending on their intrinsic properties and energies. In the GeV range, the most abundant particles are neutrinos produced in the decay of mesons. Pion decay dominates the atmospheric neutrino production, $\pi^+ \to \mu^+ \nu_\mu \to e^+ \nu_e \nu_\mu \bar{\nu}_\mu$ (and the conjugate process), and determines the neutrino energy spectra up to about 100 GeV. Above this energy, the flux become increasingly modified by the kaon contribution, which asymptotically reaches 90%. In the atmosphere mesons are subject to an interaction-decay competition. As a consequence of this, neutrinos from meson decay have a spectrum that is one power of energy steeper than the primary cosmic ray spectrum. The muon daughter neutrinos have a spectrum steeper by two powers of energy, because the muon spectrum itself is steeper by $1/E$. Electron neutrinos have a differential spectrum (approximately) $\propto E_\nu^{-4.7}$. The muon neutrino spectrum is flatter, $\propto E_\nu^{-3.7}$ up to 10^5 GeV, steepening to $\propto E_\nu^{-4.0}$. In this energy window, the flavor ratios are $N_{\nu_e} : N_{\nu_\mu} : N_{\nu_\tau} \approx 1 : 20 : 0$ and the energy spectra are functions of the zenith angle of the atmospheric cascades (Lipari, 1993). This is because mesons in inclined showers spend more time in tenuous atmosphere where they are more likely to decay rather than interact. Above about 10^5 GeV, kaons are also significantly attenuated before decaying and the "prompt" component, arising mainly from very short-lived charmed mesons ($D^\pm$, D^0, D_s and Λ_c) dominates the spectrum (Zas et al., 1993). Such a prompt neutrino flux is isotropic with flavor ratios $10 : 10 : 1$ (Beacom and Candia, 2004). These various spectra are summarized in Fig. 2. The neutrino flux arising from pion and kaon decay is reasonably well understood, with an uncertainty in the range 10%–20% (Gaisser and Honda, 2002). The prompt atmospheric neutrino flux, however, is much less understood, because of uncertainty about cosmic ray composition and relatively poor knowledge of small-x QCD processes (Enberg et al., 2008).

The flux of atmospheric neutrinos is a curse and a blessing; the background of neutrinos produced by cosmic rays in interactions with air nuclei provides a beam essential for calibrating the detectors and demonstrating the neutrino measurement technique. It also provides an opportunity to probe standard neutrino oscillations and those arising from new physics, such as violation of Lorentz invariance (Gonzalez-Garcia et al., 2005; Anchordoqui and Halzen, 2006). Over the next decade, a data set of the order of one million atmospheric neutrinos will be collected. The statistics will be so large that some mapping of the Earth's interior density profile will be possible via neutrino tomography (Gonzalez-Garcia et al., 2008). (It is not clear that this will permit improvement on the density profile deduced from seismology however.)

1.3. IceCube and extraterrestrial neutrinos

A nearly guaranteed neutrino flux originates from interactions of ultra-high energy cosmic rays (UHECRs) *en route* to Earth. Ultrahigh energy protons above the photopion production threshold interact with the cosmic microwave and infrared backgrounds as they propagate over cosmological distances, the "GZK" process (Greisen, 1966; Zatsepin and Kuzmin, 1966). These interactions generate pions and neutrons, which decay to produce neutrinos (Berezinsky and Zatsepin, 1969), known as Berezinsky–Zatsepin neutrinos, or the "BZ" flux. The accumulation of such neutrinos over cosmological time is known as the BZ or often the "cosmogenic neutrino flux" (Stecker, 1979; Hill and Schramm, 1983; Engel et al., 2001; Fodor et al., 2003). Ultra-high energy nuclei also interact with the cosmic microwave and infrared backgrounds, undergoing photo-disintegration (Greisen, 1966; Zatsepin and Kuzmin, 1966). The disassociated nucleons then interact with the cosmic microwave and infrared backgrounds to produce cosmogenic neutrinos (Hooper et al., 2005c; Ave et al., 2005). While the presence of a suppression feature in the UHECR spectrum is generally expected for all compositions, the flux of cosmogenic neutrinos and γ rays (Gelmini et al., 2007a, 2007b; Taylor and Aharonian, 2009) subsequently produced are both very sensitive to the CR source model (Allard et al., 2006; Anchordoqui et al., 2007b; Kotera et al., 2010; Ahlers and Halzen, 2012). Indeed this difference permits information on these fluxes to be used as a probe of the composition or vice-versa. For instance, an upper limit on the proton fraction in UHE extragalactic CRs can, in principle, be inferred from experimental bounds on both the diffuse flux of UHE neutrinos (Ahlers et al., 2009) and the diffuse flux of UHE photons (Hooper et al., 2011). Furthermore, these two messengers starkly contrast in their subsequent propagation, with UHE neutrinos freely propagating out to the Hubble-scale whereas UHE γ rays are limited to tens of Mpc distance scales. This difference of scales highlights the fact that these two messengers can offer complementary information about the distant and local source distribution respectively. Moreover, the accompanying output into secondary electrons and positrons, in particular from Bethe–Heitler pair production, feeds into electromagnetic cascades from the cosmic microwave background (CMB) and intergalactic magnetic fields. This leads to the accumulation of γ rays in the energy range $\text{GeV} \lesssim E_\gamma \lesssim \text{TeV}$. The observed diffuse γ ray flux by *Fermi*-LAT (Abdo et al., 2010b) hence provides a constraint on the total energy injected into such cascades over the Universe's entire history and can be translated into upper limits on the cosmic diffuse flux of photons and neutrinos (Berezinsky and Smirnov, 1975; Berezinsky et al., 2011; Ahlers et al., 2010).

By devising a search dedicated to finding these cosmogenic neutrinos, the two (now three) highest energy neutrinos ever observed were quite recently uncovered (Aartsen et al., 2013c). We will review the possible origins of these events, as well as more recently detected lower energy neutrinos from cosmic sources (Aartsen et al., 2013d; Halzen et al., 2013). The layout of the review is as follows. In Section 2 we will discuss the published IceCube data, including the characteristics of the energy spectrum, the arrival directions, and the role of atmospheric prompt neutrinos. In Section 3 we discuss the consequences of the neutrino observations for theories of Galactic neutrino production. In Section 4 we consider potential extragalactic sources, including active galactic nuclei (AGNs), gamma-ray bursts (GRBs), starburst galaxies (SBGs), and newly-born pulsars. In Section 5 we turn to beyond Standard Model physics, including the production of neutrinos from heavy particle decay, and the relevance of this to dark matter. We will also discuss possible enhancement of the neutrino–nucleon cross section and the consequence of certain new physics processes for neutrino oscillations. Finally, in Section 6 we make a few observations on the consequences of the overall picture discussed herein.

2. Evidence for extraterrestrial high energy neutrinos

In April 2013 the IceCube Collaboration published an observation of two $\sim$1 PeV neutrinos, with a p-value 2.8σ beyond the hypothesis that these events were atmospherically generated (Aartsen et al., 2013c). These two candidates were found in a search for events with a significant energy deposition as expected for cosmogenic neutrinos. These two events are the highest energy neutrino candidates as yet reported. As can be seen in Fig. 3 the events exhibit a "cascade" morphology consistent with that expected to result from CC interactions of electron neutrinos, low-energy tau neutrinos, and NC interactions for all three flavors.

New results were presented in May 2013 at the IceCube Particle Astrophysics Symposium (IPA 2013) (Kopper et al., 2013; Kurahashi-Neilson et al., 2013; Whitehorn et al., 2013). In a new search protocol, down-going events were selected based on the

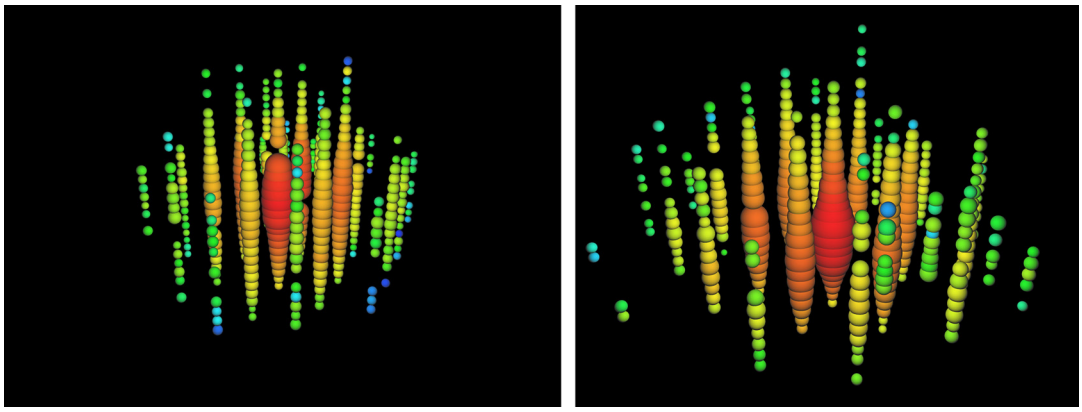

Fig. 3. The two highest energy neutrino events reported by the IceCube Collaboration. The left panel corresponds to the event called Bert that occurred in August 2011, whereas the right panel shows the event in January 2012, called Ernie. Each sphere represents a DOM. Colors represent the arrival times of the photons where red indicates early and blue late times. The size of the spheres is a measure for the recorded number of photo-electrons. Figure courtesy of the IceCube Collaboration.

Table 1
Properties of the 28 events. Shown are the deposited electromagnetic-equivalent energy (the energy deposited by the events in IceCube assuming all light was made in electromagnetic showers) as well as the arrival time and direction of each event and its topology (track or shower-like). The events are ordered according to the Modified Julian Date (MJD).

ID	Dep. energy (TeV)	Time (MJD)	Decl. (deg.)	R.A. (deg.)	Med. angular error (deg.)	Event type
1	$47.6^{+6.5}_{-5.4}$	55351.3222110	−1.8	35.2	16.3	Shower
2	117^{+15}_{-15}	55351.4659612	−28.0	282.6	25.4	Shower
3	$78.7^{+10.8}_{-8.7}$	55451.0707415	−31.2	127.9	$\lesssim 1.4$	Track
4	165^{+20}_{-15}	55477.3930911	−51.2	169.5	7.1	Shower
5	$71.4^{+9.0}_{-9.0}$	55512.5516214	−0.4	110.6	$\lesssim 1.2$	Track
6	$28.4^{+2.7}_{-2.5}$	55567.6388084	−27.2	133.9	9.8	Shower
7	$34.3^{+3.5}_{-4.3}$	55571.2585307	−45.1	15.6	24.1	Shower
8	$32.6^{+10.3}_{-11.1}$	55608.8201277	−21.2	182.4	$\lesssim 1.3$	Track
9	$63.2^{+7.1}_{-8.0}$	55685.6629638	33.6	151.3	16.5	Shower
10	$97.2^{+10.4}_{-12.4}$	55695.2730442	−29.4	5.0	8.1	Shower
11	$88.4^{+12.5}_{-10.7}$	55714.5909268	−8.9	155.3	16.7	Shower
12	104^{+13}_{-13}	55739.4411227	−52.8	296.1	9.8	Shower
13	253^{+26}_{-22}	55756.1129755	40.3	67.9	$\lesssim 1.2$	Track
14	1041^{+132}_{-144}	55782.5161816	−27.9	265.6	13.2	Shower
15	$57.5^{+8.3}_{-7.8}$	55783.1854172	−49.7	287.3	19.7	Shower
16	$30.6^{+3.6}_{-3.5}$	55798.6271191	−22.6	192.1	19.4	Shower
17	200^{+27}_{-27}	55800.3755444	14.5	247.4	11.6	Shower
18	$31.5^{+4.6}_{-3.3}$	55923.5318175	−24.8	345.6	$\lesssim 1.3$	Track
19	$71.5^{+7.0}_{-7.2}$	55925.7958570	−59.7	76.9	9.7	Shower
20	1141^{+143}_{-133}	55929.3986232	−67.2	38.3	10.7	Shower
21	$30.2^{+3.5}_{-3.3}$	55936.5416440	−24.0	9.0	20.9	Shower
22	220^{+21}_{-24}	55941.9757760	−22.1	293.7	12.1	Shower
23	$82.2^{+8.6}_{-8.4}$	55949.5693177	−13.2	208.7	$\lesssim 1.9$	Track
24	$30.5^{+3.2}_{-2.6}$	55950.8474887	−15.1	282.2	15.5	Shower
25	$33.5^{+4.9}_{-5.0}$	55966.7422457	−14.5	286.0	46.3	Shower
26	210^{+29}_{-26}	55979.2551738	22.7	143.4	11.8	Shower
27	$60.2^{+5.6}_{-5.6}$	56008.6845606	−12.6	121.7	6.6	Shower
28	$46.1^{+5.7}_{-4.4}$	56048.5704171	−71.5	164.8	$\lesssim 1.3$	Track

requirement that they display a vertex contained within the instrumented ice volume, effectively employing the edges of the IceCube detector as a veto for down-going muons. Since atmospheric neutrinos are produced by the same parent mesons which generate the shower muons, imposing this veto also provides a partial self-veto of the accompanying down-going atmospheric neutrino background, as discussed in Schonert et al. (2009). This technique is particularly effective for energies $E_\nu > 1$ TeV, where the boost is sufficient to ensure that the shower muons and neutrinos follow nearly identical trajectories. The new analysis, published in November 2013, revealed an additional 26 neutrino candidates depositing "electromagnetic equivalent energies" ranging from about 30 TeV up to 250 TeV (Aartsen et al., 2013d). The main properties of these events, which were observed between May 2010 to May 2012, are given in Table 1.[2]

[2] The energy given in Table 1 is equal to the neutrino energy for ν_e CC events, within experimental uncertainties, and is otherwise a lower limit on the neutrino energy due to exiting muons or neutrinos. Errors on energy and the angle include both statistical and systematic effects. Systematic uncertainties on directions

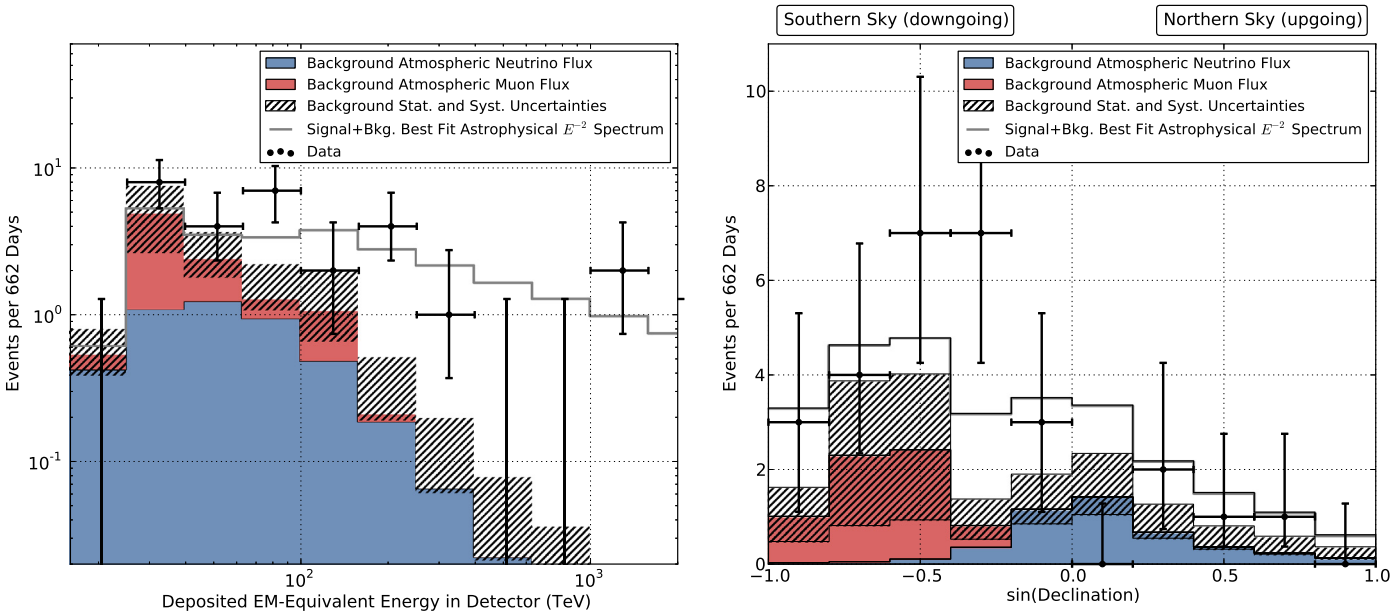

Fig. 4. Distribution of the deposited energies (left) and declination angles (right) of the IceCube observed events compared to model predictions. Energies plotted are in-detector visible energies, which are lower limits on the neutrino energy. Note that deposited energy spectra are always harder than the spectrum of the neutrinos that produced them due to the neutrino cross-section increasing with energy. The expected rate of atmospheric neutrinos is based on northern hemisphere muon neutrino observations at lower energies. The estimated distribution of the background from atmospheric muons is shown in red. Due to lack of statistics from data far above the cut threshold, the shape of the distributions from muons in this figure has been determined using Monte Carlo simulations with total rate normalized to the estimate obtained from the in-data control sample. Combined statistical and systematic uncertainties on the sum of backgrounds are indicated with a hatched area. The gray line shows the best-fit canonical E^{-2} astrophysical spectrum with all-flavor normalization (1:1:1) of $E_\nu^2 \Phi_\nu^{\rm total}(E_\nu) = 3.6 \times 10^{-8}$ GeV cm^{-2} s^{-1} sr^{-1} and a spectral cutoff of 2 PeV derived in Aartsen et al. (2013c). (An E_ν^{-2} spectrum is used here as a reference, as this spectral index is expected for canonical firs-order Fermi shock acceleration. In reality, this index may be somewhat larger or smaller.) From Aartsen et al. (2013d).

These events, together with atmospheric neutrino background expectations, are displayed in Fig. 4. The left panel shows the distribution of electromagnetic (EM) equivalent energy. At first glance, one may notice a gap between 250 TeV and the 2 highest energy events (He et al., 2013b). Keep in mind, however, that the lower energy events contain track topologies, which, as discussed before, represent only a lower bound on the neutrino energy. For example, the highest energy event in the search for ν_μ performed using data collected when IceCube was running in its 59-string configuration (May 2009 to May 2010) is most likely originated from a neutrino of energy $E_\nu \sim 0.5$–1 PeV, producing a muon that passed through the detector with an energy $E_\mu \approx 400$ TeV (Aartsen et al., 2013f).

Thus at present statistics are not sufficient to determine whether the suggestive gap in event energies represents a real structure in the spectrum (Anchordoqui et al., 2013b). Seven of the events show visible evidence of a muon track, and the remainder are consistent with cascades induced by ν_e's or ν_τ's (or their antiparticles or neutral current events). The quoted background estimate from atmospheric neutrinos is $10.6^{+4.6}_{-3.9}$. Taken together, the total sample of 28 events departs from the atmospherically-generated neutrino hypothesis by 4.3σ.[3]

Interpreting these results in terms of popular astrophysical models appears to be challenging. First of all, if the neutrino flux is indeed a Fermi-shock flux falling as an unbroken E_ν^{-2} power-law spectrum (Fermi, 1949) would lead to about 8–9 events above 1 PeV, which thus far are not observed. This null result at high-energy may be indicative of a cutoff in the spectrum at $1.6^{+1.5}_{-0.4}$ PeV (Whitehorn et al., 2013). (But note the newly reported Big Bird event (Klein et al., 2013; Halzen, 2013), with $E_\nu \gtrsim 2$ PeV which will raise this cutoff somewhat.) On the other hand, it may be possible to maintain consistency with the data with a steeper but still unbroken $E_\nu^{-\Gamma}$ spectrum, with $\Gamma > 2$.

The arrival directions of the 28 neutrinos are shown in Fig. 5. The IceCube angular resolution for shower events is poor, 15° to 20°, so firm conclusions are elusive at present. The largest concentration of events is near the Galactic center (Razzaque, 2013), consisting of 7 shower events (with a p-value of 8% (Kurahashi-Neilson et al., 2013)). It is further tempting to observe that one of the highest energy events, #14 at 1 PeV, points directly towards the Galactic Center. It has also been noted that the possible clustering could be associated to the Norma arm of the Galaxy (Neronov et al., 2013). While these interpretations are interesting, it is worth reiteration that at present statistics are limited and we have seen many incorrect suggestions of source association in the cosmic rays (Sigl et al., 2001; Torres et al., 2003; Finley and Westerhoff, 2004).

Concerning the issue of possible structure in the neutrino spectrum (either a gap or a cutoff), let us examine the consistently of a single power law over the entire energy range, with no cutoff. We consider the hypothesis that the cosmic neutrino flux per flavor, averaged over all three flavors, follows an unbroken power law of the form

$$\Phi_\nu(E_\nu) \equiv \frac{dF_\nu}{d\Omega\, dA\, dt\, dE_\nu} = \Phi_0 \left(\frac{E_\nu}{1\ \text{GeV}} \right)^{-\Gamma}, \qquad (1)$$

for a factor of several or more above the highest energies so far observed. Then we ask "What value(s) of the spectral index Γ are consistent with the recent IceCube observations?" We partition the observations into three bins:

- 26 events from 50 TeV to 1 PeV, which includes the ∼10 atmospheric background events;

for shower-like events were determined on an individual basis; track systematic uncertainties here are equal to 1°. The arrival directions are given in equatorial coordinates, right ascension (R.A.) and declination (Dec.). The topologies of all these events are shown in Aartsen et al. (2013d).

[3] See however Lipari (2013) for the possible significance of prompt neutrinos.

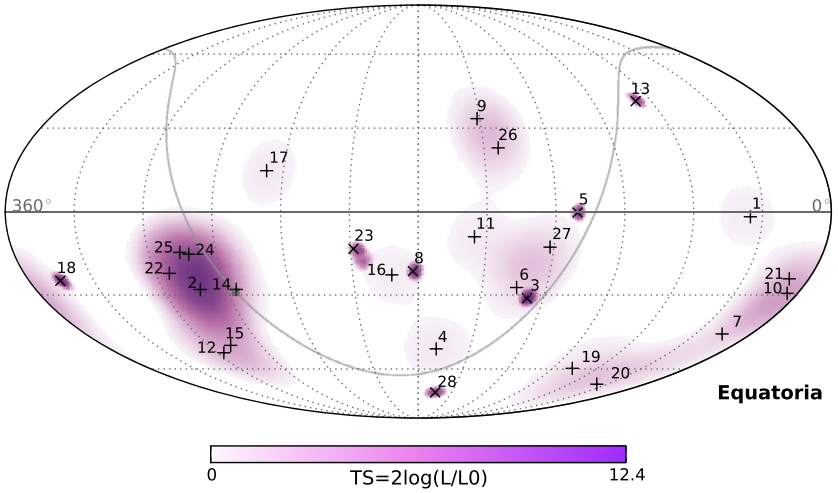

Fig. 5. IceCube skymap in equatorial coordinates of the Test Statistic value (TS) from the maximum likelihood point-source analysis. The most significant cluster consists of five events – all showers and including the second-highest energy event in the sample – with a final significance of 8%. This is not sufficient to identify any neutrino sources from the clustering study. The galactic plane is shown as a gray line with the galactic center denoted as a filled gray square. Best-fit locations of individual events (listed in Table 1) are indicated with vertical crosses (+) for showers and angled crosses (×) for muon tracks. From Aartsen et al. (2013d).

- 2 events from 1 PeV to 2 PeV;
- zero events above 2 PeV, say from 2 PeV to 10 PeV, with a background of zero events.

This choice of binning was selected a priori for the following reason. The 2 highest energy events exhibit shower topologies. For cascade events, the IceCube Collaboration has a sensitive method for determination of the energy resolution, $\Delta(\log_{10} E_\nu) \approx 0.26$, so we place these two events in 1 bin. The low energy bin contains both background as well as a number of events exhibiting track topologies. For track events, the ν_μ energy may be 5 times higher than the deposited energy. We therefore conservatively group all of these lower energy events into a single bin.

For various spectral indices from 2.0 to 2.8, we fit the neutrino flux to each of these three bins, by integrating over the energy span of the bin. A key point is that we employ IceCube's energy-dependent, flavor-dependent exposure functions for the 662 days of observation time reported thus far. The IceCube exposures are shown in Fig. 6.

The results of the fit are summarized in Table 2. Column two (three) shows the fitted flux normalization Φ_0 for the first (second) bin. The null, third bin requires more explanation: According to the statistics of small numbers (Feldman and Cousins, 1998), any flux yielding more than 1.29 (2.44) events in the null 2–10 PeV range of bin three, is excluded at 68% C.L. (90% C.L.). Accordingly, columns four and five show the maximum flux normalizations allowed by the null bin three, at the 68% and 90% C.L.'s.

Under the assumption of a single power-law across the three energy bins, consistency requires that the maximum flux normalization determined by bin three must exceed the flux normalizations from bins one and two. Moreover, the fitted normalizations from bins one and two should be the same, or nearly so. In terms of the table columns, if flux numbers from columns two or three exceed the maximums of columns 4 and 5, then the fit is ruled out at 68% and 90% C.L. Thus, Table 2 reveals that spectral indices shallower than 2.3 are inconsistent with the data at 90% C.L. or more, while indices shallower than 2.7 are inconsistent at 68% C.L.. Note also that for $\Gamma = 2.3$, and only for $\Gamma = 2.3$, are the normalizations from bins one ($E_\nu < 1$ PeV) and two (1 PeV $< E_\nu <$ 2 PeV) quite consistent with each other, and therefore with an unbroken power law. The overall consistency of the $\Gamma = 2.3$ power law across all three bins is at roughly the 90%, 1.5σ level. We therefore choose $\Gamma = 2.3$ as our reference value for the unbroken power law cutoff-free hypothesis. It is worth reiterating here that consistency with a single power low does not exclude a cutoff in the spectrum; rather, given current statistics it is *possible* to characterize the spectrum with a single power law.

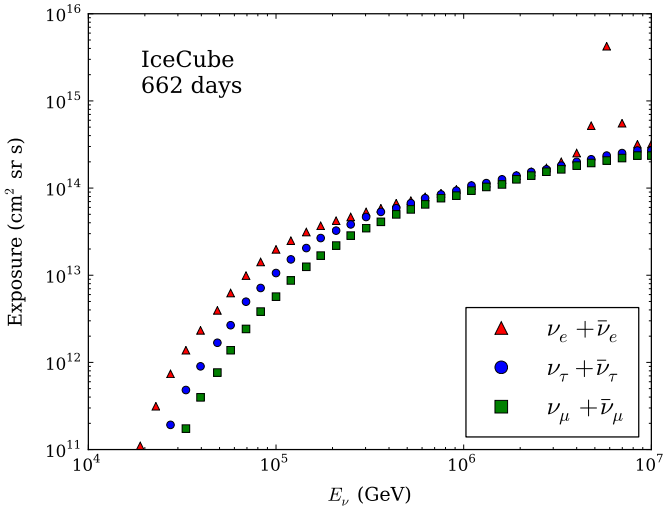

Fig. 6. IceCube exposure for 662 days of data collection, for contained events. The sharp-peaked structure for $\bar{\nu}_e$ at $10^{6.8}$ GeV is due to the Glashow resonance. One should note the relatively smaller "exposure" for muon events below 100 TeV. Taken from Anchordoqui et al. (2013b).

Table 2
Normalization Φ_0 for the "low energy" ($E < 1$ PeV) and "high energy" (1–2 PeV) bins, and normalization upper limits for the "null" bin (2–10 PeV) at 68% C.L. ($\Phi_{68}^{\max}$) and 90% C.L. ($\Phi_{90}^{\max}$) in units of (GeV cm^2 s sr)$^{-1}$, for various spectral indices, Γ.

Γ	$\Phi_0^{E_\nu<1\ \mathrm{PeV}}$	$\Phi_0^{1\ \mathrm{PeV}<E_\nu<2\ \mathrm{PeV}}$	$\Phi_{68}^{\max}$	$\Phi_{90}^{\max}$
2.0	1.66×10^{-8}	9.50×10^{-9}	3.94×10^{-9}	7.44×10^{-9}
2.1	5.70×10^{-8}	3.91×10^{-8}	1.84×10^{-8}	3.49×10^{-8}
2.2	1.95×10^{-7}	1.61×10^{-7}	8.62×10^{-8}	1.63×10^{-7}
2.3	6.63×10^{-7}	6.62×10^{-7}	4.02×10^{-7}	7.61×10^{-7}
2.4	2.24×10^{-6}	2.72×10^{-6}	1.88×10^{-6}	3.55×10^{-6}
2.5	7.54×10^{-6}	1.12×10^{-5}	8.73×10^{-6}	1.65×10^{-5}
2.6	$2.52 \times 10^{-}5$	4.59×10^{-5}	4.06×10^{-5}	7.68×10^{-5}
2.7	8.39×10^{-5}	1.88×10^{-4}	1.88×10^{-4}	3.56×10^{-4}
2.8	2.78×10^{-4}	7.71×10^{-4}	8.73×10^{-4}	1.65×10^{-3}

To assess the effect of uncertainties on our reference spectral index, we note that a 1σ upper fluctuation of the background is 15.2 events. The consequence of such a fluctuation on the hypothesis of a single power law with a high-energy cutoff would be to favor a spectral index close to $\Gamma = 2$, with a normalization for the all-neutrino flux $\Phi_0^{\rm total} = 3\Phi_0 = 2.85 \times 10^{-8}$ GeV^{-1} cm^{-2} s^{-1} sr^{-1}. Note that this normalization is about 20% smaller the normalization quoted in Fig. 4. The reason for this difference arises from the particular selection criteria applied in the analysis corresponding to Fig. 3 of Aartsen et al. (2013c) compared the selection in the analysis just discussed. In Aartsen et al. (2013c) the exposure is computed only for shower topologies, whereas in the analysis discussed herein both shower and tracks are included in the exposure calculation. From a comparison of Fig. 3 in Aartsen et al. (2013c) to Fig. 6 one can see that taking account of both CC and NC interactions in the case of muons, increases the number muon neutrino events by about a factor 5, compared to considering NC interactions alone.

To close this section, we consider some aspects of the connection among CRs, neutrinos and γ rays. We anticipate that if the neutrino spectrum ultimately turns out to be dominated by Galactic sources, the lack of observed CR anisotropy will require a soft neutrino spectrum of $\Gamma \approx 2.3$. This will be discussed further in Section 3. If cosmic neutrinos are primarily of extragalactic origin, then the 100 GeV gamma ray flux observed by *Fermi*-LAT constrains the normalization at PeV energies at injection, which in turn demands a neutrino spectral index $\Gamma < 2.1$ (Murase et al., 2013).

3. Galactic models

Above about 10 GeV, the CR energy spectrum is observed to fall roughly as a power law; the flux decreases nearly three orders of magnitude per energy decade until eventually suffering a strong suppression near $10^{10.7}$ GeV (Abbasi et al., 2008; Abraham et al., 2008, 2010a). Close examination reveals several other spectral features. A steepening of the spectrum from $J(E) \propto E^{-2.67\pm0.07}$ to $E^{-3.07\pm0.11}$ occurring at an energy $E_{\rm knee} \approx 10^{6.5}$ GeV is known in cosmic vernacular as the "knee" (Hörandel, 2003; Blasi and Amato, 2012a). A less prominent "second knee", corresponding to a further softening $J(E) \propto E^{-3.52\pm0.19}$ appears above $10^{8.5}$ GeV (Abu-Zayyad et al., 2001). At $E_{\rm ankle} \approx 10^{9.5}$ GeV a pronounced hardening of the spectrum becomes evident, generating the so-called "ankle" feature (Bird et al., 1993; Abbasi et al., 2005). Given that the CR spectrum exhibits breaks at the knee and second knee, we should ask whether it is plausible for the proton injection spectrum to be characterized by a single index over the energy range of interest. In this section we first discuss the connection between the neutrino spectrum and structures in the cosmic ray spectrum. In the process, we have to consider consistency with source power requirements as well as other multimessenger constraints including observations of TeV gamma rays and bounds at higher energies. We will also discuss the neutrino "hot-spot" near the Galactic Center, and assuming it is not a statistical fluke, we make predictions for future observations by IceCube and ANTARES.

3.1. Shape of the source spectrum

Relativistic charged particles produced in our Galaxy are likely to be confined by the Galactic magnetic field, $|\boldsymbol{B}| \sim 3\ \mu$G. The Larmor radius of a charged particle in a magnetic field is

$$r_{\rm L} = \frac{E}{Ze|\boldsymbol{B}|} \simeq \frac{1.08 \times 10^{-9}}{Z} \frac{E_{\rm GeV}}{B_{\mu\rm G}}\ \text{kpc}, \tag{2}$$

where $E_{\rm GeV} \equiv E/\text{GeV}$ and $B_{\mu\rm G} \equiv B/\mu\text{G}$. The quantity E/Ze is termed the "rigidity" of the particle. Particles may only leak from the Galaxy if their gyroradius is comparable to the size of the Galaxy (Cocconi, 1956). As a zeroth order approximation, in which we pretend the Galaxy has a spherical homogeneous halo, this leakage energy corresponds to

$$E \gtrsim ZeBR_H \simeq 1.5 \times 10^{10} Z B_{\mu\rm G} \left(\frac{R_H}{15\ \text{kpc}}\right) \text{GeV}, \tag{3}$$

where R_H is the radius of the halo. The majority of CRs possess a considerably lower energy than this and are thus trapped in the Galaxy. It is important to note here that the $\boldsymbol{B}$ field comprises approximately equal contributions from a "regular" component $B_{\rm reg}$ (that is, the galactic plane has field lines that run parallel to the spiral arms) and an irregular component $B_{\rm rand}$ generated by turbulent motions in the interstellar medium (Stanev, 1997; Jansson and Farrar, 2012). The motion of trapped cosmic rays can be reasonably approximated as a diffusive process controlled by the turbulent components of the magnetic field.

Neglecting the effects of convection, feed-down from fragmentation of heavier nuclei, and any energy losses, the CR transport in the Galaxy can be described by steady-state diffusion equation, in which the current $\boldsymbol{j}$ is related to the CR density $n_{\rm CR}$ through (Ginzburg and Syrovatskii, 1964)

$$\boldsymbol{\nabla \cdot j} \equiv -\nabla_i D_{ij} \nabla_j n_{\rm CR} = Q\,, \tag{4}$$

where Q is the generation rate of primary CRs and D_{ij} is the cosmic ray diffusion tensor, with components

$$D_{ij} = (D_\parallel - D_\perp) b_i b_j + D_\perp \delta_{ij} + D_A \epsilon_{ijk} b_k, \tag{5}$$

where $b_i = B_{{\rm reg},i}/B_{\rm reg}$ is a unit vector along the regular Galactic magnetic field, δ_{ij} is the Kronecker delta, and ϵ_{ijk} is the Levi-Civita fully antisymmetric tensor. The symmetric terms of D_{ij} contain the diffusion coefficients parallel (field-aligned) and perpendicular (transverse), $D_\parallel$ and $D_\perp$, which describe diffusion due to small-scale turbulent fluctuations. The antisymmetric (Hall) diffusion coefficient D_A is responsible for macroscopic drift currents. The anisotropy vector $\boldsymbol{\delta}$ is given by

$$\delta_i = \frac{3 j_i}{n_{\rm CR} c}. \tag{6}$$

The diffusion coefficients and their energy dependence are primarily determined by the level of turbulence in the interstellar medium. Under the assumption that the regular magnetic field is directed in the azimuthal direction and that both the Galaxy and the CR sources can be considered to have cylindrical symmetry, one finds that $D_\parallel$ plays no role in the diffusion equation. In most interesting cases the turbulent spectrum of the random magnetic field is described by a power-law, yielding $D_\perp \propto (E/Z)^\delta$ and $D_A \propto E/Z$, with $\delta = 1/3$ for a Kolmogorov spectrum (Kolmogorov, 1941) and $\delta = 1/2$ for a Kraichnan hydromagnetic spectrum (Kraichnan, 1965).

There are two broad categories of explanatory models for the knee: one ascribes the structure *mainly* to properties of the source(s) such as different acceleration mechanisms or variations in acceleration efficiency with energy (Fichtel and Linsley, 1986; Biermann, 1993; Biermann et al., 1995; Erlykin and Wolfendale, 1997, 2005; Kobayakawa et al., 2002; Hillas, 2005, 2006); the second broad category attributes the break at the knee to the details of the Galactic magnetic field and the resulting rigidity dependent leakage from the Galaxy (Syrovatskii, 1971; Ptuskin et al., 1993; Candia et al., 2002, 2003). In order to determine which type of model is more likely to be viable, it is crucial to employ both data on the energy spectrum and composition as well as the anisotropy around and above the knee.

Many of the salient features of the two models can be visualized in terms of a "leaky box," in which CRs propagate freely in the

Galaxy, contained by the magnetic field but with some probability to escape which is constant in time (Gaisser, 1990). For a homogeneous volume V (enclosed by the surface S), after averaging over that volume, gives for Eq. (4)

$$\begin{aligned}\overline{-\nabla_i D_{ij} \nabla_j n_{\rm CR}} &= -\int_V d^3x\, \nabla_i D_{ij} \nabla_j n_{\rm CR}/V \\ &= \int_S d^2x\, \hat{n}_i D_{ij} \nabla_j n_{\rm CR}/V \\ &= \int_S d^2x\, v_{\rm esc} n_{\rm CR}/V\,, \end{aligned} \tag{7}$$

where $\hat{\boldsymbol{n}}$ is the unit vector orthogonal to S. Assuming that the position where the particles escape through S is independent of $\boldsymbol{x}$, which is the leaky-box ansatz, then

$$\overline{-\nabla_i D_{ij} \nabla_j n_{\rm CR}} \sim \frac{v_{\rm esc}\, n_{\rm CR}}{x_{\rm esc}} = \frac{n_{\rm CR}}{\tau_{\rm esc}}, \tag{8}$$

where $x_{\rm esc}$ is the characteristic escape distance, $\tau_{\rm esc}$ is the characteristic escape time, and $V \sim S x_{\rm esc}$. Averaging over V on the right-hand side of Eq. (4) gives $\overline{Q}$. Thus, under the homogeneity assumption we have derived the leaky-box equation (without energy loss/gain or decay terms)

$$n_{\rm CR}(E) \equiv \frac{4\pi}{c} J(E) \approx \overline{Q(E)} \tau_{\rm esc}(E/Z). \tag{9}$$

There is a subtle point here with regard to boundary conditions. In the diffusion model, the boundary condition is that $n_{\rm CR}$ drops to zero everywhere on the border S (Dirichlet boundary condition). In the leaky-box ansatz a strong reflection is assumed at the border for particles below some energy threshold, *i.e.*, the gradient of $n_{\rm CR}$ drops to zero at any point on S (Neumann boundary condition). For cosmic ray particles that do escape, we have $|\boldsymbol{j}| > j_{\rm esc} = v_{\rm esc} n_{\rm CR}$. These different boundary conditions are associated to different Sturm–Liouville operators. In this approach the leaky-box limit can be considered as a mathematical limit (however physical or unphysical that limit may be) employed to solve the differential equation (4) at any point inside S.

The basic model for the investigation of cosmic ray propagation in the Galaxy is the flat halo diffusion model (Ginzburg and Ptuskin, 1976). The model has a simple geometry which reflects, however, the most essential features of the real system. It is assumed that the system has the shape of a cylinder with a radius $R_H \sim 15$ kpc and half height $H = 4$ kpc. The cosmic ray sources are distributed within the inner disk having characteristic thickness $h \sim 1$ kpc and radius $R_G \sim 10$ kpc. For $E < Z E_{\rm knee}$, the escape time from the Galaxy as a function of energy is solidly parametrized by Parizot (2004), De Marco et al. (2007)

$$\tau_{\rm esc}(E/Z) \simeq \frac{H^2}{6 D_\perp(E)} \propto (E/Z)^{-\delta}. \tag{10}$$

Hereafter, we consider the particular case of a source term whose energy dependence is taken as a power-law, $\overline{Q(E)} \propto E^{-\alpha}$. An effective way to determine the rigidity behavior is to uncover the spectrum of secondary nuclei. Fits to the energy dependence of secondary to primary ratios yield $\delta = 0.6$ (Gupta and Webber, 1989; Engelmann et al., 1990; Swordy et al., 1993). For a source index $\alpha \simeq 2.07$, which is close to the prediction of Fermi shock acceleration (Fermi, 1949), inclusion of propagation effects reproduces the observed spectrum. However, as shown in Fig. 7, $\delta = 0.6$ results in an excessively large anisotropy which is inconsistent with observations. Consistency with anisotropy can be achieved by adopting a Kolmogorov index, $\delta = 1/3$

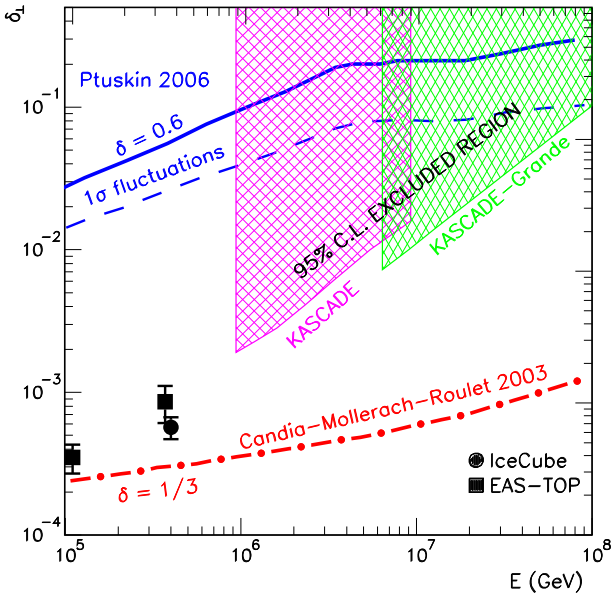

Fig. 7. Comparison of the effect of different injection spectral indices on the anisotropy amplitude in the direction of the equatorial plane, $\delta_\perp$. The solid line indicates the average value for $\delta = 0.6$ (Ptuskin, 2006), whereas the dot-dashed line corresponds to the Kolmogorov value $\delta = 1/3$ (Candia et al., 2003). In order to compare with existing observations, the anisotropy amplitude has been projected into the equatorial direction (Abreu et al., 2011), as described in Appendix A. Measurements of the first harmonic amplitude (corrected by the mean value of the cosine of the event declinations) by EAS-TOP (Aglietta et al., 2009) and IceCube (Abbasi et al., 2012b) are shown for comparison. The shaded regions are excluded by null results of searches by KASCADE (Antoni et al., 2004) and KASCADE-Grande (Stumpert, 2008) Collaborations. The dashed line indicates the 1σ downward fluctuation for $\delta = 0.6$.

(Biermann et al., 1995; Candia et al., 2003). The apparent conflict with the secondary to primary composition analyses can be alleviated through small variations of the energy dependence of the spallation cross sections, or variation in the matter distribution in the Galaxy (Biermann et al., 1995). This hypothesis implies a steeper source spectrum, $\alpha \simeq 2.34$, which agrees remarkably well with the fit of an unbroken power law to IceCube data, as discussed herein.

For rigidity $E/Z > 3$ GeV, the secondary to primary ratios and the abundances of unstable isotopes can be best fit by choosing

$$D_\perp(E) = 10^{28} D_{28} \left(\frac{E_{\rm GeV}/Z}{3\ {\rm GeV}} \right)^\delta \tag{11}$$

with $D_{28}/H_{\rm kpc} = 1.33$ for $\delta = 1/3$ and $D_{28}/H_{\rm kpc} = 0.55$ for $\delta = 0.6$ (Blasi and Amato, 2012b). For Kolmogorov diffusion, this leads to

$$\tau_{\rm esc} \approx 2 \times 10^7 \left(\frac{E_{\rm GeV}}{Z} \right)^{1/3} {\rm yr}, \tag{12}$$

which is in good agreement with the CR confinement time derived from the observed abundance of the radioactive ^{10}Be (Garcia-Munoz et al., 1977).

A model accommodating the single power law hypothesis can be concocted by assuming cosmic ray leakage is dominated by Kolmogorov diffusion, $\tau \propto (E/Z)^{-1/3}$, for $E < Z E_{\rm knee}$, with increasing leakage due to decreasing trapping efficiency with rising energy, $\tau \propto (E/Z)^{-1}$ for $E \gg Z E_{\rm knee}$ (Candia et al., 2003). The knee is etched into the spectrum by a transition from diffusion to drift motion, while the second knee results from a subsequent transition to quasirectilinear motion. Each CR nucleus is affected by drifts at $E \simeq Z E_{\rm knee}$, resulting in a progressive steepening of the CR spectrum. Since the lighter components are strongly suppressed

above 10^8 GeV, we are left with an iron dominated spectrum which progressively steepens until the overall spectrum becomes $J(E) \propto E^{-2.67+\Delta\delta}$, where $\Delta\delta = -1-(-1/3) = -2/3$, in agreement with observation of the second knee (Abu-Zayyad et al., 2001). Such a power law index is also in agreement with upper limits on flux anisotropies.

In closing, we note that detailed Monte Carlo simulations (Blasi and Amato, 2012b) demonstrate that the leaky box approximation (in which anisotropy depends in a simple way on energy) is a dramatic oversimplification that only represents an average over a large ensemble of possible source distributions in space and time. Significantly, while some realizations for $\delta = 1/3$ can accommodate all existing observations, a value $\delta = 0.6$ yields an anisotropy which is systematically larger than what is observed at any energy. From these arguments, we posit that a proton injection spectrum of $\alpha = 2.34$ is favored, and consequently a similar injection index for neutrinos.

3.2. Consistency with upper limits on the diffuse γ ray flux

Since neutrinos are produced by $\pi^\pm$ decays at the same unshielded sources where γ rays are produced by π^0 decays, and since neither is deflected or attenuated (assuming the photons are of Galactic origin), coordinated observations of these cosmic messengers will allow a new way of exploring the highest-energy Galactic sources (Anchordoqui et al., 2013b; Gupta, 2013). At present we are dealing only with bounds on PeV photons, which constrain the source injection of photons, neutrinos, and charged particles.

In this section, we address the impact of experimental bounds on the diffuse $\boldsymbol{\gamma}$ ray flux, for the hypothesis of a predominantly Galactic origin of the IceCube neutrino excess. From experimental bounds on the photon fraction we can acquire limits on the integral $\boldsymbol{\gamma}$ ray flux in regimes spanning one or more decades in energy (Matthews et al., 1991; Chantell et al., 1997; Schatz et al., 2003; Aartsen et al., 2013e). It is worth keeping in mind that this very lax binning means that we cannot strictly place a bound on the differential photon flux without making some assumption about the photon energy spectrum, though future improvements in experimental methods could nudge us closer to a bound on (or observation of) a differential flux. In this section, we therefore consider the relationship between the neutrino flux and the integral photon flux, compare this with experimental bounds, and draw some conclusions regarding how strongly the photon observations constrain the neutrino sources.

Inelastic pp collisions lead to roughly equal numbers of π^0's, π^+'s, and π^-'s, hence one expects two photons, two ν_e's, and four ν_μ's per π^0. On average, the photons carry one-half of the energy of the pion. The average neutrino energy from the direct pion decay is $\langle E_{\nu_\mu}\rangle^\pi = (1-r)E_\pi/2 \simeq 0.22E_\pi$ and that of the muon is $\langle E_\mu\rangle^\pi = (1+r)E_\pi/2 \simeq 0.78E_\pi$, where r is the ratio of muon to the pion mass squared. Now, taking the ν_μ from muon decay to have 1/3 the energy of the muon, the average energy of the ν_μ from muon decay is $\langle E_{\nu_\mu}\rangle^\mu = (1+r)E_\pi/6 = 0.26E_\pi$. This gives a total ν_μ energy per charged pion $\langle E_{\nu_\mu}\rangle \simeq 0.48E_\pi$, with a total $\langle E_{\nu_\mu}\rangle^{\rm total} = 0.96\langle E_\gamma\rangle$ for each triplet of π^+, π^-, and π^0 produced. For simplicity, we hereafter consider that all neutrinos carry one-quarter of the energy of the pion.

The total number of γ rays in the energy interval $(E_1/2, E_2/2)$ is equal to the total number of charged pions in the interval (E_1, E_2) and twice the number of neutral pions in the same energy interval,

$$\int_{E_1/2}^{E_2/2} \frac{dN_\gamma}{dE_\gamma}\,dE_\gamma = 2\int_{E_1}^{E_2} \frac{dN_{\pi^0}}{dE_\pi}\,dE_\pi = 2N_{\pi^0}. \tag{13}$$

Additionally, since $N_{\pi^\pm} = 2N_{\pi^0}$, the number of ν_μ in the energy interval $(E_1/4, E_2/4)$ scales as

$$\int_{E_1/4}^{E_2/4} \frac{dN_{\nu_\mu}}{dE_\nu}\,dE_\nu = 2\int_{E_1}^{E_2} \frac{dN_{\pi^\pm}}{dE_\pi}\,dE_\pi = 2N_{\pi^\pm}. \tag{14}$$

Now, taking d/dE_2 on each side of Eqs. (13) and (14) leads to

$$\begin{aligned} \frac{1}{2}\frac{dN_\gamma}{dE_\gamma}\bigg|_{E_\gamma=E_2/2} &= 2\frac{dN_\pi^0}{dE_\pi}\bigg|_{E_2} \quad \text{and} \\ \frac{1}{4}\frac{dN_{\nu_\mu}}{dE_\nu}\bigg|_{E_\nu=E_2/4} &= 2\frac{dN_\pi^\pm}{dE_\pi}\bigg|_{E_2}, \end{aligned} \tag{15}$$

respectively. The energy-bins dE scale with these fractions, and we arrive at

$$\begin{aligned} \frac{dN_\gamma}{dt\,dE_\gamma}\bigg|_{E_\gamma=E_\pi/2} &= 4\frac{dN_\pi}{dt\,dE_\pi}\bigg|_{E_\pi}, \\ \frac{dN_{\nu_e}}{dt\,dE_\nu}\bigg|_{E_\nu=E_\pi/4} &= 8\frac{dN_\pi}{dt\,dE_\pi}\bigg|_{E_\pi}, \\ \frac{dN_{\nu_\mu}}{dt\,dE_\nu}\bigg|_{E_\nu=E_\pi/4} &= 16\frac{dN_\pi}{dt\,dE_\pi}\bigg|_{E_\pi}, \end{aligned} \tag{16}$$

for the total fluxes at the source, where π denotes any one of the three pion charge-states and dt is the time differential.

During propagation TeV–PeV γ rays are absorbed in radiation backgrounds, with interaction length $\lambda_{\gamma\gamma}(E_\gamma)$. From Eq. (16), we see that neutrinos are produced at sources with a flavor ratio of 1:2:0. After propagating over large distances, however, oscillations convert this ratio to approximately 1:1:1 (for details, see Appendix B). From these observations, one finds a nearly identical flux for each of the three neutrino flavors, which relates to the γ ray counterpart according to Anchordoqui et al. (2004a)

$$e^{-\frac{r}{\lambda_{\gamma\gamma}}}\frac{dF_{\nu_\alpha}}{dA\,dt\,dE_\nu}\bigg|_{E_\nu=E_\gamma/2} = 2\frac{dF_\gamma}{dA\,dt\,dE_\gamma}\bigg|_{E_\gamma}. \tag{17}$$

Now that we have a relation between the neutrino and photon differential fluxes, we can check whether existing experimental bounds on the CR photon fraction at various energies leave room for the possibility that the IceCube excess is generated in optically thin sources in the Galaxy. To do this, we consider Eq. (17) for a distribution of sources, and write the integral flux of photons above some minimum energy $E_\gamma^{\rm min}$ in terms of the neutrino flux

$$\int_{E_\gamma^{\rm min}} \frac{dF_\gamma}{d\Omega\,dA\,dt\,dE_\gamma}\,dE_\gamma = \frac{1}{2}\int_{E_\gamma^{\rm min}/2} \sum_i e^{-\frac{r_i}{\lambda_{\gamma\gamma}}}\frac{dF_{\nu_\alpha}}{d\Omega\,dA\,dt\,dE_\nu}\,dE_\nu, \tag{18}$$

where

$$\frac{dF_{\nu_\alpha}}{d\Omega\,dA\,dt\,dE_\nu} \simeq 6.62\times10^{-7}\left(\frac{E_\nu}{\rm GeV}\right)^{-2.3}\left({\rm GeV\,cm^2\,s\,sr}\right)^{-1} \tag{19}$$

is the cosmic neutrino flux per flavor, averaged over all three flavors, according to the best fit of an unbroken power law to IceCube data (Anchordoqui et al., 2013b). The CASA-MIA 90% C.L. upper limits on the integral γ ray flux, I_γ, for

$$\frac{E_\gamma^{\rm min}}{\rm GeV} = 3.30\times10^5,\ 7.75\times10^5,\ 2.450\times10^6, \tag{20}$$

are

$$\frac{I_\gamma}{\mathrm{cm}^{-2}\,\mathrm{s}^{-1}\,\mathrm{sr}^{-1}} < 1.0\times10^{-13},\ 2.6\times10^{-14},\ 2.1\times10^{-15}, \quad (21)$$

respectively (Chantell et al., 1997). Under the assumption that there is no photon absorption, the integral photon flux (in units of photons $\mathrm{cm}^{-2}\,\mathrm{s}^{-1}\,\mathrm{sr}^{-1}$) above the energies specified in (20) are

$$\int_{E_\gamma^{\min}} \frac{dF_\gamma}{d\Omega\, dA\, dt\, dE_\gamma}\, dE_\gamma$$

$$= 4.2\times10^{-14},\ 1.4\times10^{-14},\ 3.1\times10^{-15}. \quad (22)$$

We can see that for the first two energies the predicted fluxes are comfortably below the 90% C.L. upper limits. For the highest energy the predicted integral photon flux slightly exceeds the 90% C.L. bound. However, *this does not necessarily signify the Galactic origin for the IceCube flux is excluded at the 90% C.L.* First of all, in this energy regime photon absorption starts to play an important role, as the mean free path of PeV photons in the CMB is about 10 kpc. Secondly we do not know the maximum neutrino energy achieved, and hence the maximum photon energy is not certain.

To more strictly comply with the CASA-MIA bound we would need about a 30% flux reduction. To see whether this is plausible we (i) conduct a calculation of the flux at the edge of the Galactic disk with an estimate of absorption effects and (ii) quantify the importance of assumption about the maximum photon energy.

Consider the case where the observer O is at the edge of the Galactic disk of radius R_G. Denote the vector from O to the center C of the galaxy by $\boldsymbol{R}_G$, from C to the source S_i by $\boldsymbol{r}_i'$, and from O to S_i, by $\boldsymbol{r}_i$. Then

$$\boldsymbol{r}_i = \boldsymbol{R}_G + \boldsymbol{r}_i'. \quad (23)$$

The energy-weighted neutrino flux from the Galactic source distribution with normal incidence at O is

$$E_\nu \frac{dF_{\nu_\alpha}}{dA\, dt\, dE_\nu} = \frac{1}{4\pi}\sum_i \frac{P_i}{r_i^2} = \frac{1}{4\pi}\sum_i \frac{P_i}{R_G^2 + 2R_G r_i' \cos\theta_i' + r_i'^2}, \quad (24)$$

where P_i is power output of source i and θ_i' is the angle subtended by $\boldsymbol{r}_i'$ and $\boldsymbol{R}_G$. Assuming equal power for all sources, and thus equal power density per unit area of the disk, we convert the sum to an integral

$$E_\nu \frac{dF_{\nu_\alpha}}{dA\, dt\, dE_\nu} = \frac{1}{4\pi}\frac{P}{\pi R_G^2}\int_0^{r'_{\max}} r'\, dr' \int_0^{2\pi} d\theta' \frac{1}{R_G^2 + 2r' R_G\cos\theta' + r'^2}$$

$$= \frac{1}{4\pi}\frac{P}{\pi R_G^2}\frac{1}{2}\int_0^{r'^2_{\max}} dr'^2 \frac{2\pi}{R_G^2 - r'^2}$$

$$= \frac{P}{4\pi R_G^2}\ln\frac{1}{1-(r'_{\max}/R_G)^2}. \quad (25)$$

The divergence is avoided by cutting off the integral for sources closer than within a ring of radius h, the thickness of the disk at the position of the observer, so that $r'_{\max} = R_G - h$. Note that this cut is unlikely to remove sources, which are expected to be clustered close to the Galactic center. After this regularization, the energy-weighted neutrino flux at Earth becomes

$$E_\nu \frac{dF_{\nu_\alpha}}{dA\, dt\, dE_\nu} = \frac{P}{4\pi R_G^2}\ln\frac{1}{\tau(2-\tau)}, \quad (26)$$

where $\tau \equiv h/R_G$. For $h/R_G = 0.1$, we get

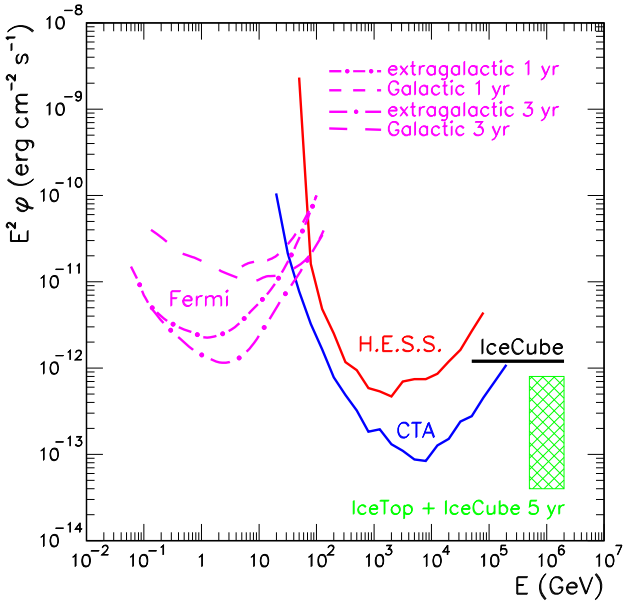

Fig. 8. The solid horizontal line shows the directional (eight degree solid angle) cosmic neutrino flux (all flavors) observed by IceCube (for details, see Table 3). We also show γ ray point source sensitivities of CTA (for 50 hours observation time in configuration I) (Bernlöhr et al., 2013), H.E.S.S. (also for 50 hours of observation time), Fermi for 1 yr (http://www.slac.stanford.edu/exp/glast/groups/canda/archive/pass6v3/lat_Performance.htm) and 3 yr (http://www.slac.stanford.edu/exp/glast/groups/canda/lat_Performance.htm), and IceTop + IceCube for 5 yr (declinations $-67^\circ \lesssim \delta \lesssim -57^\circ$) (Aartsen et al., 2013e). (The H.E.S.S. sensitivity is estimated by considering a sub-array of CTA (Bernlöhr et al., 2013) which has the same configuration as the HESS array, namely 4 telescopes of 12 m diameter at a separation of 120 m.)

$$E_\nu \frac{dF_{\nu_\alpha}}{dA\, dt\, dE_\nu} = 1.66\frac{P}{4\pi R_G^2}. \quad (27)$$

We now estimate the photon flux for $E_\gamma^{\min} > 1$ PeV. The γ absorption mean free path on the CMB is about 10 kpc, roughly the same as the distance of Earth from our Galactic center. Consequently, a simple assumption is justified, that photons traveling distances larger than R_G are completely absorbed. This absorption suppresses contributions from sources at distances greater than 10 kpc, to $0.2P/(4\pi R_G^2)$ (a result that was computed by changing the integration range $(0, 2\pi) \to (-\pi/2, \pi/2)$ in the angular integral of (25)). For a Galactic disk thickness of 1 kpc, we find a 12% reduction in the photon flux.

Now we explore the effect of varying the maximum energy cutoff. If we set the upper limit of integration in (22) to

$$\frac{E_\gamma^{\max}}{\mathrm{PeV}} = 6,\ 7,\ 8, \quad (28)$$

we obtain

$$\int_{E_\gamma^{\min}}^{E_\gamma^{\max}} \frac{dF_\gamma}{d\Omega\, dA\, dt\, dE_\gamma}\, dE_\gamma$$

$$= 2.1\times10^{-15},\ 2.3\times10^{-15},\ 2.4\times10^{-15}. \quad (29)$$

From these results we can see there are several possible ways to comply with the CASA-MIA upper bound at the highest energy bin of (21). For example, even without absorption, $E_\gamma^{\max} = 6$ PeV is consistent with the CASA-MIA bound; if the cutoff is at $E_\gamma^{\max} = 8$ PeV, γ ray absorption on the CMB provides enough additional suppression of the photon flux to be consistent with data.

In summary, current data still allow sufficient plausible wiggle room for consistency with a Galactic origin of the IceCube flux

even if the sources are optically thin. In fact, the highest fluctuation in the IceCube γ ray map (Aartsen et al., 2013e) is in the direction of one of the PeV neutrino events (Ahlers and Murase, 2013). It is also worth noting that sources which are optically thin up to $E_\gamma \sim 100$ TeV, may not be optically thin above $E_\gamma \sim 100$ TeV, suggesting that the importance of photon bounds in establishing the origin of IceCube events should be considered with some caution. In Fig. 8 we compare the IceCube sensitivity to neutrino point sources with the γ ray sensitivity of several current and pending experiments. Note that if the source emissivity is roughly the same for photons and neutrinos, then the Cherenkov Telescope Array (CTA) will be able to observe the associated γ ray flux at IceCube energies

3.3. Waxman–Bahcall energetics

Next we turn to the question of what the Galactic power-law model developed above would imply regarding the average efficiency of transferring proton energy to charged pions. Assume that the source spectral index of CRs in the range 0.1–100 PeV is Γ from here on. In the spirit of Ahlers et al. (2005), we define the two constants

$$C^p_{\rm CR}(\Gamma) \equiv \frac{dF^p_{\rm CR}}{dE\,dA\,dt} E^\Gamma, \quad \text{and} \quad C_\nu(\Gamma) \equiv \frac{dF_\nu}{dE\,dA\,dt} E^\Gamma, \tag{30}$$

where $C_\nu = 4\pi \Phi_0^{\rm total}$ GeV$^\Gamma$ and $\Phi_0^{\rm total} = 3\Phi_0$, given our assumption of flavor equilibration. In conventional notation, we next define $\epsilon_{\pi^\pm}$ to be the ratio of CR power (energy/time) emitted in charged pions to that in the parent nucleons. We also need ϵ_ν, defined as the fractional energy in neutrinos per single charged pion decay. If the pion decay chain is complete ($\pi^\pm \to e\nu_e\nu_\mu\bar\nu_\mu$), then $\epsilon_\nu \simeq 3/4$, whereas if the pion decay chain is terminated in the source region by energy loss of the relatively long-lived muon, then $\epsilon_\nu \simeq 1/4$. Comparing the energy produced in charged pions at the source to the neutrino energy detected at Earth, one gets the energy conservation relation

$$\epsilon_\nu \epsilon_{\pi^\pm} \int_{E_1}^{E_2} \frac{dF^p_{\rm CR}}{dE\,dA\,dt} E\,dE = \int_{E_{\nu 1}}^{E_{\nu 2}} \frac{dF_\nu}{dE_\nu\,dA\,dt} E_\nu\,dE_\nu, \tag{31}$$

where $E_{\nu 1} = \frac{E_1}{16}$, and $E_{\nu 2} = \frac{E_2}{16}$; these integrals may be done analytically to yield (for $\Gamma \neq 2$)

$$\epsilon_\nu \epsilon_{\pi^\pm} C^p_{\rm CR} \frac{E_1^{2-\Gamma} - E_2^{2-\Gamma}}{\Gamma - 2} = \frac{(\frac{E_1}{16})^{2-\Gamma} - (\frac{E_2}{16})^{2-\Gamma}}{\Gamma - 2} C_\nu. \tag{32}$$

Then, solving for $\epsilon_{\pi^\pm}$ we arrive at

$$\epsilon_{\pi^\pm} = \left(\frac{1}{16}\right)^{2-\Gamma} \frac{C_\nu(\Gamma)}{\epsilon_\nu C^p_{\rm CR}(\Gamma)}. \tag{33}$$

The numerology for C_ν is given in Table 2. For the favored spectral index $\Gamma = 2.3$, we have

$$C_\nu(2.3) = 12\pi \times 6.6 \times 10^{-7}\ {\rm GeV}^{2.3}\ \left({\rm GeV\,s\,cm}^2\right)^{-1}. \tag{34}$$

The constant $C^p_{\rm CR}(2.3)$ is related to the injection power of CR protons, $d\epsilon^p_{\rm CR}/dt$, as follows:

$$\begin{aligned} \frac{d\epsilon^p_{\rm CR}}{dt}[E_1, E_2] &= A \int_{E_1}^{E_2} \frac{dF^p_{\rm CR}}{dE\,dA\,dt} E\,dE \\ &= A \int_{E_1}^{E_2} \left(\frac{dF^p_{\rm CR}}{dE\,dA\,dt} E^\Gamma\right) E^{(1-\Gamma)}\,dE \\ &= A C^p_{\rm CR} \frac{({E_1}^{(2-\Gamma)} - {E_2}^{(2-\Gamma)})}{\Gamma - 2}, \end{aligned} \tag{35}$$

where $A = 4\pi r^2$ is an appropriately weighted surface area for the arriving cosmic ray or neutrino flux. In Gaisser et al. (1995), A is set equal to $4\pi R_G^2 \equiv A_0$. However, keeping in mind that $\langle r^{-2}\rangle$ diverges as $\ln(R/2r_{\rm min})$, with $r_{\rm min}$ being the distance to the nearest source, A^{-1} can easily be a factor of 2 larger than A_0^{-1}. Two independent arguments support such an enhancement. The first is to simply note that a local void radius of 0.7 kpc gives $A_0/A = 2$. The second is to note that the thin-disk approximation breaks down at a small distance z of order of the disk height, leading to a similar estimate of integration cutoff and resulting enhancement factor; the second argument was previously discussed in the text preceding Eq. (26).

Inverting (35) and using the fact that ${E_2}^{(2-\Gamma)} \ll {E_1}^{(2-\Gamma)}$, we get the conversion

$$C^p_{\rm CR} = \frac{d\epsilon^p_{\rm CR}}{dt}[E_1, E_2] \frac{(\Gamma - 2) E_1^{(\Gamma-2)}}{A}. \tag{36}$$

How, and how well, is $d\epsilon^p_{\rm CR}/dt$ known? The assumption underlying the leaky box model is that the energy density in CRs observed locally is typical of other regions of the Galactic disk. If so, the total power required to maintain the cosmic radiation in equilibrium can be obtained by integrating the generation rate of primary CRs over energy and space. Using (9), we obtain

$$\frac{d\epsilon_{\rm CR}}{dt} = \int d^3x \int Q(E)\,dE = V_G \frac{4\pi}{c} \int \frac{J(E)}{\tau(E/Z)}\,dE, \tag{37}$$

where $V_G \sim 10^{67}$ cm^3 is the Galactic disk volume (Gaisser, 2005). For $E_{\rm knee} < E < E_{\rm ankle}$, we conservatively assume that the trapping time in the Galaxy scales with energy as in (12). (Note that an evolution into quasirectilinear motion would increase the power allowance.) In this case the power budget required to fill in the spectrum from the knee to the ankle is found to be $d\epsilon_{\rm CR}/dt \simeq 2 \times 10^{39}$ erg/s (Gaisser, 2006).

We also note that recent data from KASCADE-Grande (Apel et al., 2013) indicate that at ~30 PeV the flux of protons is about an order of magnitude smaller than the all-species CR flux. Taken at face value, this implies that the fraction of the power budget allocated to nucleons of energy E_p which do not escape the Galaxy is about 0.1 of the all-species power. However, light elements possess higher magnetic rigidity and are therefore more likely to escape the Galaxy. From the functional form of $\tau(E/Z)$ above, we estimate the survival probability for protons at 30 PeV to be 46% of that at $E_{\rm knee}$. This leads to a value for the proton fraction of total flux at injection (ζ) of $\zeta = 0.1/0.46 = 0.22$. In the following discussion, we will consider a wide range for $\bar\zeta \equiv \zeta A_0/A$, with $0.22 \lesssim \bar\zeta \lesssim 0.44$ seemingly the most realistic range.

Then, we find for $C^p_{\rm CR}$ the particular result

$$C^p_{\rm CR}(2.3) = \frac{0.3 \times (0.1\ {\rm PeV})^{0.3} \times 2\bar\zeta \times 10^{39}\ {\rm erg/s}}{4\pi\,(10\ {\rm kpc})^2}. \tag{38}$$

Finally, inserting Eqs. (34) and (38) into (33), we get

$$\epsilon_{\pi^\pm}(2.3) = \left(\frac{1}{16}\right)^{-0.3} \frac{C_\nu(2.3)}{\epsilon_\nu C^p_{\rm CR}(2.3)} = \frac{0.055}{\bar\zeta \epsilon_\nu}, \tag{39}$$

where in the final expression, we have set Γ equal to the favored value of 2.3. Substituting in Eq. (39) $\epsilon_\nu = \frac{3}{4}$ and $\frac{1}{4}$ for the complete and damped pion decay chain, respectively, we finally arrive at $\epsilon_{\pi^\pm}(2.3) = 0.073/\zeta$ and $0.22/\zeta$.[4]

[4] Though the damped pion decay chain does not yield flavor equipartition on Earth, any deviation from $\Phi_0^{\rm total}$ falls in the range of uncertainty.

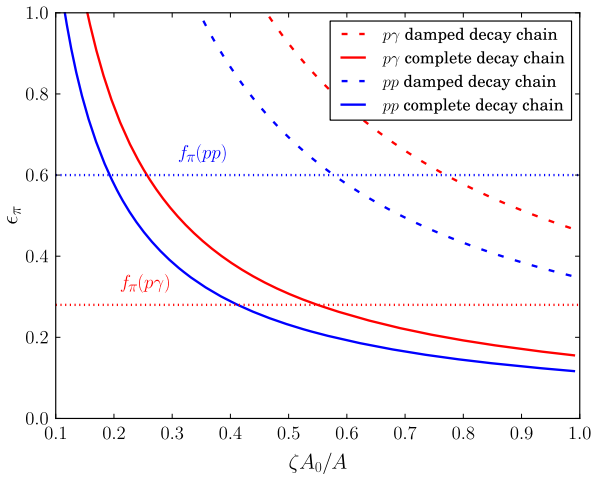

Fig. 9. Total pion energy fractions of parent proton, for favored spectral index $\Gamma = 2.3$. The average inelasticity f_π for pp and $p\gamma$ collisions is also shown for comparison. From Anchordoqui et al. (2013b).

If neutrinos are produced in pp collisions, one can interpret $\epsilon_{\pi^\pm}$ in terms of the efficiency of transferring proton energy to all three pion species, ϵ_π, by simply scaling $\epsilon_{\pi^\pm}$ by $\frac{3}{2}$ to yield $\epsilon_\pi = 0.12/\zeta$ and $\epsilon_\pi = 0.33/\zeta$ for the complete and damped chains, respectively. Alternatively, if neutrinos are produced in $p\gamma$ collisions, we scale by 2, yielding $\epsilon_\pi = 0.15/\zeta$ and $\epsilon_\pi = 0.44/\zeta$ for the complete and damped pion chains, respectively.[5] We show $\epsilon_\pi(\zeta A_0/A)$ for all four cases in Fig. 9.

In pp collisions, hadronic models predict that $f_\pi \sim 0.6$ of the "beam" proton energy is channeled into pions (Frichter et al., 1997). Since the value of ϵ_π reflects both the inelasticity as well as the fraction of protons which escape the source without producing pions, we expect ϵ_π to be smaller than f_π. This turns out to be the case for a complete pion decay chain if $\zeta A_0/A > 0.19$. Note, however, that the incomplete pion decay chain requires a considerably larger fraction, $\zeta A_0/A > 0.59$, which pushes the realm of plausibility. For $p\gamma$ interactions, $f_\pi \sim 0.28$ (Stecker, 1968), thereby excluding the incomplete decay chain hypothesis for this case. On the other hand, the complete decay chain appears to be allowed only for $\zeta A_0/A > 0.56$.

We have seen that the energetics of the Galaxy are sufficient to explain the neutrino flux, assuming that the neutrinos are produced in pp interactions. Potential Galactic neutrino sources have long been considered, see *e.g.* Levinson and Waxman, 2001; Distefano et al., 2002; Alvarez-Muniz and Halzen, 2002; Anchordoqui et al., 2003, 2004b, 2007a, 2007c; Amato et al., 2003; Kistler and Beacom, 2006; Torres and Halzen, 2007; Beacom and Kistler, 2007; Kappes et al., 2007; Lunardini and Razzaque, 2012; some recent refinements to previous models in light of new IceCube data are discussed in Joshi et al. (2013), Gonzalez-Garcia et al. (2013). As an example, we discuss in the next section the Galactic Center as one of the more likely neutrino engines.

3.4. Clustering at the center of the Milky Way?

We previously discussed the distribution of arrival directions. Let us revisit Fig. 5, where we see that the largest concentration of events is near the Galactic Center. In Fig. 10 we reproduce the skymap with all the events, considering a shower average reconstruction angular uncertainty of 15°. We can see that 5 shower-like

[5] Resonant $p\gamma$ interactions produce twice as many neutral pions as charged pions. Direct pion production via virtual meson exchange contributes about 20% to the total cross section, almost exclusively producing π^+. Hence, $p\gamma$ interactions produce roughly equal numbers of π^+ and π^0.

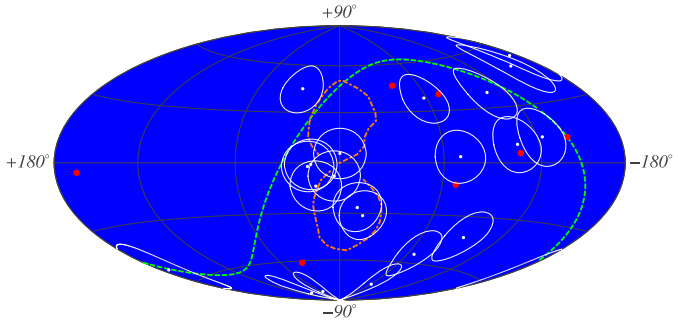

Fig. 10. IceCube neutrino events in Galactic coordinates. The 21 shower-like events are shown with 15° error circles around the approximate positions (small white points) reported by the IceCube Collaboration. The 7 track-like events are shown as larger red points. Also shown are the boundaries of the Fermi bubbles (dot-dashed line) and the Equatorial plane (dashed line). From Razzaque (2013).

Table 3
Normalization φ_0 for 4 events in the "low energy" ($E < 1$ PeV) bin and 1 event in the "high energy" (1–2 PeV) bin, and normalization upper limits for the "null" bin (2–10 PeV) at 68% C.L. ($\varphi_{68}^{\max}$) and 90% C.L. ($\varphi_{90}^{\max}$) in units of $(\text{GeV cm}^2\,\text{s})^{-1}$, for various spectral indices, Γ, and $\Omega_{8^\circ} = 0.06$ sr.

Γ	$\varphi_0^{E_\nu<1\ \text{PeV}}$	$\varphi_0^{1\ \text{PeV}<E_\nu<2\ \text{PeV}}$	$\varphi_{68}^{\max}$	$\varphi_{90}^{\max}$
2.0	2.49×10^{-10}	2.85×10^{-10}	2.36×10^{-10}	4.64×10^{-10}
2.1	8.55×10^{-10}	1.17×10^{-9}	1.10×10^{-9}	2.09×10^{-9}
2.2	2.92×10^{-9}	4.83×10^{-9}	5.17×10^{-9}	9.78×10^{-9}
2.3	9.94×10^{-9}	1.99×10^{-8}	2.41×10^{-8}	4.57×10^{-8}
2.4	3.36×10^{-8}	8.16×10^{-8}	1.13×10^{-7}	2.01×10^{-7}
2.5	1.31×10^{-7}	3.36×10^{-7}	5.24×10^{-7}	9.90×10^{-7}

Table 4
Normalization φ_0 for 6 events in the "low energy" ($E < 1$ PeV) bin and 1 event in the "high energy" (1–2 PeV) bin, and normalization upper limits for the "null" bin (2–10 PeV) at 68% C.L. ($\varphi_{68}^{\max}$) and 90% C.L. ($\varphi_{90}^{\max}$) in units of $(\text{GeV cm}^2\,\text{s})^{-1}$, for various spectral indices, Γ, and $\Omega_{20^\circ} = 0.38$ sr.

Γ	$\varphi_0^{E_\nu<1\ \text{PeV}}$	$\varphi_0^{1\ \text{PeV}<E_\nu<2\ \text{PeV}}$	$\varphi_{68}^{\max}$	$\varphi_{90}^{\max}$
2.0	2.36×10^{-9}	1.80×10^{-9}	1.50×10^{-9}	2.82×10^{-9}
2.1	8.12×10^{-9}	7.45×10^{-9}	6.99×10^{-9}	1.33×10^{-8}
2.2	2.78×10^{-8}	3.06×10^{-8}	3.27×10^{-8}	6.19×10^{-8}
2.3	9.45×10^{-8}	1.26×10^{-7}	1.53×10^{-7}	2.89×10^{-7}
2.4	3.19×10^{-7}	5.17×10^{-7}	7.14×10^{-7}	1.27×10^{-6}
2.5	1.07×10^{-6}	2.13×10^{-6}	3.31×10^{-6}	6.27×10^{-6}

events fall near the Galactic center, one of which is the second-highest energy event in the data, with an additional 3 shower events (Lunardini et al., 2013) consistent with the extent of the *Fermi* bubbles (Su et al., 2010). Curiously, there are no track-like events in this region, although statistics are very limited at present and the selection efficiency for cascades is higher than it is for tracks below 10^6 GeV (see Fig. 6).

In the spirit of Razzaque (2013), we define the "directional" cosmic neutrino flux per flavor, averaged over all flavors, as

$$\varphi_\nu(E_\nu) \equiv \frac{dF_{\nu_\alpha}}{dA\,dt\,dE_\nu} \simeq \varphi_0 \left(\frac{E_\nu}{\text{GeV}}\right)^{-\Gamma}. \tag{40}$$

Next, we compute the normalizations for an 8° circular window encompassing the Galactic Center, *i.e.* solid angle $\Omega_{8^\circ} = 2\pi(1 - \cos 8^\circ) = 0.06$ sr, with the results shown in Table 3. We find that an unbroken spectrum with $\Gamma = 2$ and a cutoff at ~ 2 PeV yields the observed number of high and low energy events in this region, with normalizations differing only by 12%. If we are willing to tolerate consistency of an empty bin at the 90% C.L., then we do not require a cutoff.

Using data collected from 2007 to 2010 the ANTARES Collaboration performed a time integrated search for point sources of cosmic neutrinos (Adrian-Martinez et al., 2012). No statistically

significant signal has been found and upper limits on the neutrino flux have been obtained. Assuming an E_ν^{-2} spectrum, with a 20° circular window around the source, the Collaboration reported an upper limit from the direction of the Galactic Center,

$$E_\nu^2\,\varphi_\nu^{\rm total}(E_\nu) < 3.8\times 10^{-8}\,{\rm GeV\,cm^{-2}\,s^{-1}}, \tag{41}$$

at the 90% C.L. Comparison with the normalizations given in Table 3, for a spectrum $\propto E_\nu^{-2}$, shows that the flux required to explain IceCube data is safely two orders of magnitude below the current ANTARES bound.

In closing we make a speculative observation, to be digested with a dash of salt. If we take the cascade angular resolution of IceCube to be closer to 20° than the fiducial 15°, then 6 events are consistent with a common origin near the Galactic Center. The relevant normalizations are summarized in Table 4. For spectral indices $\Gamma \geqslant 2.2$, the data do not demand a cutoff at the highest energies. For $\Gamma = 2.2$, the normalizations in the first two bins differ by 10%, whereas for $\Gamma = 2.3$, there is a 25% difference. To cross-check whether these scenarios are consistent with ANTARES observations, we must translate the E_ν-square-weighted bound reported by ANTARES into integral limits. For $\Gamma = 2.3$, we obtain

$$\varphi_\nu^{\rm total}(E_\nu > 50\,{\rm TeV}) < 7.6\times 10^{-13}\,{\rm cm^{-2}\,s^{-1}}, \tag{42}$$

at the 90% C.L.

Using the normalization in the low energy bin for the all flavor neutrino flux,

$$\varphi_0^{\rm total} = 2.8\times 10^{-7}\,\left({\rm GeV\,cm^2\,s}\right)^{-1}, \tag{43}$$

we obtain the integrated flux required to reproduced the IceCube data

$$\varphi_\nu^{\rm total}(E_\nu > 50\,{\rm TeV}) = 1.7\times 10^{-13}\,{\rm cm^{-2}\,s^{-1}}, \tag{44}$$

which is still a factor of ≈ 4 below the bound of ANTARES. Interestingly the H.E.S.S. Collaboration has reported a point-like source at the Galactic center with a spectral index $2.21 \pm 0.09 \pm 0.15$ (Aharonian et al., 2004), which is, within errors, consistent with $\Gamma = 2.2$–2.3.

4. Extragalactic models

In many respects, extragalactic cosmic ray accelerators provide the most natural sources for the extraterrestrial neutrinos observed by IceCube. In particular, interactions of high energy and UHECRs with energetic photons can generate charged pions, and thus neutrinos in their decays. The flux of neutrinos produced through the photo-meson interactions of cosmic ray protons can be directly tied to the cosmic ray injection rate (Waxman and Bahcall, 1999):

$$\begin{aligned} E_\nu^2\Phi_\nu(E_\nu) &\approx \frac{3}{8}\epsilon_\pi\,\xi_Z\,t_{\rm H}\,\frac{c}{4\pi}\,E_{\rm CR}^2\,\frac{d\dot N_{\rm CR}}{dE_{\rm CR}}, \\ &\approx 2.3\times 10^{-8}\epsilon_\pi\,\xi_Z\ {\rm GeV\,cm^{-2}\,s^{-1}\,sr^{-1}}, \end{aligned} \tag{45}$$

where $t_{\rm H}$ is the Hubble time and ϵ_π is the fraction of the energy which is injected in protons lost to photo-meson interactions.[6] The factor of 3/8 comes from the fact that, near the threshold for pion production, roughly half of the pions produced in photo-meson interactions are neutral and do not generate neutrinos, and three quarters of the energy of charged pion decays ($\pi^+ \to \mu^+\nu_\mu \to e^+\nu_e\nu_\mu\bar\nu_\mu$) go into neutrinos. The quantity ξ_Z accounts for the effects of redshift dependent source evolution ($\xi_Z = 1$ in the case of no evolution, and $\xi_Z \approx 5.75$ for sources distributed according to the star formation rate, for example), and $d\epsilon_{\rm CR}/dt \equiv E_{\rm CR}^2 d\dot N_{\rm CR}/dE_{\rm CR}$ is the (cosmologically) local energy injection rate of cosmic rays. In a target consisting of ice, the flux given in Eq. (45) is predicted to yield a rate of approximately $14\times\epsilon_\pi\xi_Z$ showers per km^3 per year with energies above 1 PeV (Cholis and Hooper, 2013). This simple calculation illustrates that a generic class of extragalactic cosmic ray sources with $\epsilon_\pi\xi_Z$ of order unity would be expected to produce a flux of neutrinos approximately equal to that observed by IceCube. This is highly suggestive of a connection between the observed neutrinos and the extragalactic sources of the high energy cosmic ray spectrum.

In the remainder of this section, we review a number of specific classes of extragalactic sources that could potentially be responsible for the neutrinos observed by IceCube, including GRBs, AGN, SBGs, and newly-born pulsars.

4.1. Gamma-ray bursts

GRBs constitute one of the most promising sources of high and UHECRs, and may be capable of accelerating protons to energies as high as $\sim 10^{20}$ eV (Milgrom and Usov, 1995; Waxman, 1995; Vietri, 1997; Wick et al., 2004). Furthermore, as their name implies, gamma-ray burst fireballs contain high densities of γ rays, enabling the efficient production of neutrinos via the photo-meson interactions of high energy protons (Waxman and Bahcall, 1997; Meszaros, 2006).

Typical GRBs exhibit a broken power-law spectrum of the form: $dN_\gamma/dE_\gamma \propto E_\gamma^{-2}$ for $E_\gamma \gtrsim 0.1$–1 MeV and $dN_\gamma/dE_\gamma \propto E_\gamma^{-1}$ at lower energies (Band et al., 1993). The radiation pressure resulting from the very high optical depth of GRB fireballs leads to their ultra-relativistic expansion, accelerating the plasma to Lorentz factors on the order of $\Gamma \sim 10^2$–10^3. In order for proton–photon collisions in this environment to exceed the threshold for pion production, the proton must have an energy that, in the observer's frame, meets the following condition (Waxman and Bahcall, 1997; Dermer and Atoyan, 2003; Guetta et al., 2004):

$$E_p \gtrsim 40\ {\rm PeV}\left(\frac{\Gamma}{300}\right)^2\left(\frac{0.3\ {\rm MeV}}{E_\gamma}\right)\left(\frac{1}{1+z}\right)^2, \tag{46}$$

where z is the redshift of the burst. In any falling spectrum of high-energy protons, such interactions will predominantly take place near this threshold. After taking into account that only about 1/5 of the proton's energy goes into the charged pion produced in such an interaction, and that each neutrino carries away only about a quarter of the charged pion's energy, this leads to the production of neutrinos of characteristic energy:

$$E_\nu \sim 2\ {\rm PeV}\left(\frac{\Gamma}{300}\right)^2\left(\frac{0.3\ {\rm MeV}}{E_\gamma}\right)\left(\frac{1}{1+z}\right)^2. \tag{47}$$

Thus for protons interacting with photons near the observed spectral break, the resulting neutrinos will have energies near that of the two most energetic events reported by IceCube.

Most GRBs are observed to have maximum isotropic luminosities in the range of $L_{\rm max} \sim 10^{51}$–10^{53} erg/s.[7] This class of "high

[6] A similar argument applies to the case of cosmic ray nuclei (Anchordoqui et al., 2008).

[7] As the observed hard X ray and γ ray luminosity is synchrotron emission from internal shocks in the relativistic fireball (Rees and Meszaros, 1994), this emission will be relativistically beamed to within an opening angle on the order of $\theta \sim 1/\Gamma$. The isotropic equivalent luminosity is related to the true luminosity by: $L_{\rm iso} = L_{\rm true}/(1-\cos\theta)$. The total isotropic energy emitted is $E_{\rm iso} \simeq L_{\rm iso}^{\rm max}\tau_{\rm dur}$. $L_{\rm iso}^{\rm max} \equiv L_{\rm max}$ (for simplicity in the remaining text) is the maximum isotropic equivalent luminosity. The duration timescale (as observed in hard X rays and γ rays), is taken to be $\tau_{\rm dur} = 2$ s for high luminosity GRBs and $\tau_{\rm dur} = 50$ s for the low luminosity sample (see Cholis and Hooper, 2013; Goldstein et al., 2012; Paciesas et al., 2012).

luminosity" GRBs is further divided into short and long duration bursts with observed timescales of 0.1–1 and 10–100 seconds, respectively, with the majority of observed bursts being of long duration (Goldstein et al., 2012; Paciesas et al., 2012; Zhang et al., 2012). In addition, another population of low luminosity GRBs with $L_{\rm max} \sim 10^{47}$ erg/s has been suggested (Liang et al., 2007) (see also Lv et al., 2010). These low luminosity GRBs, which are potentially much more numerous than their high luminosity counterparts, generally exhibit smooth light curves, wider emission cones and durations that are typically in the range 50–1000 s (Murase et al., 2006; Gupta and Zhang, 2007; Coward, 2005; Cobb et al., 2006; Pian et al., 2006; Daigne and Mochkovitch, 2007; Bromberg et al., 2011). At present, there is considerable variation in the GRB luminosity functions, $\Phi(L)$, appearing in the literature (Liang et al., 2007; Gupta and Zhang, 2007; Wanderman and Piran, 2010). The redshift distribution of GRBs, $R_{\rm GRB}(z)$, is generally assumed to approximately follow the star formation rate (Porciani and Madau, 2001), with high luminosity GRBs occurring at a local rate of $\sim$1 Gpc^{-3} yr^{-1} and low luminosity GRBs at a rate of 230 (Soderberg et al., 2006a) to 5000 (Soderberg et al., 2006b) Gpc^{-3} yr^{-1}.

For a given luminosity function and redshift distribution, one can calculate the diffuse flux of neutrinos or photons at the location of the Earth from the population of all GRBs:

$$\Phi_{\nu(\gamma)} = \int_0^{z_{\rm max}} dz \int_{L_{\rm min}}^{L_{\rm max}} dL\, \Phi(L) \frac{R_{\rm GRB}(z)}{1+z} \frac{4\pi D_L(z)^2}{(1+z)^2} \times \frac{c}{H_0\sqrt{\Omega_\Lambda + \Omega_M (1+z)^3}} \varphi_{\nu(\gamma)}, \tag{48}$$

where D_L is the luminosity distance and $\varphi_{\nu(\gamma)}$ refers to the observable neutrino/photon fluence from an individual GRB located at comoving distance, $D(z)$:

$$\varphi_{\nu(\gamma)} = \frac{dN_{\nu(\gamma)}}{dE^{\rm inj}_{\nu(\gamma)}} \frac{1+z}{4\pi D(z)^2}. \tag{49}$$

$dN_{\nu(\gamma)}/dE^{\rm inj}_{\nu(\gamma)}$ is the equivalent injection neutrino/photon spectrum.

The spectrum of neutrinos (and antineutrinos) at injection can be approximated by a doubly broken power-law (Waxman and Bahcall, 1999):

$$\frac{dN_\nu}{dE^{\rm inj}_\nu} \propto \begin{cases} (\frac{E^{\rm inj}_\nu}{E_1})^{-1} & \text{for } E^{\rm inj}_\nu \leqslant E_1 \\ (\frac{E^{\rm inj}_\nu}{E_1})^{-2} & \text{for } E_1 \leqslant E^{\rm inj}_\nu \leqslant E_2 \\ (\frac{E_2}{E_1})^{-2} \times (\frac{E^{\rm inj}_\nu}{E_2})^{-3} & \text{for } E^{\rm inj}_\nu \geqslant E_2. \end{cases} \tag{50}$$

The first of these spectral features (at $E_\nu = E_1$) corresponds to the pion production threshold for scattering off photons at the observed break in the gamma ray spectrum of GRBs, while the higher energy break (at $E_\nu = E_2$) appears as a result of the synchrotron cooling of muons and pions. The exact locations of these breaks differs between individual GRBs due to differences in the strengths of the fireballs' magnetic and radiation fields. Deviations from the standard Waxman–Bahcall spectrum reproducible by the Δ^+ resonance can result from additional neutrino production modes (Baerwald et al., 2011). Yet, such modifications of the spectrum do not affect the diffuse neutrino flux by more than a factor of 2. (See however Hummer et al., 2012; Li, 2012; He et al., 2012.) In fact the most important uncertainty is the amount of the burst's internal energy that goes into accelerating protons to energies of $\sim 10^{16}$ eV and above. Zhang (2007) and Racusin (2011) have suggested that the energy into accelerated protons may be a factor of $\sim$10 higher than that into accelerated electrons. Of the energy in protons, $\sim$1–10% is expected to go into neutrinos, with significant variation from burst-to-burst (Guetta et al., 2004). It is the averaged value for the overall population of GRBs that is the most significant uncertainty yet.

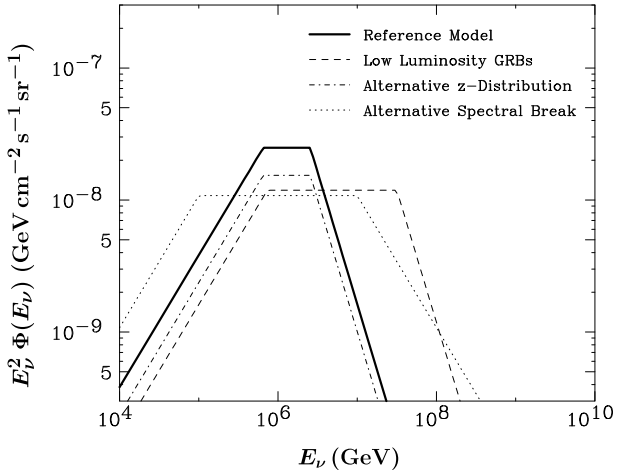

Fig. 11. The contribution of GRBs to the diffuse neutrino (plus antineutrino) spectrum. Results are shown for high luminosity (solid) and low luminosity (dashed) GRBs, calculated using default parameters, and for high luminosity GRB models with a suppressed high redshift distribution (dot–dash) and alternative spectral characteristics (dots). Each of these models yields a rate of PeV events which is comparable to that implied by the two most energetic events reported by IceCube. Plot taken from Cholis and Hooper (2013).

In Fig. 11, taken from Cholis and Hooper (2013), the total diffuse flux of neutrinos and antineutrinos from GRBs is shown for default parameter choices, and for some representative variations of these parameters. The solid and dashed lines represent the predicted flux from high and low luminosity GRBs, respectively, each assumed to evolve according to the rate of star formation. The dot-dashed line represents the contribution from high luminosity GRBs with a redshift distribution that is suppressed above $z = 3$. The dotted line shows the flux from high luminosity GRB with alternative choices for the parameters leading to the location of the spectral breaks. These variations show a fairly wide range of assumptions for GRBs; expected to generate fluxes of PeV neutrinos that are similar to that implied by IceCube's two most energetic events. As also suggested by Liu and Wang (2013), luminosity functions with steeper slopes on the low luminosity end, or redshift distributions with higher rates at high redshifts, favor the existence of more dim and untriggered GRBs in the X rays and γ rays.

Additionally, ultra-long GRBs with γ ray luminosities in the range of 10^{49}–10^{51} erg s^{-1} and durations of $\sim 10^4$ s (associated with larger progenitors, such as Wolf–Rayet stars with radius $R \sim 0.6$–$3.0 R_\odot$) have been proposed for the source of IceCube's observed neutrinos (Murase and Ioka, 2013) (see also, Liu and Wang, 2013; Vieyro et al., 2013 on Pop. III GRBs at high redshifts). The calculations of Murase and Ioka (2013) suggest that such sources could produce a neutrino flux of $\sim 10^{-9}$ GeV cm^{-2} s^{-1} sr^{-1} from successful jets and of $\sim 10^{-8}$ GeV cm^{-2} s^{-1} sr^{-1} from choked jets. For such a case, the spectral slope is expected to steepen above a few PeV, and an associated multi-TeV neutrino signal is also predicted (Murase and Ioka, 2013).

By taking into account the times and/or directions of known GRBs, it is possible to conduct a nearly background free search for neutrinos originating from such sources. Recently, the IceCube Collaboration has applied such a strategy, and used the results to derive a stringent upper limit on the flux of high energy neutrinos from observed GRBs (Abbasi et al., 2012c). Under standard astrophysical assumptions, this limit implies that GRBs cannot be the only sources of the highest energy ($>10^{18}$ eV) cosmic rays

(see also, Ahlers et al., 2011).[8] The events reported by IceCube, however, could still originate from GRBs if either, (i) a greater fraction than expected of the high energy neutrinos from GRBs originate from bursts which are not sufficiently luminous to be observed by γ ray or X ray observatories (Cholis and Hooper, 2013; Liu and Wang, 2013; Murase and Ioka, 2013; Fraija, 2013), or (ii) a significant fraction of the 10^{16}–10^{18} eV cosmic ray spectrum originates from GRBs, while most of the $>10^{18}$ eV cosmic ray spectrum originates from other sources (Cholis and Hooper, 2013; Li, 2013; Winter, 2013). Having an alternative source for the CRs above $E > 10^{18}$ eV is attractive from the perspective of the cosmic ray spectrum's chemical composition. Measurements from the Pierre Auger Observatory of the depth of shower maxima and its variation suggest that the highest energy cosmic rays are largely of heavy chemical composition (closer in mass to iron nuclei than protons), while the composition becomes steadily lighter at lower energies, appearing to be dominated by protons at 10^{18} eV (Abraham et al., 2010b; Abreu et al., 2013). As ultra high-energy nuclei accelerated in a GRB are expected to be entirely disintegrated into individual nucleons before escaping the fireball (Anchordoqui et al., 2008), the possibility that GRBs provide most of the CRs below $\sim 10^{18}$ eV, but that another class of sources provide the bulk of the highest energy (heavy nuclei) CRs, is a well motivated one.

The fact that the events reported by IceCube do not correlate in time with any known GRBs does not necessarily rule out the hypothesis that these events originate from this class of sources. Many GRBs, while in the field-of-view of either the *Swift* Burst Alert Telescope (BAT) and the *Fermi* Gamma-ray Burst Monitor (GBM), may still go undetected if they are of sufficiently low luminosity, or are sufficiently distant. Given the fluence sensitivity of *Swift*'s BAT and *Fermi*'s GBM ($\sim 1 \times 10^{-8}$ erg cm^{-2} s^{-1} and $\sim 2 \times 10^{-8}$ erg cm^{-2} s^{-1} at 20 keV, respectively), one can estimate how distant a GRB of a given luminosity could be and still trigger these detectors. These experiments should be capable of detecting essentially all high luminosity GRBs ($L \gtrsim 10^{51}$ erg/s) within their fields-of-view out to a distance of about 8 Gpc ($z \approx 5$). Thus the observed collection of high luminosity GRBs is fairly complete (within the given fields-of-view). In contrast, low luminosity GRBs ($L \sim 10^{47}$ erg/s) are likely to be detected only within a radius of $\sim$100 Mpc, suggesting that the vast majority of the diffuse neutrino flux from low luminosity GRBs will be uncorrelated in time or direction with any observed γ ray or X ray signals (Cholis and Hooper, 2013).

4.2. Active Galactic nuclei

The kinematics of high-energy neutrino production in AGNs is similar to that of GRBs, with protons accelerated in the cores of AGN close to the accretion disk (Kazanas and Ellison, 1986). Yet there are important differences; the Lorentz factors of AGN jets are significantly lower than those of GRB shocks, with values of $\Gamma \sim 30$ rather than $\sim$300 (Atoyan and Dermer, 2001; Mannheim, 1993, 1998). As a result, $\sim$10–100 PeV protons can exceed the threshold for pion production much more easily, requiring only the presence of $\sim$keV photons (rather than the $\sim$100 keV photons required in GRBs).

In GRBs, the observed photon spectral break ($\sim$0.1–1 MeV) leads to a break at $\sim$1 PeV in the neutrino spectrum. Thus we may expect the first detections of GRB neutrinos to appear at around this energy scale. In contrast, AGN do not typically exhibit a spectral peak at keV energies, but instead in the ultra-violet, typically at around $\sim$10 eV. This leads one to expect the neutrino spectrum to peak EeV energies, much higher than that from GRBs. There is a considerable degree of model dependence in this conclusion, however, deriving in large part from uncertainties in the spectrum of the target radiation fields. In addition, there is significant uncertainty in the magnitude of the diffuse neutrino flux associated to the number density of AGN (Stecker, 2013a).

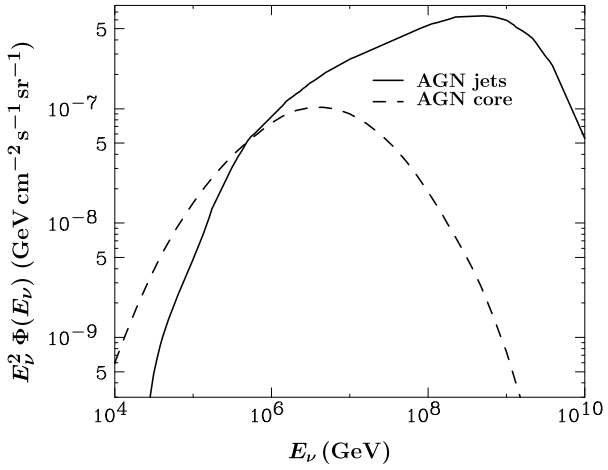

Fig. 12. The contribution of AGNs to the diffuse neutrino (plus antineutrino) flux. Results are shown for the energy spectrum of the AGN core model (Stecker et al., 1991, 2005) and the maximal neutrino intensity from AGN jets (Mannheim et al., 2001). Plot from Cholis and Hooper (2013).

In Fig. 12 we show a comparison of two canonical models for the diffuse neutrino emission from AGN cores and from optically thick AGN jets (Cholis and Hooper, 2013). In both cases, the diffuse neutrino flux has been normalized to that observed at $\sim$1 PeV by IceCube. In the model of Mannheim et al. (2001), the scattering of ultra-high energy protons with ultra-violet radiation leads to a neutrino spectrum which peaks at EeV energies. For this spectral shape, most showers initiated within IceCube's volume will be of energy 20 PeV or greater. Assuming that IceCube's existing data does not contain a sizable number of enormous (non-contained) showers in this energy range (Aartsen et al., 2013d), this AGN model will likely not be able to account for the reported events. In contrast, the model of Stecker et al. (1991, 2005) predicts a neutrino spectrum from AGN which peaks at a much lower energy of a few PeV, not unlike the predictions for GRBs. This is in large part due to an assumed high density of ambient X rays present around the AGN.

While neutrino emission from known GRBs can be efficiently constrained by searching in the time window around the occurrence of a given burst, such a background-free strategy is not possible for AGN. As a result, it will be much more difficult to definitively test the hypothesis that these neutrinos originate from AGN.

Due to the ability of AGN jets to accelerate CRs up to the EeV scale, there are additional constraints that can be imposed on such model. First, the injected CR spectrum and composition must be consistent with the observations of CRs at very high energies (Apel et al., 2012; Aartsen et al., 2013g; Berezhnev et al., 2012; Garyaka et al., 2008; Amenomori et al., 2008). Secondly, the electromagnetic cascades generated in CR production and propagation cannot lead to a γ ray flux in excess of the extragalactic background measured by *Fermi*-LAT (Abdo et al., 2010b). In Kalashev et al. (2013) it was shown that in order to explain the observed flux of $\sim$ PeV neutrinos without overproducing neutrinos at even higher energies, and satisfying CR and gamma ray constraints, AGN jets should emit anywhere between 2×10^{39} erg s^{-1} Mpc^{-3} and 7×10^{40} erg s^{-1} Mpc^{-3} (see also, Kistler et al., 2013). This implies an individual AGN luminosity of

[8] Of course this constraint can be evaded if cosmic rays escape from GRBs without scattering (Baerwald et al., 2013).

approximately $L \sim 10^{44}$ erg s^{-1} (Kalashev et al., 2013).[9] In the next subsection we discuss in more detail the energetics of the AGN jet model.

4.3. Blazars

Blazars are AGNs with a relativistic jet pointing in the general direction of Earth. They are very bright gamma ray sources observed over a broad range of energies. Powered by a central engine believed to be a supermassive black hole, a blazar jet is capable of accelerating electrons, protons, and nuclei to very high energies. Detailed numerical simulations support the possibility of accelerating protons up to $E_{p,\max} \sim 10^{17}$ eV (Sironi and Spitkovsky, 2011; Sironi et al., 2013), and even higher energies are possible under some exceptional conditions, such as alignment of magnetic fields in the internal shocks. It is unclear how much AGNs contribute at the highest end of observed UHECR spectrum, which extends well above 10^{19} eV. Contributions of unusual supernova explosions, GRBs, and, possibly, nuclei from nearby sources remain viable possibilities for explaining UHECR at energies above 10^{18} eV (Gaisser et al., 2013; Anchordoqui et al., 1999; Aloisio et al., 2011; Calvez et al., 2010; Taylor et al., 2011). However, there is little doubt that AGNs can produce substantial fluxes of cosmic rays at least up to the "ankle."

There is growing evidence that intergalactic cascades initiated by line-of-sight interactions of cosmic rays produced by AGNs are responsible for the highest-energy gamma rays observed from blazars (Kalashev et al., 2013; Esse and Kusenko, 2010, 2013, 2012; Essey et al., 2010, 2011b; Murase et al., 2012; Razzaque et al., 2012; Prosekin et al., 2012; Aharonian et al., 2013; Zheng and Kang, 2013; Takami et al., 2013; Inoue et al., 2013b). As long as the intergalactic magnetic fields (IGMFs) are in the range 10^{-17} G $\lesssim B \lesssim 3 \times 10^{-14}$ G (Essey et al., 2011a), the spectra of distant blazars are explained remarkably well with secondary photons from such cascades (Essey and Kusenko, 2010; Essey et al., 2010, 2011b). In the absence of cosmic ray contribution (for example, if one assumes large IGMFs), the observed spectra from distant blazars should be much softer because of the gamma ray interactions with extragalactic background light. Models for hard intrinsic spectra of γ rays can be constructed (Stecker et al., 2007; Lefa et al., 2011; Dermer and Lott, 2012), but neither source-intrinsic features, nor selection effects can explain the observed anomaly in the broad range of energies and redshifts for which the data are available (Horns and Meyer, 2012). Furthermore, there is a growing list of remarkably distant TeV sources, such as a VHE blazar PKS 1424+240: the recent measurement of its redshift $z \geqslant 0.6035$ (Furniss et al., 2013) puts it at an optical depth $\tau > 5$ for the highest energy gamma rays observed by VERITAS (Acciari et al., 2010). At such an optical depth, all the primary gamma rays should be attenuated and filtered out, while proton-induced secondary component agrees with the observed spectrum of PKS 1424+240 for redshifts $0.6 \leqslant z \leqslant 1.3$ (Essey and Kusenko, 2013). There is a tantalizing possibility that new axion-like particles exist and couple to photons with a coupling that is large enough to allow for gamma ray conversions (De Angelis et al., 2007; Simet et al., 2008; Horns et al., 2012). This effect could reduce the effective opacity of the universe dramatically, as could some forms of Lorentz-invariance violation (Kifune, 1999). However, the natural ease with which secondary photons from cosmic ray interactions reproduce the data makes the explanation based on cosmic rays very appealing. Furthermore, the lack of time variability of the most distant blazars at energies above TeV is in agreement with this hypothesis, which predicts that the shortest variability time scales for $z \gtrsim 0.15$ and $E \gtrsim 1$ TeV should be greater than (0.1–10^3) years, depending on the model parameters (Prosekin et al., 2012).

Secondary gamma rays are generated in two types of interactions of cosmic rays along the line of sight. First, the proton interactions with the CMB photons produce electron–positron pairs and give rise to an electromagnetic cascades due to proton pair production (PPP) or Bethe–Heitler process, $p\gamma_{\rm CMB} \to pe^+e^-$ (Blumenthal, 1970). Second, the proton interactions with the extragalactic background light (EBL) can produce pions in the reactions $p\gamma_{\rm EBL} \to p\pi^0$ or $p\gamma_{\rm EBL} \to n\pi^+$. While the PPP process is not associated with any neutrinos, the pion photoproduction generates a neutrino flux related to the gamma ray flux. The relative importance of the two processes depends on the proton injection spectrum. Remarkably, the observed gamma ray spectrum is very robust and does not depend on the spectrum of protons, as shown in Fig. 13 (left panel) and, in detail, in Essey et al. (2010, 2011b). This feature is particularly appealing in application to the spectra of distant blazars, because the shape of the spectrum is not model-dependent, and the data for each distant blazar are explained with a one-parameter fit by varying the total proton luminosity within the range allowed by AGN energetics (Essey and Kusenko, 2010; Essey et al., 2010, 2011b).

While the spectra of gamma rays are practically independent of the model parameters, as long as the maximal proton energy $E_{p,\max} > 10^{17}$ eV (Essey et al., 2010, 2011b), the spectrum of neutrinos does depend on $E_{p,\max}$, as well as on the EBL model. The lowest-energy neutrinos are those produced just above the threshold for pion production on EBL. If $E_{p,\max} \sim 10^{17}$ eV, the proton spectrum cuts off just above the pion production threshold, and the resulting neutrino spectrum has a peak at 1 PeV, as shown in Fig. 13 (left panel) by the solid red line. For higher values of $E_{p,\max}$, the peak moves to higher energies.

However, according to detailed numerical simulations (Sironi and Spitkovsky, 2011; Sironi et al., 2013), acceleration beyond $E_{p,\max} \sim 10^{17}$ eV in AGN jets would require some very special conditions, such as magnetic field alignment in shocks. Therefore, it is likely that the distribution of AGNs with respect to the maximal proton energies is a decreasing function of $E_{p,\max}$, with the values $E_{p,\max} \gtrsim 10^{18}$ eV still allowed, but uncommon. The interactions of cosmic rays with EBL produce neutrinos via the reaction $p\gamma_{\rm EBL} \to p\pi^+$, which has a sharp threshold around $E_{\rm th} \sim 10^{17}$ eV (broadened by the energy distribution of the EBL photons). As long as the distribution of AGN with $E_{\rm p,max}$ decreases fast enough to make the contribution of CMB photons unimportant, most neutrinos are produced in interactions of protons near the threshold, $E_p \sim 10^{17}$ eV. The neutrino spectrum is, therefore, limited by the fraction $\sim$ (0.01–0.1) of the threshold energy from below and by $\sim$ (0.01–0.1) $\times E_{p,max}$ from above, so that the neutrino spectrum has a peak at $E_\nu \sim$ (0.01–0.1) $\times 10^{17}$ eV ~ 1 PeV.

Taking into account a likely evolution of AGN with redshift, one obtains a spectrum for diffuse neutrino background produced by blazars as shown in Fig. 13 (right panel) (Kalashev et al., 2013). The consistency with IceCube results depends on the model of redshift evolution and on the model of extragalactic background light (Kalashev et al., 2013).

4.4. Starburst galaxies

Collisions of cosmic rays with the radiation in galaxies undergoing periods of rapid star formation, referred to as SBGs, are predicted to yield significant fluxes of $\sim$ TeV–PeV neutrinos (Loeb and Waxman, 2006). Among the supernovae that occur in such galaxies, a small fraction produce ejecta with velocities that can be as fast as 0.1c and release kinetic energy at the level of 10^{52} erg

[9] In Treister et al. (2009) the observed volume density of AGN with luminosity in the X rays $L_X > 10^{43}$ erg s^{-1} has been measured to be $\simeq 10^{-5}$ Mpc^{-3} for $z > 0.5$. This density refers to the observable AGN, and does not account for distant AGN with their jets pointing at an angle far from our line-of-sight.

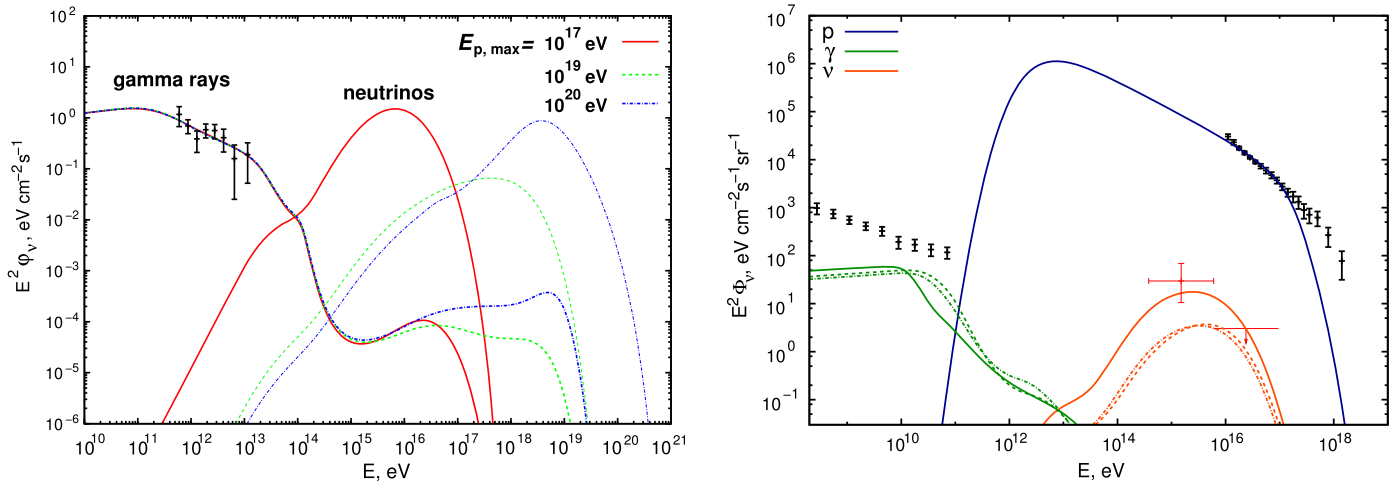

Fig. 13. Left: A peaked neutrino spectrum accompanies secondary gamma rays produced in line-of-sight interactions of cosmic rays emitted by blazars (Essey and Kusenko, 2010; Essey et al., 2010, 2011b). The lowest position of the peak is at 1 PeV. Assuming that a distribution of AGN with respect to maximal proton energy $E_{p,\max}$ is a decreasing function of $E_{p,\max}$, as implied by numerical simulations (Sironi and Spitkovsky, 2011; Sironi et al., 2013), the diffuse neutrino spectrum shown in the right panel has a peak at 1 PeV (Kalashev et al., 2013). **Right:** Predicted spectra of PeV neutrinos (red lines) compared with the flux measured by the IceCube experiment. The IceCube data points (red) are model-dependent 68% confidence level flux estimates obtained by convolving the IceCube exposure with the predicted neutrino spectrum. The predicted spectra are shown for the sum of three flavors; each flavor contributes, roughly, 1/3. The solid, dashed, and dotted red lines correspond to different EBL models (Kneiske et al., 2004; Stecker et al., 2006, 2012; Inoue et al., 2013a). The proton injection spectrum has a spectral index $\alpha = 2.6$ and maximun energy $E_{p,\max} = 3 \times 10^{17}$ eV. Also shown are the predicted gamma ray (lower curves below 10 TeV) and cosmic ray (upper curve) fluxes. The cosmic ray data points above 10 PeV are based on KASCADE-Grande (Apel et al., 2012); the diffuse gamma ray background data points below 1 TeV are due to Fermi (Abdo et al., 2010b). See text and Kalashev et al. (2013) for details.

(Soderberg et al., 2006a; Liu et al., 2013). These extreme supernovae, called hypernovae, and are able to accelerate protons up to 10^{17} eV. If these protons travel through a galactic medium of dense infrared and optical radiation background, they will produce neutrinos through photo-meson interactions with energies up to the PeV-scale (Murase et al., 2013; Cholis and Hooper, 2013). For reasonable assumptions, and calibrating to the observed fluxes of gamma rays (Lacki et al., 2011) and radio emission from such objects, contributions to the diffuse neutrino flux are expected to be on the order of 1×10^{-8} GeV cm^{-2} s^{-1} sr^{-1} (Loeb and Waxman, 2006; Lacki et al., 2011; Stecker, 2007; Thompson et al., 2006) (see also Torres, 2004; Domingo-Santamaria and Torres, 2005; del Pozo et al., 2009b, 2009a; Rephaeli et al., 2010; Persic et al., 2008; Lacki et al., 2010; Torres et al., 2012 for detailed models on multi-frequency emission from starburst galaxies and Acero et al., 2009; Acciari et al., 2009; Abdo et al., 2010a for γ ray observations). He et al. (2013a) have considered the case of ultra-luminous infrared galaxies, which are the most intense and luminous galaxies among the SBGs with high gas densities. The diffuse neutrino flux from hypernova remnants in these galaxies can be at the level of $\sim 2 \times 10^{-9}$ GeV cm^{-2} s^{-1} sr^{-1} with an estimated cut-off at $\sim$5 PeV for an assumed CR proton injected spectrum of $dN_p/dE_p \propto E_p^{-2}$ (He et al., 2013a).

Allowing for more optimistic acceleration conditions for protons in hypernovae (E_p up to 10^{18} eV and 5×10^{51} erg s in CR protons), and for larger confinement timescales inside the SBGs than He et al. (2013a),[10] Liu et al. (2013) have suggested that hypernovae in SBGs could be responsible for the $\sim 10^{-8}$ GeV cm^{-2} s^{-1} sr^{-1} PeV neutrino flux. Their suggested neutrino spectrum has a power-law spectral slope of $\Phi_\nu(E_\nu) \propto E_\nu^{-2}$, without any sharp cutoff above the PeV energies, and with only a smooth softening of the neutrino spectrum at $\sim$10 PeV.

4.5. Newborn pulsars

Another proposed source-type is newborn pulsars. Like GRBs, newborn pulsars are transients. However, unlike GRBs, newborn pulsars accelerate the iron-rich surface elements on young neutron stars, to populate the highest-energy cosmic rays with mainly heavy elements like ^{56}Fe. Nearby pulsars show direct evidence of accelerated electrons and positrons. Their ability to accelerate hadrons is speculative.

Heavy nuclei carry two advantages compared to light elements for a given energy. First of all, due to their lower energy per baryon, heavy nuclei can travel hundreds of megaparsecs before losing their energy by photo-disintegration processes on the cosmic backgrounds (Puget et al., 1976; Anchordoqui et al., 1998; Stecker and Salamon, 1999; Epele and Roulet, 1998; Ahlers and Taylor, 2010). Secondly, nuclei of charge Z can be accelerated to an energy typically Z times larger than protons in a given electromagnetic configuration (Anchordoqui et al., 1999; Aloisio et al., 2011). Results from the Pierre Auger Observatory indicate an increasing average primary mass with energy above a few EeV (though this result is not observed by HiRes or Telescope Array) (Anchordoqui et al., 2013a).

Pulsars have been suggested as possible accelerators of cosmic rays since their discovery, due to their important rotational and magnetic energy reservoirs (Gunn and Ostriker, 1969). The fastest spinning young neutron stars exhibit pulsar magnetic fields typically in the range 10^{12}–10^{13} G. Neutron stars with much larger surface magnetic fields, *i.e.*, magnetars, have also been proposed as sources of ultrahigh energy protons (Arons, 2003). Galactic pulsars have been suggested as the sources of cosmic rays around the knee region up to the ankle (Karakula et al., 1974; Bednarek and Protheroe, 1997, 2002; Giller and Lipski, 2002; Bednarek and Bartosik, 2004). That iron nuclei accelerated in the fastest spinning young neutron stars could explain the observed cosmic rays above the ankle in a Galactic source scenario was proposed in Blasi et al. (2000).

[10] For CR protons the two important timescales that define the confinement time of CRs in a galaxy are the diffusion timescale $\tau_{\rm diff} \simeq h^2/4D$ and the advection timescale $\tau_{\rm adv} \simeq h/v_{\rm wind}$, where h is the hight of the galaxy's gas disk, $D = (1/3)\cdot\lambda c$ is the diffusion coefficient (λ is the diffusion length), and $v_{\rm wind}$ is the velocity of the galactic wind. There are uncertainties in each of the h, D and $v_{\rm wind}$ at the level of a factor of few, allowing for a wide range of values on the confinement time of the very high energy CR protons (from $\simeq$ few $\times 10^4$ to few $\times 10^5$ years for 60 PeV protons). Also the timescale of energy losses for the CR protons can be of relevance under assumptions for very high gas galactic densities (see for more discussions of He et al., 2013a and Liu et al., 2013).

The acceleration mechanism in a young pulsar is unipolar induction: In the out-flowing relativistic plasma, the combination of the fast star rotation and its strong magnetic field can induce, in principle, potential differences of order $\phi = \Omega^2 \mu / c^2$, where $\mu = B R_*^3/2$, B is the surface dipole field strength and R_* is the pulsar radius. Provided that particles of charge Z can experience a fraction η of that potential, they will be accelerated to the energy

$$E(\Omega) = Ze\phi\eta = \frac{Z}{26}\frac{\eta}{0.03}\left(\frac{\Omega}{10^4\ \mathrm{s}^{-1}}\right)^2 \frac{\mu}{10^{30.5}\mathrm{cgs}} \times 10^{20}\ \mathrm{eV}. \quad (51)$$

The potential success of a UHECR source scenario lies in its ability to reproduce these four observations: (i) the energy spectrum; (ii) the composition; (iii) the anisotropy, and (iv) a rate of sources consistent with the population studies inferred from other astronomical observations. Newly-born pulsars are natural candidates to reproduce points (ii) and (iii), due to their iron-peaked surface (if the composition at the highest energies proves to be heavy as suggested by Auger) and their transient nature. Point (iv) is not daunting, as newborn pulsars are copiously produced in supernovae. Point (i) is challenged by the fact that the toy model of unipolar induction generates a hard spectrum that does not fit the observed UHECR spectrum. However, the slope could be naturally softened during the escape from the supernova envelopes of the 0.01% of the "normal" (as opposed to binary millisecond) pulsar birth rate required to achieve the requisite flux. Results obtained in Fang et al. (2012) suggest that all four points could be reasonably achieved in the extragalactic rotation-powered pulsar scenario. The highest energy protons and light elements can traverse only very dilute pulsar envelopes. However, iron nuclei appear able to escape from the supernova envelope with energies above 10^{20} eV. The escaped spectrum displays a transition from light to heavy composition at a few EeV, and, due to the production of secondary nucleons, a softer slope than the initially injected one, two results which enable a good fit to Auger observations. The flux up to the ankle is mainly fit by Galactic newborn pulsars, while the flux above the ankle mainly derives from extragalactic newborns (Fang et al., 2013a).

The transient nature of the source makes direct source identification very difficult. The deflection in the extragalactic magnetic fields should indeed induce important time delays ($\sim 10^4$ yr for one degree deflection over 100 Mpc) between charged particles and the photons propagating in geodesics, so that the sources should already be extinguished when cosmic rays are detected on Earth. However, neutrinos from a single close-by source born within $\sim$5 Mpc may be detectable at IceCube (Fang et al., 2012). Moreover, while the overall background neutrino flux from newborn pulsars would be at least an order of magnitude smaller for iron than for proton injection, the resulting level of the diffuse neutrino flux might still be detectable with the IceCube experiment. Future IceCube data will provide a decisive test for the young pulsar origin of UHECRs (Fang et al., 2013b).

4.6. Cosmogenic neutrinos from ultra-high energy cosmic rays

It is natural to ask whether interactions of cosmic rays of the highest observed energies, above 10^{18} eV, can generate a spectrum of neutrinos consistent with the data (Barger et al., 2012b). This, however, is not the case (Roulet et al., 2013; Laha et al., 2013; Aartsen et al., 2013h). There is a significant uncertainty in predicted spectra of cosmogenic neutrinos that must accompany the observed spectra of UHECR. However, normalizing the expected neutrino flux to that observed by IceCube at 1 PeV leads to an excessive prediction for EeV neutrinos, which are not observed. The spectral shape of requisite cosmic rays, implied by the observation of PeV neutrinos and by non-observation of EeV neutrinos, is not consistent with the observed spectrum of UHECR above 1 EeV (Roulet et al., 2013; Laha et al., 2013; Aartsen et al., 2013h). Cosmic rays at lower energies, such as those discussed in Section 4.3, evade the constraint because the spectrum of injected protons does not extend beyond 1 EeV.

5. Cosmic probes of fundamental physics

In this section we explore new physics processes which could give rise to the observed neutrino flux. In particular we discuss: (i) the potential of superheavy dark matter to produce a monochromatic neutrino signal, interestingly not inconsistent with current IceCube observations of two isolated events at about the same energy (Feldstein et al., 2013; Esmaili and Serpico, 2013; Bai et al., 2013); (ii) a model in which a leptoquark (of mass ≈ 0.6 TeV), coupling the tau-flavor to light quarks, enhances the CC interaction for shower production at 1 PeV, and the NC interactions at lower energies. This model is currently consistent with the possible gap in the spectrum, and the paucity of muon tracks (Barger and Keung, 2013); (iii) some exotic neutrino property (such as neutrino decay or pseudo-Dirac neutrino states) which could reduce the muon neutrino flux at high energies from distant sources (Pakvasa et al., 2013). However, it is important to stress that with present statistics the observed neutrino flavor ratios are consistent with the Standard Model, and there are not yet signs of new physics in the data (Chen et al., 2013). To date, neutrino observations have shown an absence of certain Lorentz-violating operators to extraordinary energies (Stecker, 2013b; Diaz et al., 2013), and no sign of Planck scale dissipative phenomena (Liberati and Maccione, 2013).

5.1. Superheavy dark matter decay

Some features of the IceCube results point to a tantalizing possibility that PeV neutrinos may come from decays of dark matter particles with masses of a few PeV (Feldstein et al., 2013). These features may lack statistical significance at present, but they will be tested very soon with upcoming new data. The lack of events above a PeV and, in particular, in the vicinity of the Glashow resonance, suggests that the spectrum should decrease significantly at the energy of a few PeV. Spectra from dark matter decays (and annihilations) always exhibit a sharp cutoff determined by the particle mass. Furthermore, the two PeV events appear to have identical energies, up to experimental uncertainties. A line in the neutrino spectrum would be a "smoking gun" signature for dark matter. A monochromatic neutrino line should be accompanied by a continuous spectrum of lower-energy neutrinos (Feldstein et al., 2013), which can explain both the PeV events and some of the sub-PeV events, a conclusion that emerges from particle physics considerations (Feldstein et al., 2013) and appears to be in agreement with the data (Esmaili and Serpico, 2013; Esmaili et al., 2012). Finally, angular distribution of arrival directions is consistent with dark matter decay (Bai et al., 2013).

The existence of dark matter is confirmed by a number of independent observations, and many particle physics candidates have been proposed (Feng, 2010). In general, both annihilations and decays of dark matter particles could be considered for explaining the IceCube results. However, since the $m_{\rm DM} \sim$ PeV mass scale is determined by the PeV neutrino energies, annihilations can be ruled out (Feldstein et al., 2013). For dark matter with an annihilation cross section into neutrinos saturating the unitarity limit, $\sigma_{\rm Ann} \leqslant 4\pi/(m_{\rm DM}^2 v^2)$, the event rate expected at a neutrino telescope of fiducial volume V and nucleon number density $n_{\rm N}$ is

$$\Gamma_{\rm events} \sim V L_{\rm MW} n_{\rm N} \sigma_{\rm N} \left(\frac{\rho_{\rm DM}}{m_{\rm DM}}\right)^2 \langle \sigma_{\rm Ann} v \rangle$$

$$\lesssim 10^{-3}\left(\frac{1\ \text{PeV}}{m_{\rm DM}}\right)^{3.6}(1\ \text{year})^{-1}, \tag{52}$$

where we have used the fiducial volume of the IceCube experiment, and the energy-dependent neutrino–nucleon scattering cross section from Gandhi et al. (1998) for the energy $E \sim m_{\rm DM}$. Obviously, dark matter annihilation cannot produce a sufficient number of events.

However, decays of dark matter particles can produce the required flux for cosmologically acceptable decay times, much longer than the present age of the universe (Feldstein et al., 2013; Esmaili and Serpico, 2013). A systematic study of effective operators capable of producing the requisite decay signal leads to a number of very interesting dark matter candidates (Feldstein et al., 2013). The list includes a gravitino with R-Parity violation, hidden sector gauge bosons, and singlet fermions and bosons in extra dimensions.

Even much heavier relic particles, with masses well above a PeV, can generate the required neutrino spectrum from their decays if their lifetime is much shorter than the present age of the universe (Ema et al., 2013). The spectrum of neutrinos is modified by a combination of redshift and interactions with the background neutrinos, and the observed spectrum can have a cutoff just above 1 PeV for a broad range of the relic particle masses, from ∼1 PeV to ∼10 EeV (Ema et al., 2013). Each of these possibilities represents a new window on physics beyond the Standard Model with profound implications for one's understanding of the universe.

5.2. Enhancement of neutrino–nucleon cross section

A possible explanation of the PeV IceCube events is a resonant enhancement of the neutrino cross-section. The Glashow resonance in electron–antineutrinos scattering on electrons is one such example (Glashow, 1960). Shower events would result from the hadronic decays of the produced W-boson (Barger et al., 2012b; Bhattacharya et al., 2012). However, the 6.3 PeV energy of the Glashow resonance is too high to explain the observed 1 PeV shower energies.

Another resonance candidate is an s-channel leptoquark (LQ) in neutrino scattering on light quarks (Anchordoqui et al., 2006b; Berezinsky, 1985). A leptoquark of mass ∼0.6 TeV that couples to τ-lepton and down-quark flavors provides a plausible explanation of the IceCube data (Barger and Keung, 2013). The LQ resonance enhanced processes are $\nu_\tau + q \to \text{LQ} \to \tau + q'$ and $\nu_\tau + q \to \text{LQ} \to \nu_\tau + q$.

At PeV energies, upward-going neutrinos that pass through the Earth should mainly be τ-flavor, because the Earth is almost opaque to electron–neutrinos and muon–neutrinos while τ-neutrinos can be regenerated via τ-decays. The τ decays to hadrons and electrons, with a combined branching fraction of 82%, produce shower events, whereas only 18% of τ's-decays give a muon-track.

How does this general expectation compare with the IceCube observations? The contribution from cascades and track topologies has been studied in detail in Winter (2013). Above 20 TeV deposited EM energy, there are fewer upward than downward events, as expected from absorption of electron–neutrinos and muon–neutrinos by the Earth. Furthermore, all but one of the muon-track events are upward or horizontal. Above 150 TeV, there is only one muon-track event, which is upward as compared to 6 shower events, 2 upward and 4 downward. The present statistics are low, but the IceCube data suggest that mainly ν_τ events are being seen above 150 TeV, in accord with this leptoquark scenario.

The PeV IceCube events could be due to CC reactions with showers from the hadronic τ decays and the hadron jet from the produced quark. The observed shower energy would be a little less than the mass of the leptoquark because the secondary neutrino from the τ decay is undetected. When the produced τ decays to a muon, giving a track, or the τ decays to an electron, the shower energy is lower than for events associated with the hadronic τ-decays. In the NC reaction, the shower energy of the event will be approximately half that of the CC reaction. The shower energy gap between the PeV events and the onset of lower energy events seems indicative of what is expected from the LQ processes.

A general list of leptoquark models and the corresponding experimental limits are given in Rolli and Tanabashi (2012). For a scalar leptoquark S of charge $-\frac{1}{3}$, the Lagrangian interaction is given by

$$\mathscr{L}_{\rm LQ} = f_L S^\dagger (u,d)_L \varepsilon \begin{pmatrix} \nu_\tau \\ \tau \end{pmatrix}_L + f_R S^\dagger u_R \tau_R + \text{ h.c.}, \tag{53}$$

where the Levi-Civita symbol ε antisymmetrizes the two $SU(2)$ doublets to match the singlet S. The couplings f_L, f_R are the leptoquark couplings to the left and right chiral quarks. In the narrow LQ width approximation, the neutrino cross-section is given by Anchordoqui et al. (2006b), Alikhanov (2013), Doncheski and Robinett (1997)

$$\sigma_{\rm LQ}(\nu N) = \frac{\pi f_L^2}{2M_S^2} x d_N(x,\mu^2), \tag{54}$$

where $x = M_S^2/s$ is the parton fractional momentum, with $s = 2m_N E_\nu$. The down-quark parton distribution function $d_N(x,\mu^2)$ in the target nucleon N is evaluated at the scale $\mu^2 = M_S^2$ in the leading order calculation. To obtain the corresponding rates for each channel, we multiply the LQ production cross section (shown in the left panel of Fig. 14) by the associated branching fractions

$$\begin{aligned} &\mathcal{B}(S \to \nu_\tau d) = \mathcal{B}(S \to \tau_L u) = f_L^2/(2f_L^2 + f_R^2), \\ &\mathcal{B}(S \to \tau_R u) = f_R^2/(2f_L^2 + f_R^2). \end{aligned} \tag{55}$$

The LQ width is found to be

$$\Gamma_{\rm LQ} = \frac{1}{16\pi} M_S (2f_L^2 + f_R^2), \tag{56}$$

which is a small fraction of its mass even for a unit coupling f, so the narrow width approximation is justifiable.

As a benchmark, we consider the neutrino flux given in (1), with the power index $\Gamma = 2.3$. For $t = 662$ days, the predicted number of events is given by

$$\mathcal{N} = n_N t \Omega \int dE_\nu\, \sigma_{\rm LQ} \cdot \mathcal{B}(S \to ij) \cdot \Phi_\nu(E_\nu), \tag{57}$$

where $n_N = 6 \times 10^{38}$ is the effective target nucleon number in IceCube and we take the solid angle of the full 4π coverage ($\Omega = 4\pi$). The event distribution $d\mathcal{N}/dE_\nu$, for the coupling choice $f_L = 1$, is shown in the right panel of Fig. 14. At a neutrino energy of ∼1 PeV a few cascade events are predicted for LQ mass of ∼0.6 TeV.

A leptoquark of 0.6 TeV mass can be probed at the LHC (Cieza Montalvo et al., 1998; Belyaev et al., 2005; Blumlein et al., 1997). Based on its pair production, the CMS/LHC search at 7 TeV (Chatrchyan et al., 2013) for a scalar τ-type LQ placed a constraint $M_S \gtrsim 525$ GeV. Single LQ production at the LHC occurs through the subprocesses $gu \to \bar{\tau} S$ and $gd \to \bar{\nu}_\tau S$. The down-type LQ, S, subsequently decays into τu or $\nu_\tau d$, leading to the final states $\bar{\tau}\tau u$, or $\bar{\tau}\nu_\tau d$, or $\bar{\nu}_\tau \nu_\tau d$, etc. These subprocesses lead to distinctive events of $\bar{\tau}\tau$ pair plus a jet or a monojet and missing energy with or without a τ. Searches at LHC14 for these LQ signals can confirm or reject the LQ interpretation of the PeV events at IceCube.

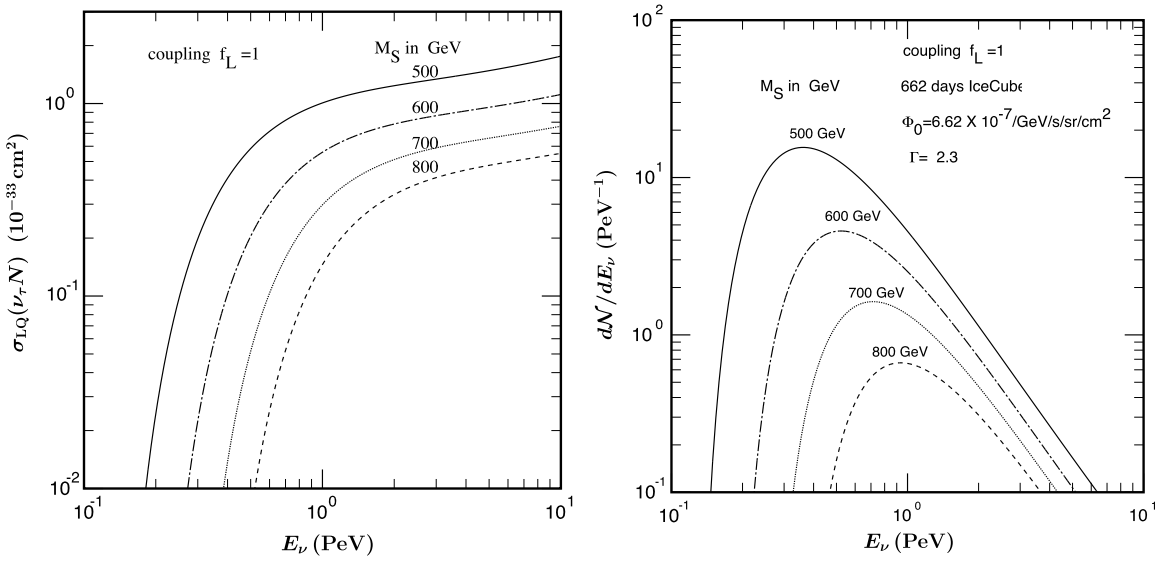

Fig. 14. Left: LQ production cross-section in $\nu_\tau N$ scattering. **Right:** Event rate distribution $d\mathcal{N}/dE_\nu$, from the LQ cross section convoluted with the flux of Eq. (1). The CTEQ6.10 parton distributions at NLO are used in this calculation (Lai et al., 2010).

5.3. Neutrino flavor physics

A natural question is whether the observation of 7 track (T) events and 21 shower (S) events is consistent with the expected $1:1:1$ neutrino flavor signal. Denoting the fractional neutrino flux of flavor i by $\eta_{\nu_i} = \Phi_{\nu_i}/(\Phi_{\nu_e} + \Phi_{\nu_\mu} + \Phi_{\nu_\tau})$, with Φ_{ν_i} the neutrino flux of flavor i, the ratio,

$$\frac{T}{T+S} \simeq \frac{(e_T/e_S)(\eta_{\nu_\mu} + 0.2\eta_{\nu_\tau})}{(e_T/e_S)(\eta_{\nu_\mu} + 0.2\eta_{\nu_\tau}) + \eta_{\nu_e} + 0.8\eta_{\nu_\tau} + \sigma_{NC}/\sigma_{CC}}, \tag{58}$$

where e_T and e_S are the efficiencies for detecting tracks and showers, respectively. Taking the efficiencies to be equal (which is approximately true, since all 28 events have a vertex within the instrumented volume), $\sigma_{NC}/\sigma_{CC} = 0.4$ for PeV neutrinos, and $\eta_{\nu_e} = \eta_{\nu_\mu} = \eta_{\nu_\tau} = 1/3$, we get

$$\frac{T}{T+S} \simeq 0.286, \tag{59}$$

which given the limited statistics is consistent with the observed value of 0.25. Nevertheless, with the promise of larger datasets, it is worth considering deviations from the $1:1:1$ flavor mix, and there are quite a few ways of achieving this. In the following, we draw from Pakvasa (2008).

The simplest possibility is that initial flavor mix is not $1:2:0$. In the damped muon case in which the initial flavor mix is $0:1:0$, the final result after the oscillations are averaged out is $0.57:1:1$ on arrival (for details, see Appendix B). The "beta" beam which starts out as $1:0:0$ becomes $2.5:1:1$ on arrival. A "prompt" beam from heavy flavor decays which starts out as $1:1:0$ arrives as $1.27:1:1$. These are sufficiently different from the universal mix that the nature of the source can be easily distinguished. The two kinds of production processes that lead to the initial flavor mix of $1:2:0$, namely the pp and γp interactions can also be distinguished from each other, at least in principle (Anchordoqui et al., 2005b). In the former case the flux of $\bar{\nu}_e$ relative to the total neutrino flux is 1/6, whereas in the latter case it is 2/27; the $\bar{\nu}_e$ flux can be measured at an incident energy of 6.3 PeV as showers due to the Glashow resonance.

Neutrino decay is another way for the flavor mix to deviate significantly from the democratic mix (Beacom et al., 2003a, 2004b) (see also Anchordoqui and Goldberg, 2008; Baerwald et al., 2012). If the neutrino mass hierarchy is normal and the source distances are large, the ν_2 and ν_3 mass eigenstates will have decayed away completely. For a quasi-hierarchical mass spectrum, *i.e.*, $m_2, m_3 \gg m_1$, the daughter neutrino energy is much lower than that of the parent and the final ν_1 does not contribute to the flux at that energy; see *e.g.*, Beacom and Bell (2002). This may explain the absence of ν_μ events above 1 PeV (Pakvasa et al., 2013).

In this picture, neutrinos originating from GRBs arrive at the earth as pure ν_1 whose flavor content is $\Phi_{\nu_e} : \Phi_{\nu_\mu} : \Phi_{\nu_\tau} = |U_{e1}|^2 : |U_{\mu 1}|^2 : |U_{\tau 1}|^2$ (Pakvasa, 1981). The current best fit values for the neutrino mixing parameters (Schwetz et al., 2012; Gonzalez-Garcia et al., 2012; Fogli et al., 2012) and the unknown Dirac CP phase yield $|U_{\mu 1}|^2$ between 0.1 and 0.3 with a central value of about 0.16. This is a suppression beyond the factor of two due to standard flavor oscillations, so that a suppression of the muon neutrino flux by an order of magnitude is possible. Since the value of $|U_{e1}|^2$ lies between 0.65 and 0.72, the ν_e flux is only slightly affected by the decays of ν_2 and ν_3. Note that $\Phi_{\nu_e}/\Phi_{\nu_\mu}$ ranges from 2.5 to 8 with a central value of about 4, depending on the value of the phase δ.

Another possibility for deviations from the universal flavor mix arises in scenarios of pseudo-Dirac neutrinos in which each of the three neutrino mass eigenstates is a doublet with mass differences smaller than 10^{-6} eV, thereby evading detection (Wolfenstein, 1981; Petcov, 1982; Bilenky and Pontecorvo, 1983). In fact, the only way to detect mass differences in the range $10^{-18}\ \mathrm{eV}^2 < \Delta m^2 < 10^{-12}\ \mathrm{eV}^2$ is by measuring flavor mixes of the high energy neutrinos from cosmic sources.

For large L/E, flavor ratios deviate from the canonical value of 1/3 by

$$\delta P_\beta = \frac{1}{3}\left[|U_{\beta 1}|^2\chi_1 + |U_{\beta 2}|^2\chi_2 + |U_{\beta 3}|^2\chi_3\right], \tag{60}$$

where $\chi_i = \sin^2(\Delta m_i^2 L/4E)$, with the pseudo-Dirac mass-squared differences,

$$\Delta m_i^2 = \left(m_i^+\right)^2 - \left(m_i^-\right)^2, \tag{61}$$

of the nearly degenerate pair ν_i^+ and ν_i^- (Beacom et al., 2004a) (see also Esmaili, 2010; Esmaili and Farzan, 2012). The flavor ratios deviate from $1:1:1$ when one or two of the pseudo-Dirac oscillation modes is accessible. In the limit where L/E is so large that all three oscillating factors have averaged to 1/2, the flavor

ratios return to 1 : 1 : 1, with only a net suppression of the measurable flux, by a factor of 1/2.

If neutrinos traverse regions with large magnetic fields and their magnetic moments are large enough, the flavor mix can be affected (Enqvist et al., 1998). The main effect of the passage through a magnetic field is the conversion of a given helicity into an equal mixture of both helicity states. This is also true in passage through random magnetic fields (Domokos and Kovesi-Domokos, 1997). It has been shown that a magnetic field of 10 or more Gauss at the source can cause the neutrinos to decohere as they traverse cosmic distances (Farzan and Smirnov, 2008).

If neutrinos are Dirac particles with comparable magnetic moments, then the effect of the spin-flip is to simply reduce the overall flux of all flavors by half, the other half becoming the sterile Dirac partners. On the other hand, if neutrinos are Majorana particles, the flavor mix remains 1 : 1 : 1 with the absolute flux unchanged.

What happens when large magnetic fields are present in or near the neutrino production region? In the case of Dirac neutrinos, the situation is as above, and the outgoing flavor ratio remains 1 : 1 : 1 with the absolute fluxes reduced by half. In the case of Majorana neutrinos, the initial flavor mix 1 : 2 : 0 is unmodified at the source because of the antisymmetry of the magnetic moment matrix, but the final flavor mix after oscillations is still 1 : 1 : 1.

If neutrinos have flavor violating couplings to gravity then resonance effects may allow one way transitions *e.g.*, $\nu_\mu \to \nu_\tau$ but not vice versa (Minakata and Smirnov, 1996; Barger et al., 2000). This can give rise to an anisotropic deviation of the $\Phi_{\nu_\mu}/\Phi_{\nu_\tau}$ from 1, becoming less than 1 for events coming from the direction of the Great Attractor, while remaining 1 in other directions (Minakata and Smirnov, 1996). If such striking effects are not seen, current bounds on such violations can be improved by six to seven orders of magnitude.

Another possibility that can give rise to deviations of the flavor mix from the canonical 1 : 1 : 1 is the idea of mass-varying neutrinos (Fardon et al., 2004), that was proposed to solve the cosmic coincidence problem. Neutrino masses vary in such a way that the dark energy density and neutrino energy density are related over cosmic time scales. The dark energy density is made neutrino-mass-dependent by coupling a sterile neutrino and a light scalar field. If the sterile neutrino mixes with a flavor neutrino, the mass difference varies along the path of propagation, with the potential for resonance enhancement of the transition probability into the sterile neutrino, and a resulting change in the flavor mix (Hung and Pas, 2005). For example, if only one resonance is crossed *en route*, the heaviest (mostly) flavor state may transform into the (mostly) sterile state, thus changing the flavor mix to $1-|U_{e1}|^2 : 1-|U_{\mu 1}|^2 : 1-|U_{\tau 1}|^2 \approx 0.4 : 1 : 1$ for the inverted hierarchy and to $1-|U_{e3}|^2 : 1-|U_{\mu 3}|^2 : 1-|U_{\tau 3}|^2 \approx 2 : 1 : 1$ for the normal hierarchy.

Complete quantum decoherence gives rise to a flavor mix of 1 : 1 : 1, which is identical to the case of averaged oscillations. The distinction is that complete decoherence always leads to this result, whereas averaged oscillations give this result only for an initial flavor mix of 1 : 2 : 0. Therefore, to find evidence for decoherence requires a source which has a different flavor mix. An example is the "beta" beam source with an initial flavor mix of 1 : 0 : 0. In this case decoherence gives the universal 1 : 1 : 1 mix whereas averaged oscillations give 2.5 : 1 : 1 (Anchordoqui et al., 2005a). The two cases can be easily distinguished from each other.

Violations of Lorentz invariance and/or *CPT* invariance can change the final flavor mix from the universal mix significantly. With a specific choice of a modified dispersion relation due to Lorentz Invariance Violation, the effects can be dramatic. For example, the final flavor mix at sufficiently high energies can become 7 : 2 : 0 (Hooper et al., 2005b).

To summarize, a measurement of a flavor ratio different from 1 : 1 : 1 would suggest new physics. If measurements of the flavor mix at Earth of high energy astrophysical neutrinos find it to be

$$\Phi_{\nu_e} : \Phi_{\nu_\mu} : \Phi_{\nu_\tau} = \alpha : 1 : 1, \tag{62}$$

then: (i) $\alpha \approx 1$ confirms our knowledge of the neutrino mixing matrix and our prejudice about the production mechanism; (ii) $\alpha \approx 1/2$ indicates a pure ν_μ source and conventional mixing; (iii) $\alpha > 1$ indicates that neutrinos with a normal hierarchy are decaying; and (iv) a value of α between 2.5 and 10, and a deviation of the ν_μ/ν_τ ratio from 1 (between 0.2 to 4) can yield valuable information about the *CP* phase δ, whereas a value of α between 0.7 and 1.5 can probe pseudo-Dirac Δm^2 smaller than 10^{-12} eV^2. These results have no dependence on the initial flavor mix, and are consequently independent of the production model. One either learns about the production mechanism and the initial flavor mix, or about neutrino properties.

6. Looking ahead

In summary, a decades-long development program, culminating in the fruits of the IceCube Collaboration, have introduced not only the dawn of the age of neutrino astronomy and astrophysics but also provides a beacon for future directions in particle physics. We have reviewed the possible origins of the soon-to-be famous 28 IceCube neutrino events (Aartsen et al., 2013c, 2013d). Thus far the IceCube excess is consistent with both Galactic and extragalactic origin(s).

In particular, we showed that the IceCube neutrino excess is consistent with optically thin Galactic sources producing an unbroken power-law with a spectral index of $\Gamma = 2.3$ (Anchordoqui et al., 2013b). A shallower spectrum would overproduce events in the null region above ∼2 PeV, and hence require a cutoff. We employed this hypothesis to argue that cosmic neutrinos are more likely to arise from pp interactions than $p\gamma$ interactions. We also explored the validity of this hypothesis considering other factors including the spectral shape and anisotropy of baryonic CRs around and above 3 PeV predicted by various Galactic magnetic field models as well as the compatibility of nearby (Galactic) sources with bounds on the photon fraction measured by the CASA-MIA Collaboration. We conclude from the CR anisotropy searches that a Galactic magnetic field model favoring a CR injection index of $\alpha = 2.3$ is more likely to be correct than the usual $\alpha \simeq 2$ of a Fermi engine. Furthermore, we find that existing photon bounds do not rule out a Galactic origin at optically thin sources as a viable model for the IceCube excess. In all, given present statistics, the Galactic hypothesis is plausible with an unbroken power without cutoff. Note that these conclusions apply only if the neutrino sources are Galactic, since, for instance, we do not know the extragalactic CR power at PeV energies.

It is inspiring to realize that we are at the cusp of a new era of multimessenger astronomy, now with cosmic neutrinos thrown into the mix. Indeed a recent analysis (Murase et al., 2013) shows that a bound on the steepness of an extragalactic pp-generated neutrino spectrum can be estimated based on *Fermi*-LAT observations of the isotropic γ ray background, showing $\Gamma \lesssim 2.1$–2.2 is required for consistency with extragalactic neutrino origin. It is notable then that IceCube spectrum alone will ultimately reveal something about the source of cosmic neutrinos, even in the absence of an observation of an excess in specific regions of the sky.

We have seen that various classes of extragalactic sources are consistent with emission spectrum $\propto E_\nu^{-2}$ in the energy range of interest. These include GRBs (Cholis and Hooper, 2013), AGNs (Stecker, 2013a; Kalashev et al., 2013; Kistler et al., 2013), and hypernova remnants in star forming galaxies (Liu et al., 2013).

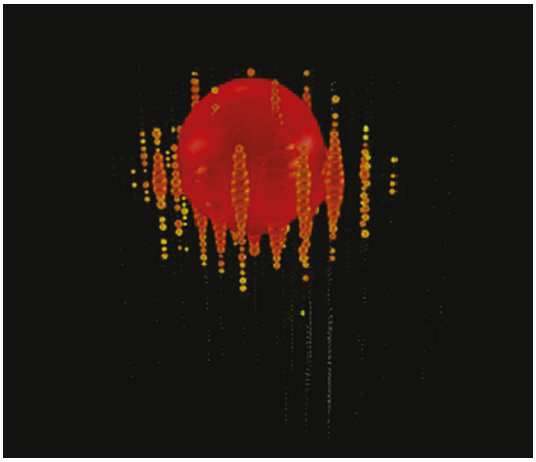

Fig. 15. Event display showing Big Bird, with 378 optical modules hit. Each sphere shows a hit optical module. The size of the spheres shows the number of photoelectrons observed by the DOM, while the color indicates the time, with red being earliest, and blue latest. Figure courtesy of the IceCube Collaboration.

The distribution of arrival directions would provide a way of distinguishing among these models. In the case of GRBs, coincidence in time will be the key. In the case of possible correlations with AGN, we can learn about the intergalactic magnetic field via possible correlations with associated γ rays, as a result of photon showering during propagation to Earth.

In a few years of data taking IceCube will collect sufficient statistics to ascertain whether there are structures in the spectrum. A gap could be associated with NC and CC processes of a new physics resonance (Barger and Keung, 2013). Alternatively, a neutrino spectral line could then point to the decay or annihilation of the elusive dark matter particles (Feldstein et al., 2013).

Examination of the data collected in 2012 has begun. One very high energy event, called Big Bird, appeared in the 10% of the data that was used to tune the selection cuts. This event is shown in Fig. 15. A total of 378 DOMs were hit, making it the brightest neutrino event thus far observed. This is suggestive that the energy spectrum will continue, in one form or another, beyond the 1 PeV limit found thus far, perhaps into the sweet spot for ν_τ-detection. The potential to access the region of high sensitivity to ν_τ, together with growing statistics for ν_μ and ν_e events will wedge open a portal for flavor physics exploration, making the coming era watershed years for electroweak physics accessible via high energy cosmic neutrinos (Pakvasa et al., 2013).

The discovery of cosmic rays just over 100 years ago was not only remarkable in its own right, but it also provided a cornerstone for the field of particle physics. Many of the most important early breakthroughs in particle physics were achieved through observation of cosmic rays, including the watershed discoveries of antimatter, the pion, the muon, the kaon, and several other particles. In this article, we have both reviewed the nascent field of cosmic neutrino astronomy and considered some of the potential ways CR science will once again point the way in the quest to understand Nature at its most fundamental.

Acknowledgments

We would like to thank Francis Halzen, Stephen King, Soeb Razzaque, and the IceCube Collaboration for allowing us to use various figures from their papers in this review. L.A.A. is supported by U.S. National Science Foundation (NSF) CAREER Award PHY1053663 and by the National Aeronautics and Space Administration (NASA) Grant No. NNX13AH52G. V.B. is supported by the U.S. Department of Energy (DoE) Grant No. DE-FG-02-95ER40896. I.C. and D.H. are supported by DoE. H.G. is supported by NSF Grant No. PHY-0757959. A.K. is supported by DoE Grant No. DE-SC0009937 and by the World Premier International Research Center Initiative (WPI Initiative), MEXT, Japan. J.G.L. and S.P. are supported by DoE Grant No. DE-FG02-04ER41291. D.M. is supported by DoE Grant No. DE-FG02-13ER42024. T.C.P. is supported by NSF Grant No. PHY-1205854 and NASA Grant No. NNX13AH52G. T.J.W. is supported by DoE Grant No. DE-FG05-85ER40226. Any opinions, findings, and conclusions or recommendations expressed in this material are those of the authors and do not necessarily reflect the views of the NSF, DoE, or NASA.

Appendix A. Harmonic analysis for anisotropy searches

Cosmic ray detectors which experience stable operation over a period of a year or more attain a uniform exposure in right ascension, α. In such a case, the right ascension distribution of the flux arriving at a detector can be characterized by the amplitudes and phases of its Fourier expansion,

$$J(\alpha) = J_0\big[1 + r\cos(\alpha - \phi) + r'\cos\big(2(\alpha - \phi')\big) + \cdots\big]. \tag{A.1}$$

For N measurements α_i, the first harmonic amplitude r and its phase ϕ can be determined by applying the classical Rayleigh formalism (Linsley, 1975),

$$r = \sqrt{x^2 + y^2}, \qquad \phi = \arctan\frac{y}{x}, \tag{A.2}$$

where

$$x = \frac{2}{\mathcal{N}}\sum_{i=1}^{N} w_i\cos\alpha_i, \qquad y = \frac{2}{\mathcal{N}}\sum_{i=1}^{N} w_i\sin\alpha_i, \tag{A.3}$$

$\mathcal{N} = \sum_{i=1}^{N} w_i$ is the normalization factor, and the weights, $w_i = \omega^{-1}(\delta_i)$, are the reciprocal of the relative exposure, ω, as a function of the declination, δ_i (Sommers, 2001). As deviations from an uniform right ascension exposure are small, the probability $P(>r)$ that an amplitude equal or larger than r arises from an isotropic distribution can be approximated by the cumulative distribution function of the Rayleigh distribution $P(>r) = \exp(-k_0)$, where $k_0 = \mathcal{N}r^2/4$.

The first harmonic amplitude of the right ascension distribution can be directly related to the amplitude $|\boldsymbol{\delta}|$ of a dipolar distribution of the form

$$J(\alpha,\delta) = \big(1 + |\boldsymbol{\delta}|\,\hat{\boldsymbol{d}}\cdot\hat{\boldsymbol{u}}\big)J_0, \tag{A.4}$$

where $\hat{\boldsymbol{u}}$ denotes the unit vector in the direction (α,δ) of the sky and $\hat{\boldsymbol{d}}$ denotes the unit vector in the direction of the dipole. We can rewrite x, y, and $\mathcal{N}$ as

$$x = \frac{2}{\mathcal{N}}\int_{\delta_{\min}}^{\delta_{\max}} d\delta \int_0^{2\pi} d\alpha\cos\delta\; J(\alpha,\delta)\omega(\delta)\cos\alpha,$$

$$y = \frac{2}{\mathcal{N}}\int_{\delta_{\min}}^{\delta_{\max}} d\delta \int_0^{2\pi} d\alpha\cos\delta\; J(\alpha,\delta)\omega(\delta)\sin\alpha,$$

$$\mathcal{N} = \int_{\delta_{\min}}^{\delta_{\max}} d\delta \int_0^{2\pi} d\alpha\;\cos\delta\; J(\alpha,\delta)\omega(\delta). \tag{A.5}$$

In (A.5) we have neglected the small dependence on right ascension in the exposure. Next, we write the angular dependence in $J(\alpha,\delta)$ as

$$\hat{\boldsymbol{d}}\cdot\hat{\boldsymbol{u}}_{\boldsymbol{i}} = \cos\delta_i\cos\delta_0\cos(\alpha_i - \alpha_0) + \sin\delta_i\sin\delta_0, \tag{A.6}$$

where α_0 and δ_0 are the right ascension and declination of the direction where the flux is maximum, and α_i and δ_i are the right ascension and declination of the ith event. Performing the α integration in (A.5) it follows that

$$r = \left| \frac{A\delta_\perp}{1 + B\delta_\parallel} \right|, \tag{A.7}$$

where $\delta_\parallel = \boldsymbol{\delta} \sin\delta_0$ is the component of the dipole along the Earth rotation axis, and $\delta_\perp = \boldsymbol{\delta} \cos\delta_0$ is the component in the equatorial plane (Aublin and Parizot, 2005). The coefficients A and B can be estimated from the data as the mean values of the cosine and the sine of the event declinations,

$$A = \frac{\int d\delta\, \omega(\delta) \cos^2\delta}{\int d\delta\, \omega(\delta) \cos\delta} \quad \text{and} \quad B = \frac{\int d\delta \omega(\delta) \cos\delta \sin\delta}{\int d\delta\, \omega(\delta) \cos\delta}. \tag{A.8}$$

For a dipole amplitude $|\boldsymbol{\delta}|$, the measured amplitude of the first harmonic in right ascension r thus depends on the region of the sky observed, which is essentially a function of the latitude of the observatory and the range of zenith angles considered. In the case of a small $B\delta_\parallel$ factor, the dipole component in the equatorial plane is obtained as $\delta_\perp \simeq r/A$. The phase ϕ corresponds to the right ascension of the dipole direction α_0.

Appendix B. Cosmic neutrino flavor ratio

The discovery of neutrino oscillations provoked quite a revolution in elementary particle physics, demonstrating the need for physics beyond the Standard Model. The flavor oscillation patterns can be convincingly interpreted as a non-trivial mixing among neutrino mass eigenstates, with a small "solar" mass splitting $\Delta m^2_\odot \simeq 7.65 \times 10^{-5}$ eV^2 and a large "atmospheric" splitting $\Delta m^2_{\rm atm} \simeq 2.40 \times 10^{-3}$ eV^2 (Gonzalez-Garcia et al., 2012).

The superposition of neutrino mass eigenstates ν_j ($j = 1, 2, 3, \ldots$) produced in association with the charged lepton of flavor α,

$$|\nu_\alpha\rangle = \sum_j U^*_{\alpha j} |\nu_j\rangle, \tag{B.1}$$

is the state we refer to as the neutrino of flavor α, where $U_{\alpha j}$'s are elements of the unitary neutrino mass-to-flavor mixing matrix fundamental to particle physics, the so-called Pontecorvo–Maki–Nagakawa–Sakata (PMNS) matrix (Pontecorvo, 1957, 1968; Maki et al., 1962). The unitary PMNS mixing matrix has 9 degrees of freedom, which are reduced to 6 after absorbing three global phases into re-definitions of the three charged lepton states, e, μ, τ. (For Majorana neutrinos, no further phases may be absorbed, while for Dirac neutrinos, two further relative phases among the three neutrinos may be absorbed by neutrino-field redefinitions.) With six undetermined parameters, the neutrino mixing matrix $\mathbb{U}_{\rm PMNS}$ is conveniently parametrized by three Euler rotations θ_{12}, θ_{23}, and θ_{13}, and three CP-violating phases δ, α_1 and α_2,

$$\mathbb{U}_{\rm PMNS} = R_{23}(\theta_{23}) \begin{pmatrix} c_{13} & 0 & s_{13} e^{-i\delta} \\ 0 & 1 & 0 \\ -s_{13} e^{i\delta} & 0 & c_{13} \end{pmatrix} R_{12}(\theta_{12}) \times \mathrm{diag}\left(e^{i\alpha_1/2}, e^{i\alpha_2/2}, 1\right), \tag{B.2}$$

where we used the abbreviations $\sin\theta_{ij} = s_{ij}$ and $\cos\theta_{ij} = c_{ij}$. R_{ij} denotes a rotation in the $\nu_i\nu_j$-plane, see Fig. B.16. The "Majorana" phases α_1 and α_2 are unique to Majorana neutrinos, *i.e.* neutrinos which are their own antiparticles. Note, that the phase δ ("Dirac phase") appears only in combination with a non-vanishing mixing angle θ_{13}. Additional details are eloquently discussed in Barger et al. (2012a). For the curious public, Weiler (2013) provides a very readable account.

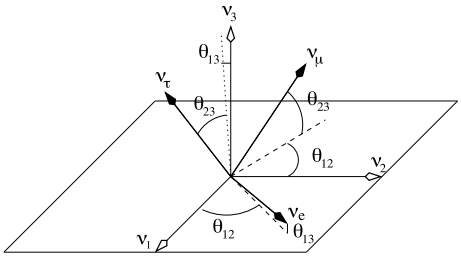

Fig. B.16. Display of the three mixing angles that characterize the orientation of the flavor axes relative to mass axes. From King and Luhn (2013).

The density matrix of a flavor state, $\rho_\alpha = |\nu_\alpha\rangle\langle\nu_\alpha|$, can be expressed in terms of mass eigenstates by $\rho_\alpha = \sum_{i,j} U^*_{\alpha i} U_{\alpha j} |\nu_i\rangle\langle\nu_j|$. This is a pure quantum system, therefore the density matrix satisfies $\mathrm{Tr}\,\rho^2 = \mathrm{Tr}\,\rho = 1$. The time evolution of the density matrix,

$$\frac{\partial\rho}{\partial t} = -\mathrm{i}[H, \rho], \tag{B.3}$$

is governed by the Hamiltonian of the system,

$$H \simeq \sum_i \frac{m_i^2}{2E_\nu} \Pi_i, \tag{B.4}$$

where we have introduced the projection operator $\Pi_i \equiv |\nu_i\rangle\langle\nu_i|$.[11] Substituting the Hamiltonian (B.4) into (B.3) we obtain

$$\frac{\partial\rho_{ij}}{\partial t} = \frac{\mathrm{i}\Delta m^2_{ij}}{2E_\nu} \rho_{ij}, \tag{B.5}$$

where $\Delta m^2_{ij} \equiv m_i^2 - m_j^2$. For the initial condition $\rho_\alpha(0) = \Pi_\alpha$, the density matrix at a distance L is given by

$$\rho_\alpha(L) = \sum_{i,j} U^*_{\alpha i} U_{\alpha j} \exp\left(\frac{\mathrm{i}\Delta m^2_{ij} L}{2E_\nu}\right) |\nu_i\rangle\langle\nu_j|. \tag{B.6}$$

Therefore, after traveling a distance L an initial state ν_α becomes a superposition of all flavors, with probability of transition to flavor β given by $P_{\nu_\alpha \to \nu_\beta} = \mathrm{Tr}[\rho_\alpha(L)\Pi_\beta]$, or equivalently (Gonzalez-Garcia and Maltoni, 2008)

$$P_{\nu_\alpha \to \nu_\beta} = \delta_{\alpha\beta} - 4 \sum_{i>j} \Re\left(U^*_{\alpha i} U_{\beta i} U_{\alpha j} U^*_{\beta j}\right) \sin^2 \Delta_{ij} + 2 \sum_{i>j} \Im\left(U^*_{\alpha i} U_{\beta i} U_{\alpha j} U^*_{\beta j}\right) \sin 2\Delta_{ij}. \tag{B.7}$$

The oscillation phase Δ_{ij} is conveniently parameterized as

$$\Delta_{ij} = \frac{\Delta m^2_{ij} L}{4E_\nu} \simeq 1.27 \left(\frac{\Delta m^2_{ij}}{\mathrm{eV}^2}\right) \left(\frac{L}{\mathrm{km}}\right) \left(\frac{E_\nu}{\mathrm{GeV}}\right)^{-1}. \tag{B.8}$$

Note, that the third term in Eq. (B.7) comprises CP-violating effects, *i.e.* this term changes sign for the antineutrino process $P_{\bar\nu_\alpha \to \bar\nu_\beta}$, corresponding to the replacement $U \to U^*$. For the standard parameterization (B.2), the single CP-violating contribution is attributable to the Dirac phase δ; oscillation experiments are *not* sensitive to Majorana phases.

For many years, the sparse data on the angle θ_{13} allowed consistency with zero. However, in Spring of 2012, the angle was definitively measured to be nonzero (but still small on the scale of $\theta_{23} \sim 45°$ and $\theta_{12} \sim 35°$), $\theta_{13} \approx 9°$

[11] Dissipative effects due to charged current interactions in matter can be simply included by an extra term $-\sum_\alpha \frac{1}{2\lambda_\alpha}\{\Pi_\alpha, \rho\}$ to the r.h.s. of Eq. (B.3), where $\Pi_\alpha = |\nu_\alpha\rangle\langle\nu_\alpha|$ and λ_α is the dissipation length.

(An et al., 2012, 2013; Ahn et al., 2012). At present, the low statistics of IceCube limits its capacity to disentangle neutrino flavors with sufficient precision to be sensitive to small θ_{13}. To simplify the following discussion, we will adopt maximal mixing for atmospheric $\nu_\mu \leftrightharpoons \nu_\tau$ neutrinos (*i.e.* $\theta_{23} \sim 45^\circ$) along with a negligible $|U_{e3}|^2 = \sin^2(\theta_{13})$. The latter approximation allows us to ignore *CP* violation and assume real matrix elements. (The small effects of nonzero θ_{13} have been investigated in Fu et al. (2012). Other small corrections that we need not consider here arise from the fact that flavor ratios at injection deviate from whole numbers due to subtle particle physics effects (Lipari et al., 2007; Pakvasa et al., 2008; see also Esmaili and Farzan, 2009).)

With our simplifying assumptions in mind, one can define a mass basis as follows,

$$|\nu_1\rangle = \sin\theta_\odot \left|\nu^\star\right\rangle + \cos\theta_\odot |\nu_e\rangle, \tag{B.9}$$

$$|\nu_2\rangle = \cos\theta_\odot \left|\nu^\star\right\rangle - \sin\theta_\odot |\nu_e\rangle, \tag{B.10}$$

and

$$|\nu_3\rangle = \frac{1}{\sqrt{2}}\big(|\nu_\mu\rangle + |\nu_\tau\rangle\big), \tag{B.11}$$

where $\theta_\odot \equiv \theta_{12} \approx 34^\circ$ is the solar mixing angle (Ahmed et al., 2004), and

$$\left|\nu^\star\right\rangle = \frac{1}{\sqrt{2}}\big(|\nu_\mu\rangle - |\nu_\tau\rangle\big) \tag{B.12}$$

is the eigenstate orthogonal to $|\nu_3\rangle$. Inversion of the neutrino mass-to-flavor mixing matrix leads to

$$|\nu_e\rangle = \cos\theta_\odot |\nu_1\rangle - \sin\theta_\odot |\nu_2\rangle \tag{B.13}$$

and

$$\left|\nu^\star\right\rangle = \sin\theta_\odot |\nu_1\rangle + \cos\theta_\odot |\nu_2\rangle. \tag{B.14}$$

Finally, by adding Eqs. (B.11) and (B.12) one obtains the ν_μ flavor eigenstate,

$$|\nu_\mu\rangle = \frac{1}{\sqrt{2}}\big[|\nu_3\rangle + \sin\theta_\odot |\nu_1\rangle + \cos\theta_\odot |\nu_2\rangle\big], \tag{B.15}$$

and by subtracting these same equations the ν_τ eigenstate.

For real PMNS matrix elements (B.7) becomes

$$P(\nu_\alpha \to \nu_\beta) = \delta_{\alpha\beta} - 4\sum_{i>j} U_{\alpha i}U_{\beta i}U_{\alpha j}U_{\beta j}\sin^2\Delta_{ij}. \tag{B.16}$$

In addition, for $\Delta_{ij} \gg 1$, the phases will be erased by uncertainties in L and E. Consequently, averaging over $\sin^2\Delta_{ij}$ one finds the decohered flavor-changing probability

$$P(\nu_\alpha \to \nu_\beta) = \delta_{\alpha\beta} - 2\sum_{i>j} U_{\alpha i}U_{\beta i}U_{\alpha j}U_{\beta j}. \tag{B.17}$$

Now, using $2\sum_{1>j} = \sum_{i,j} - \sum_{i=j}$, Eq. (B.17) can be re-written as

$$\begin{aligned} P(\nu_\alpha \to \nu_\beta) &= \delta_{\alpha\beta} - \sum_{i,j} U_{\alpha i}U_{\beta i}U_{\alpha j}U_{\beta j} + \sum_i U_{\alpha i}U_{\beta i}U_{\alpha i}U_{\beta i} \\ &= \delta_{\alpha\beta} - \left(\sum_i U_{\alpha i}U_{\beta i}\right)^2 + \sum_i U_{\alpha i}^2 U_{\beta i}^2. \end{aligned} \tag{B.18}$$

Since $\delta_{\alpha\beta} = \delta_{\alpha\beta}^2$, the first and second terms in (B.18) cancel each other, yielding

$$P(\nu_\alpha \to \nu_\beta) = \sum_i U_{\alpha i}^2 U_{\beta i}^2. \tag{B.19}$$

In matrix notation, we have

$$P(\nu_\alpha \to \nu_\beta) = \mathbb{P}\mathbb{P}^{\mathrm{T}}, \tag{B.20}$$

where the decohered neutrino propagation matrix is

$$\mathbb{P} \equiv \begin{pmatrix} |U_{e1}|^2 & |U_{e2}|^2 & |U_{e3}|^2 \\ |U_{\mu 1}|^2 & |U_{\mu 2}|^2 & |U_{\mu 3}|^2 \\ |U_{\tau 1}|^2 & |U_{\tau 2}|^2 & |U_{\tau 3}|^2 \end{pmatrix}. \tag{B.21}$$

(It is seen that decoherence returns the quantum mechanical realm to that of classical overlap probabilities.)

The probabilities for flavor oscillation are then easily calculated to be

$$\begin{aligned} P(\nu_\mu \to \nu_\mu) = P(\nu_\tau \to \nu_\tau) = P(\nu_\mu \leftrightarrow \nu_\tau) \\ = \frac{1}{8}\big[4 - \sin^2(2\theta_\odot)\big], \end{aligned} \tag{B.22}$$

$$P(\nu_\mu \leftrightarrow \nu_e) = P(\nu_e \leftrightarrow \nu_\tau) = \frac{1}{4}\sin^2(2\theta_\odot), \tag{B.23}$$

and

$$P(\nu_e \to \nu_e) = 1 - \frac{1}{2}\sin^2(2\theta_\odot), \tag{B.24}$$

with $\sin^2(2\theta_\odot) \sim 8/9$.

Neutrinos from astrophysical sources are expected to arise dominantly from the decays of pions and their muon daughters, which results in initial flavor ratios $N_{\nu_e} : N_{\nu_\mu} : N_{\nu_\tau}$ of nearly $1 : 2 : 0$. Using (B.22), (B.23), and (B.24), it is straightforward to verify that the neutrinos will arrive at Earth with equipartition on the three flavors, $1 : 1 : 1$. The prediction for a pure $\bar{\nu}_e$ source, originating via neutron β-decay, has different implications for the flavor ratios; namely, a source flavor ratio $1 : 0 : 0$ yields Earthly ratios $\approx 5 : 2 : 2$ (Anchordoqui et al., 2004b). And finally, the "damped muon" source, wherein muon energy-losses at the source effectively terminate the pion decay chain at $\pi^\pm \to \mu^\pm + \overset{(-)}{\nu}_\mu$, evolves the initial $0 : 1 : 0$ flavor ratios to $4 : 7 : 7$.

References

Aartsen, M.G., et al., IceCube Collaboration, 2013a. Phys. Rev. Lett. 110, 131302. arXiv:1212.4097 [astro-ph.HE].

Aartsen, M.G., et al., IceCube Collaboration, 2013b. Phys. Rev. Lett. 110, 151105. arXiv:1212.4760 [hep-ex].

Aartsen, M.G., et al., IceCube Collaboration, 2013c. Phys. Rev. Lett. 111, 021103. arXiv:1304.5356 [astro-ph.HE].

Aartsen, M.G., et al., IceCube Collaboration, 2013d. Science 342, 1242856. arXiv:1311.5238 [astro-ph.HE].

Aartsen, M.G., et al., IceCube Collaboration, 2013e. Phys. Rev. D 87, 062002. arXiv:1210.7992 [astro-ph.HE].

Aartsen, M.G., et al., IceCube Collaboration, 2013f. arXiv:1311.7048 [astro-ph.HE].

Aartsen, M.G., et al., IceCube Collaboration, 2013g. arXiv:1307.3795 [astro-ph.HE].

Aartsen, M.G., et al., IceCube Collaboration, 2013h. arXiv:1310.5477 [astro-ph.HE].

Abbasi, R.U., et al., HiRes Collaboration, 2005. Phys. Lett. B 619, 271. arXiv: astro-ph/0501317.

Abbasi, R., et al., HiRes Collaboration, 2008. Phys. Rev. Lett. 100, 101101. arXiv: astro-ph/0703099.

Abbasi, R., et al., IceCube Collaboration, 2009a. Nucl. Instrum. Meth. A 601, 294. arXiv: 0810.4930 [physics.ins-det].

Abbasi, R., et al., IceCube Collaboration, 2009b. Phys. Rev. D 79, 102005. arXiv: 0902.0675 [astro-ph.HE].

Abbasi, R., et al., IceCube Collaboration, 2010. Astropart. Phys. 34, 48. arXiv: 1004.2357 [astro-ph.HE].

Abbasi, R., et al., IceCube Collaboration, 2011a. Phys. Rev. D 84, 072001. arXiv: 1101.1692 [astro-ph.HE].

Abbasi, R., et al., IceCube Collaboration, 2011b. Phys. Rev. D 84, 082001. arXiv: 1104.5187 [astro-ph.HE].

Abbasi, R., et al., IceCube Collaboration, 2011c. Phys. Rev. D 83, 012001. arXiv: 1010.3980 [astro-ph.HE].

Abbasi, R., et al., IceCube Collaboration, 2012a. Astropart. Phys. 35, 615. arXiv:1109.6096 [astro-ph.IM].

Abbasi, R., et al., IceCube Collaboration, 2012b. Astrophys. J. 746, 33. arXiv:1109.1017 [hep-ex].

Abbasi, R., et al., IceCube Collaboration, 2012c. Nature 484, 351. arXiv:1204.4219 [astro-ph.HE].

Abbasi, R., et al., IceCube Collaboration, 2013a. Nucl. Instrum. Meth. A 700, 188. arXiv:1207.6326 [astro-ph.IM].

Abbasi, R., et al., IceCube Collaboration, 2013b. Nucl. Instrum. Meth. A 703, 190. arXiv:1208.3430 [physics.data-an].

Abdo, A.A., Fermi LAT Collaboration, 2010a. Astrophys. J. 709, L152. arXiv:0911.5327 [astro-ph.HE].

Abdo, A.A., et al., Fermi-LAT Collaboration, 2010b. Phys. Rev. Lett. 104, 101101. arXiv:1002.3603 [astro-ph.HE].

Abraham, J., et al., Pierre Auger Collaboration, 2008. Phys. Rev. Lett. 101, 061101. arXiv:0806.4302.

Abraham, J., et al., Pierre Auger Collaboration, 2010a. Phys. Lett. B 685, 239. arXiv:1002.1975 [astro-ph.HE].

Abraham, J., et al., Pierre Auger Collaboration, 2010b. Phys. Rev. Lett. 104, 091101. arXiv:1002.0699 [astro-ph.HE].

Abreu, P., et al., Pierre Auger Collaboration, 2011. Astropart. Phys. 34, 627. arXiv:1103.2721 [astro-ph.HE].

Abreu, P., et al., Pierre Auger Collaboration, 2013. JCAP 1302, 026. arXiv:1301.6637 [astro-ph.HE].

Abu-Zayyad, T., et al., 2001. Astrophys. J. 557, 686. arXiv:astro-ph/0010652.

Acciari, V.A., et al., VERITAS Collaboration, 2009. Nature 462, 770. arXiv:0911.0873 [astro-ph.CO].

Acciari, V.A., et al., VERITAS and Fermi Collaborations, 2010. Astrophys. J. Lett. 708, L100. arXiv:0912.0730 [astro-ph.CO].

Acero, F., et al., H.E.S.S. Collaboration, 2009. Science 326, 1080. arXiv:0909.4651 [astro-ph.HE].

Achterberg, A., et al., IceCube Collaboration, 2006. Astropart. Phys. 26, 155. arXiv:astro-ph/0604450.

Ackermann, M., et al., AMANDA Collaboration, 2004. Astropart. Phys. 22, 127. arXiv:astro-ph/0405218.

Adrian-Martinez, S., et al., ANTARES Collaboration, 2012. Astrophys. J. 760, 53. arXiv:1207.3105 [hep-ex].

Ageron, M., et al., ANTARES Collaboration, 2011. Nucl. Instrum. Meth. A 656, 11. arXiv:1104.1607 [astro-ph.IM].

Aglietta, M., et al., EAS-TOP Collaboration, 2009. Astrophys. J. 692, L130. arXiv:0901.2740 [astro-ph.HE].

Aharonian, F., et al., H.E.S.S. Collaboration, 2004. Astron. Astrophys. 425, L13. arXiv:astro-ph/0408145.

Aharonian, F., Essey, W., Kusenko, A., Prosekin, A., 2013. Phys. Rev. D 87, 063002. arXiv:1206.6715 [astro-ph.HE].

Ahlers, M., Halzen, F., 2012. Phys. Rev. D 86, 083010. arXiv:1208.4181 [astro-ph.HE].

Ahlers, M., Murase, K., 2013. arXiv:1309.4077 [astro-ph.HE].

Ahlers, M., Taylor, A.M., 2010. Phys. Rev. D 82, 123005. arXiv:1010.3019 [astro-ph.HE].

Ahlers, M., Anchordoqui, L.A., Goldberg, H., Halzen, F., Ringwald, A., Weiler, T.J., 2005. Phys. Rev. D 72, 023001. arXiv:astro-ph/0503229.

Ahlers, M., Anchordoqui, L.A., Sarkar, S., 2009. Phys. Rev. D 79, 083009. arXiv:0902.3993 [astro-ph.HE].

Ahlers, M., Anchordoqui, L.A., Gonzalez-Garcia, M.C., Halzen, F., Sarkar, S., 2010. Astropart. Phys. 34, 106. arXiv:1005.2620 [astro-ph.HE].

Ahlers, M., Gonzalez-Garcia, M.C., Halzen, F., 2011. Astropart. Phys. 35, 87. arXiv:1103.3421 [astro-ph.HE].

Ahmed, S.N., et al., SNO Collaboration, 2004. Phys. Rev. Lett. 92, 181301. arXiv:nucl-ex/0309004.

Ahn, J.K., et al., RENO Collaboration, 2012. Phys. Rev. Lett. 108, 191802. arXiv:1204.0626 [hep-ex].

Ahrens, J., et al., IceCube Collaboration, 2003. Nucl. Phys. Proc. Suppl. 118, 388. arXiv:astro-ph/0209556.

Alikhanov, I., 2013. arXiv:1305.2905 [hep-ph].

Allard, D., Ave, M., Busca, N., Malkan, M.A., Olinto, A.V., Parizot, E., Stecker, F.W., Yamamoto, T., 2006. JCAP 0609, 005. arXiv:astro-ph/0605327.

Aloisio, R., Berezinsky, V., Gazizov, A., 2011. Astropart. Phys. 34, 620. arXiv:0907.5194 [astro-ph.HE].

Alvarez-Muniz, J., Halzen, F., 2002. Astrophys. J. 576, L33. arXiv:astro-ph/0205408.

Amato, E., Guetta, D., Blasi, P., 2003. Astron. Astrophys. 402, 827. arXiv:astro-ph/0302121.

Amenomori, M., et al., TIBET III Collaboration, 2008. Astrophys. J. 678, 1165. arXiv:0801.1803 [hep-ex].

An, F.P., et al., DAYA-BAY Collaboration, 2012. Phys. Rev. Lett. 108, 171803. arXiv:1203.1669 [hep-ex].

An, F.P., et al., Daya Bay Collaboration, 2013. Chin. Phys. C 37, 011001. arXiv:1210.6327 [hep-ex].

Anchordoqui, L., Goldberg, H., 2008. Phys. Lett. B 659, 345. arXiv:0709.0678 [hep-ph].

Anchordoqui, L., Halzen, F., 2006. Annals Phys. 321, 2660. arXiv:hep-ph/0510389.

Anchordoqui, L.A., Montaruli, T., 2010. Ann. Rev. Nucl. Part. Sci. 60, 129. arXiv:0912.1035 [astro-ph.HE].

Anchordoqui, L.A., Dova, M.T., Epele, L.N., Swain, J.D., 1998. Phys. Rev. D 57, 7103. arXiv:astro-ph/9708082.

Anchordoqui, L.A., Romero, G.E., Combi, J.A., 1999. Phys. Rev. D 60, 103001. arXiv:astro-ph/9903145.

Anchordoqui, L.A., Torres, D.F., McCauley, T.P., Romero, G.E., Aharonian, F.A., 2003. Astrophys. J. 589, 481. arXiv:hep-ph/0211231.

Anchordoqui, L.A., Goldberg, H., Halzen, F., Weiler, T.J., 2004a. Phys. Lett. B 600, 202. arXiv:astro-ph/0404387.

Anchordoqui, L.A., Goldberg, H., Halzen, F., Weiler, T.J., 2004b. Phys. Lett. B 593, 42. arXiv:astro-ph/0311002.

Anchordoqui, L.A., Goldberg, H., Gonzalez-Garcia, M.C., Halzen, F., Hooper, D., Sarkar, S., Weiler, T.J., 2005a. Phys. Rev. D 72, 065019. arXiv:hep-ph/0506168.

Anchordoqui, L.A., Goldberg, H., Halzen, F., Weiler, T.J., 2005b. Phys. Lett. B 621, 18. arXiv:hep-ph/0410003.

Anchordoqui, L.A., Cooper-Sarkar, A.M., Hooper, D., Sarkar, S., 2006a. Phys. Rev. D 74, 043008. arXiv:hep-ph/0605086.

Anchordoqui, L.A., Garcia Canal, C.A., Goldberg, H., Dumm, D.G., Halzen, F., 2006b. Phys. Rev. D 74, 125021. arXiv:hep-ph/0609214.

Anchordoqui, L.A., Beacom, J.F., Goldberg, H., Palomares-Ruiz, S., Weiler, T.J., 2007a. Phys. Rev. D 75, 063001. arXiv:astro-ph/0611581.

Anchordoqui, L.A., Goldberg, H., Hooper, D., Sarkar, S., Taylor, A.M., 2007b. Phys. Rev. D 76, 123008. arXiv:0709.0734 [astro-ph].

Anchordoqui, L., Halzen, F., Montaruli, T., O'Murchadha, A., 2007c. Phys. Rev. D 76, 067301. arXiv:astro-ph/0612699;
Anchordoqui, L., Halzen, F., Montaruli, T., O'Murchadha, A.. Phys. Rev. D 77 (2008) 069906 (Erratum).

Anchordoqui, L.A., Hooper, D., Sarkar, S., Taylor, A.M., 2008. Astropart. Phys. 29, 1. arXiv:astro-ph/0703001.

Anchordoqui, L.A., Farrar, G.R., Krizmanic, J.F., Matthews, J., Mitchell, J.W., Nitz, D., Olinto, A.V., Paul, T.C., Sokolsky, P., Thomson, G.B., Weiler, T.J., 2013a. arXiv:1307.5312 [astro-ph.HE].

Anchordoqui, L.A., Goldberg, H., Lynch, M.H., Olinto, A.V., Paul, T.C., Weiler, T.J., 2013b. arXiv:1306.5021 [astro-ph.HE].

Andres, E., et al., 2000. Astropart. Phys. 13, 1. arXiv:astro-ph/9906203.

Andres, E., et al., 2001. Nature 410, 441.

Antoni, T., et al., KASCADE Collaboration, 2004. Astrophys. J. 604, 687. arXiv:astro-ph/0312375.

Apel, W.D., et al., 2013. Astropart. Phys. 47, 54. arXiv:1306.6283.

Apel, W.D., et al., 2012. arXiv:1206.3834 [astro-ph.HE].

Arons, J., 2003. Astrophys. J. 589, 871. arXiv:astro-ph/0208444.

Atoyan, A., Dermer, C.D., 2001. Phys. Rev. Lett. 87, 221102. arXiv:astro-ph/0108053.

Aublin, J., Parizot, E., 2005. Astron. Astrophys. 441, 407. arXiv:astro-ph/0504575.

Ave, M., Busca, N., Olinto, A.V., Watson, A.A., Yamamoto, T., 2005. Astropart. Phys. 23, 19. arXiv:astro-ph/0409316.

Babson, J., et al., DUMAND Collaboration, 1990. Phys. Rev. D 42, 3613.

Baerwald, P., Hummer, S., Winter, W., 2011. Phys. Rev. D 83, 067303. arXiv:1009.4010.

Baerwald, P., Bustamante, M., Winter, W., 2012. JCAP 1210, 020. arXiv:1208.4600 [astro-ph.CO].

Baerwald, P., Bustamante, M., Winter, W., 2013. Astrophys. J. 768, 186. arXiv:1301.6163 [astro-ph.HE].

Bahcall, J.N., Waxman, E., 2001. Phys. Rev. D 64, 023002. arXiv:hep-ph/9902383.

Bai, Y., Lu, R., Salvado, J., 2013. arXiv:1311.5864 [hep-ph].

Band, D., et al., 1993. Astrophys. J. 413, 281.

Barger, V., Keung, W.-Y., 2013. Phys. Lett. B. arXiv:1305.6907 [hep-ph].

Barger, V.D., Pakvasa, S., Weiler, T.J., Whisnant, K., 2000. Phys. Rev. Lett. 85, 5055. arXiv:hep-ph/0005197.

Barger, V.D., Halzen, F., Hooper, D., Kao, C., 2002. Phys. Rev. D 65, 075022. arXiv:hep-ph/0105182.

Barger, V., Kumar, J., Marfatia, D., Sessolo, E.M., 2010. Phys. Rev. D 81, 115010. arXiv:1004.4573 [hep-ph].

Barger, V., Gao, Y., Marfatia, D., 2011. Phys. Rev. D 83, 055012. arXiv:1101.4410 [hep-ph].

Barger, V., Marfatia, D., Whisnant, K., 2012a. The Physics of Neutrinos. Princeton University Press, New Jersey.

Barger, V., Learned, J., Pakvasa, S., 2012b. arXiv:1207.4571 [astro-ph.HE].

Barr, G.D., Gaisser, T.K., Robbins, S., Stanev, T., 2006. Phys. Rev. D 74, 094009. arXiv:astro-ph/0611266.

Beacom, J.F., Bell, N.F., 2002. Phys. Rev. D 65, 113009. arXiv:hep-ph/0204111.

Beacom, J.F., Candia, J., 2004. JCAP 0411, 009. arXiv:hep-ph/0409046.

Beacom, J.F., Kistler, M.D., 2007. Phys. Rev. D 75, 083001. arXiv:astro-ph/0701751.

Beacom, J.F., Bell, N.F., Hooper, D., Pakvasa, S., Weiler, T.J., 2003a. Phys. Rev. Lett. 90, 181301. arXiv:hep-ph/0211305.

Beacom, J.F., Bell, N.F., Hooper, D., Pakvasa, S., Weiler, T.J., 2003b. Phys. Rev. D 68, 093005. arXiv:hep-ph/0307025;
Beacom, J.F., Bell, N.F., Hooper, D., Pakvasa, S., Weiler, T.J.. Phys. Rev. D 72 (2005) 019901 (Erratum).

Beacom, J.F., Bell, N.F., Hooper, D., Learned, J.G., Pakvasa, S., Weiler, T.J., 2004a. Phys. Rev. Lett. 92, 011101. arXiv:hep-ph/0307151.

Beacom, J.F., Bell, N.F., Hooper, D., Pakvasa, S., Weiler, T.J., 2004b. Phys. Rev. D 69, 017303. arXiv:hep-ph/0309267.
Becattini, F., Bottai, S., 2001. Astropart. Phys. 15, 323. arXiv:astro-ph/0003179.
Becker, J.K., 2008. Phys. Rept. 458, 173. arXiv:0710.1557 [astro-ph].
Bednarek, W., Bartosik, M., 2004. Astron. Astrophys. 423, 405. arXiv:astro-ph/0405310.
Bednarek, W., Protheroe, R.J., 1997. Phys. Rev. Lett. 79, 2616. arXiv:astro-ph/9704186.
Bednarek, W., Protheroe, R.J., 2002. Astropart. Phys. 16, 397. arXiv:astro-ph/0103160.
Belolaptikov, I.A., et al., BAIKAL Collaboration, 1997. Astropart. Phys. 7, 263.
Belyaev, A., Leroy, C., Mehdiyev, R., Pukhov, A., 2005. JHEP 0509, 005. arXiv:hep-ph/0502067.
Berezhnev, S.F., et al., 2012. Nucl. Instrum. Meth. A 692, 98. arXiv:1201.2122 [astro-ph.HE].
Berezinsky, V.S., 1985. Earlier use of the leptoquark in the UHE neutrino interaction can be found. Yad. Fiz. 41, 393.
Berezinsky, V.S., Smirnov, A.Y., 1975. Astrophys. Space Sci. 32, 461.
Berezinsky, V.S., Zatsepin, G.T., 1969. Phys. Lett. B 28, 423.
Berezinsky, V., Gazizov, A., Kachelriess, M., Ostapchenko, S., 2011. Phys. Lett. B 695, 13. arXiv:1003.1496 [astro-ph.HE].
Bernlöhr, K., et al., for the CTA Consortium, 2013. Astropart. Phys. 43, 171. arXiv:1210.3503 [astro-ph.IM].
Bhattacharya, A., Gandhi, R., Rodejohann, W., Watanabe, A., 2012. arXiv:1209.2422 [hep-ph].
Biermann, P.L., 1993. Astron. Astrophys. 271, 649.
Biermann, P.L., Gaisser, T.K., Stanev, T., 1995. Phys. Rev. D 51, 3450. arXiv:astro-ph/9501001.
Bilenky, S.M., Pontecorvo, B., 1983. Sov. J. Nucl. Phys. 38, 248. Lett. Nuovo Cim. 37 (1983) 467. Yad. Fiz. 38 (1983) 415.
Bionta, R.M., et al., 1987. Phys. Rev. Lett. 58, 1494.
Bird, D.J., et al., HiRes Collaboration, 1993. Phys. Rev. Lett. 71, 3401.
Blasi, P., Amato, E., 2012a. JCAP 1201, 010. arXiv:1105.4521 [astro-ph.HE].
Blasi, P., Amato, E., 2012b. JCAP 1201, 011. arXiv:1105.4529 [astro-ph.HE].
Blasi, P., Epstein, R.I., Olinto, A.V., 2000. Astrophys. J. 533, L123. arXiv:astro-ph/9912240.
Block, M.M., Ha, P., McKay, D.W., 2010. Phys. Rev. D 82, 077302. arXiv:1008.4555 [hep-ph].
Blumenthal, G.R., 1970. Phys. Rev. D 1, 1596.
Blumlein, J., Boos, E., Kryukov, A., 1997. Z. Phys. C 76, 137. arXiv:hep-ph/9610408.
Bolesta, J., 1997. Upper limits to the diffuse emission from active galactic nuclei. PhD dissertation. University of Hawaii. see p. 96 Fig. 6.6. Available at http://www.phys.hawaii.edu/~dumand/.
Bosetti, P. et al., DUMAND Collaboration, 1980. DUMAND Proposal (Report No. HDC-2-88, unpublished).
Bromberg, O., Nakar, E., Piran, T., 2011. Astrophys. J. 739, L55. arXiv:1107.1346 [astro-ph.HE].
Calvez, A., Kusenko, A., Nagataki, S., 2010. Phys. Rev. Lett. 105, 091101. arXiv:1004.2535 [astro-ph.HE].
Candia, J., Roulet, E., Epele, L.N., 2002. JHEP 0212, 033. arXiv:astro-ph/0206336.
Candia, J., Mollerach, S., Roulet, E., 2003. JCAP 0305, 003. arXiv:astro-ph/0302082.
Chantell, M.C., et al., CASA-MIA Collaboration, 1997. Phys. Rev. Lett. 79, 1805. arXiv:astro-ph/9705246.
Chatrchyan, S., et al., CMS Collaboration, 2013. Phys. Rev. Lett. 110, 081801. arXiv:1210.5629 [hep-ex].
Chen, C.-Y., Dev, P.S.B., Soni, A., 2013. arXiv:1309.1764 [hep-ph].
Cholis, I., Hooper, D., 2013. JCAP 06, 030. arXiv:1211.1974.
Cieza Montalvo, J.E., Eboli, O.J.P., Magro, M.B., Mercadante, P.G., 1998. Phys. Rev. D 58, 095001. arXiv:hep-ph/9805472.
Cobb, B.E., Bailyn, C.D., van Dokkum, P.G., Natarajan, P., 2006. Astrophys. J. 645, L113. arXiv:astro-ph/0603832.
Cocconi, G., 1956. Nuovo Cimento 3, 1433.
Connolly, A., Thorne, R.S., Waters, D., 2011. Phys. Rev. D 83, 113009. arXiv:1102.0691 [hep-ph].
Cooper-Sarkar, A., Sarkar, S., 2008. JHEP 0801, 075. arXiv:0710.5303 [hep-ph].
Cooper-Sarkar, A., Mertsch, P., Sarkar, S., 2011. JHEP 1108, 042. arXiv:1106.3723 [hep-ph].
Coward, D.M., 2005. Mon. Not. Roy. Astron. Soc. 360, L77. arXiv:astro-ph/0504493.
Daigne, F., Mochkovitch, R., 2007. Astron. Astrophys. 465. arXiv:0707.0931.
Daum, K., et al., FREJUS Collaboration, 1995. Z. Phys. C 66, 417.
De Angelis, A., Mansutti, O., Roncadelli, M., 2007. Phys. Rev. D 76, 121301. arXiv:0707.4312 [astro-ph].
De Marco, D., Blasi, P., Stanev, T., 2007. JCAP 0706, 027. arXiv:0705.1972 [astro-ph].
del Pozo, E.d.C., Torres, D.F., Marrero, A.Y.R., 2009a. Astrophys. J. 698, 1054. arXiv:0901.2688 [astro-ph.GA].
del Pozo, E.d.C., Torres, D.F., Rodriguez, A.Y., Reimer, O., 2009b. arXiv:0912.3497 [astro-ph.HE].
Dermer, C.D., Atoyan, A., 2003. Phys. Rev. Lett. 91, 071102. arXiv:astro-ph/0301030.
Dermer, C., Lott, B., 2012. J. Phys. Conf. Ser. 355, 012010. arXiv:1110.3739 [astro-ph.HE].
Diaz, J.S., Kostelecky, A., Mewes, M., 2013. arXiv:1308.6344 [astro-ph.HE].
Distefano, C., Guetta, D., Waxman, E., Levinson, A., 2002. Astrophys. J. 575, 378. arXiv:astro-ph/0202200.
Domingo-Santamaria, E., Torres, D.F., 2005. Astron. Astrophys. 444, 403. arXiv:astro-ph/0506240.
Domokos, G., Kovesi-Domokos, S., 1997. Phys. Lett. B 410, 57. arXiv:hep-ph/9703265.
Doncheski, M.A., Robinett, R.W., 1997. Phys. Rev. D 56, 7412. arXiv:hep-ph/9707328.
Ema, Y., Jinno, R., Moroi, T., 2013. arXiv:1312.3501 [hep-ph].
Enberg, R., Reno, M.H., Sarcevic, I., 2008. Phys. Rev. D 78, 043005. arXiv:0806.0418 [hep-ph].
Engel, R., Seckel, D., Stanev, T., 2001. Phys. Rev. D 64, 093010. arXiv:astro-ph/0101216.
Engelmann, J.J., Ferrando, P., Soutoul, A., Goret, P., Juliusson, E., Koch-Miramond, L., Lund, N., Masse, P., Peters, B., Petrou, N., Rasmussen, I.L., 1990. Astron. Astrophys. 233, 96.
Enqvist, K., Keranen, P., Maalampi, J., 1998. Phys. Lett. B 438, 295. arXiv:hep-ph/9806392.
Epele, L.N., Roulet, E., 1998. JHEP 9810, 009. arXiv:astro-ph/9808104.
Erlykin, A.D., Wolfendale, A.W., 1997. J. Phys. G 23, 979.
Erlykin, A.D., Wolfendale, A.W., 2005. Astropart. Phys. 23, 1.
Esmaili, A., 2010. Phys. Rev. D 81, 013006. arXiv:0909.5410 [hep-ph].
Esmaili, A., Farzan, Y., 2009. Nucl. Phys. B 821, 197. arXiv:0905.0259 [hep-ph].
Esmaili, A., Farzan, Y., 2012. JCAP 1212, 014. arXiv:1208.6012 [hep-ph].
Esmaili, A., Serpico, P.D., 2013. arXiv:1308.1105 [hep-ph].
Esmaili, A., Ibarra, A., Peres, O.L.G., 2012. JCAP 1211, 034. arXiv:1205.5281 [hep-ph].
Essey, W., Kusenko, A., 2010. Astropart. Phys. 33, 81. arXiv:0905.1162 [astro-ph.HE].
Essey, W., Kusenko, A., 2012. Astrophys. J. 751, L11. arXiv:1111.0815 [astro-ph.HE].
Essey, W., Kusenko, A., 2013. arXiv:1310.3440 [astro-ph.HE].
Essey, W., Kalashev, O.E., Kusenko, A., Beacom, J.F., 2010. Phys. Rev. Lett. 104, 141102. arXiv:0912.3976 [astro-ph.HE].
Essey, W., Ando, S., Kusenko, A., 2011a. Astropart. Phys. 35, 135. arXiv:1012.5313 [astro-ph.HE].
Essey, W., Kalashev, O., Kusenko, A., Beacom, J.F., 2011b. Astrophys. J. 731, 51. arXiv:1011.6340 [astro-ph.HE].
Fang, K., Kotera, K., Olinto, A.V., 2012. Astrophys. J. 750, 118. arXiv:1201.5197 [astro-ph.HE].
Fang, K., Kotera, K., Olinto, A.V., 2013a. JCAP 1303, 010. arXiv:1302.4482 [astro-ph.HE].
Fang, K., Kotera, K., Murase, K., Olinto, A.V., 2013b. arXiv:1311.2044 [astro-ph.HE].
Fardon, R., Nelson, A.E., Weiner, N., 2004. JCAP 0410, 005. arXiv:astro-ph/0309800.
Farzan, Y., Smirnov, A.Y., 2008. Nucl. Phys. B 805, 356. arXiv:0803.0495 [hep-ph].
Feldman, G.J., Cousins, R.D., 1998. Phys. Rev. D 57, 3873. arXiv:physics/9711021.
Feldstein, B., Kusenko, A., Matsumoto, S., Yanagida, T.T., 2013. Phys. Rev. D 88, 015004. arXiv:1303.7320 [hep-ph].
Feng, J.L., 2010. Ann. Rev. Astron. Astrophys. 48, 495. arXiv:1003.0904 [astro-ph.CO].
Fermi, E., 1949. Phys. Rev. 75, 1169.
Fichtel, C.E., Linsley, J., 1986. Astrophys. J. 300, 474.
Finley, C.B., Westerhoff, S., 2004. Astropart. Phys. 21, 359. arXiv:astro-ph/0309159.
Fodor, Z., Katz, S.D., Ringwald, A., Tu, H., 2003. JCAP 0311, 015. arXiv:hep-ph/0309171.
Fogli, G.L., Lisi, E., Marrone, A., Montanino, D., Palazzo, A., Rotunno, A.M., 2012. Phys. Rev. D 86, 013012. arXiv:1205.5254 [hep-ph].
Fraija, N., 2013. arXiv:1310.7061 [astro-ph.HE].
Frichter, G.M., Gaisser, T.K., Stanev, T., 1997. Phys. Rev. D 56, 3135. arXiv:astro-ph/9704061.
Fu, L., Ho, C.M., Weiler, T.J., 2012. Phys. Lett. B 718, 558. arXiv:1209.5382 [hep-ph].
Fukuda, Y., et al., Super-Kamiokande Collaboration, 1998. Phys. Rev. Lett. 81, 1562. arXiv:hep-ex/9807003.
Furniss, A., et al., 2013. arXiv:1304.4859 [astro-ph.HE].
Gaisser, T.K., 1990. Cosmic Rays and Particle Physics. Cambridge Univ. Press, Cambridge, UK.
Gaisser, T.K., 2005. arXiv:astro-ph/0501195.
Gaisser, T.K., 2006. J. Phys. Conf. Ser. 47, 15.
Gaisser, T.K., Honda, M., 2002. Ann. Rev. Nucl. Part. Sci. 52, 153. arXiv:hep-ph/0203272.
Gaisser, T.K., Halzen, F., Stanev, T., 1995. Phys. Rept. 258, 173. arXiv:hep-ph/9410384; Gaisser, T.K., Halzen, F., Stanev, T.. Phys. Rept. 271 (1996) 355 (Erratum).
Gaisser, T.K., Stanev, T., Tilav, S., 2013. arXiv:1303.3565.
Gandhi, R., Quigg, C., Reno, M.H., Sarcevic, I., 1996. Astropart. Phys. 5, 81. arXiv:hep-ph/9512364.
Gandhi, R., Quigg, C., Reno, M.H., Sarcevic, I., 1998. Phys. Rev. D 58, 093009. arXiv:hep-ph/9807264.
Garcia-Munoz, M., Mason, G.M., Simpson, J.A., 1977. Astrophys. J. 217, 859.
Garyaka, A.P., Martirosov, R.M., Ter-Antonyan, S.V., Erlykin, A.D., Nikolskaya, N.M., Gallant, Y.A., Jones, L.W., Procureur, J., 2008. J. Phys. G 35, 115201. arXiv:0808.1421 [astro-ph].
Gelmini, G., Kalashev, O.E., Semikoz, D.V., 2007a. Astropart. Phys. 28, 390. arXiv:astro-ph/0702464.
Gelmini, G., Kalashev, O.E., Semikoz, D.V., 2007b. JCAP 0711, 002. arXiv:0706.2181 [astro-ph].
Giller, M., Lipski, M., 2002. J. Phys. G 28, 1275.
Ginzburg, V.L., Ptuskin, V.S., 1976. Rev. Mod. Phys. 48, 161; Ginzburg, V.L., Ptuskin, V.S.. Rev. Mod. Phys. 48 (1976) 675 (Erratum).

Ginzburg, V.L., Syrovatskii, S.I., 1964. The Origin of Cosmic Rays. Pergamon Press, Oxford.
Glashow, S.L., 1960. Phys. Rev. 118, 316.
Goldstein, A., et al., 2012. Astrophys. J. Suppl. 199, 19. arXiv:1201.2981.
Gonzalez-Garcia, M.C., Maltoni, M., 2008. Phys. Rept. 460, 1. arXiv:0704.1800 [hep-ph].
Gonzalez-Garcia, M.C., Halzen, F., Maltoni, M., 2005. Phys. Rev. D 71, 093010. arXiv:hep-ph/0502223.
Gonzalez-Garcia, M.C., Maltoni, M., Rojo, J., 2006. JHEP 0610, 075. arXiv:hep-ph/0607324.
Gonzalez-Garcia, M.C., Halzen, F., Maltoni, M., Tanaka, H.K.M., 2008. Phys. Rev. Lett. 100, 061802. arXiv:0711.0745 [hep-ph].
Gonzalez-Garcia, M.C., Maltoni, M., Salvado, J., Schwetz, T., 2012. JHEP 1212, 123. arXiv:1209.3023 [hep-ph].
Gonzalez-Garcia, M.C., Halzen, F., Niro, V., 2013. arXiv:1310.7194 [astro-ph.HE].
Greisen, K., 1966. Phys. Rev. Lett. 16, 748.
Guetta, D., Hooper, D., Alvarez-Muniz, J., Halzen, F., Reuveni, E., 2004. Astropart. Phys. 20, 429. arXiv:astro-ph/0302524.
Gunn, J.E., Ostriker, J.P., 1969. Phys. Rev. Lett. 22, 728.
Gupta, N., 2013. arXiv:1305.4123 [astro-ph.HE].
Gupta, M., Webber, W.R., 1989. Astrophys. J. 340, 1124.
Gupta, N., Zhang, B., 2007. Astropart. Phys. 27, 386. arXiv:astro-ph/0606744.
Halzen, F., 2007. Science 315, 66.
Halzen, F., for the IceCube Collaboration, 2013. IceCube: Neutrino Physics from GeV–PeV. arXiv:1308.3171 [astro-ph.HE].
Halzen, F., 2013. arXiv:1311.6350 [hep-ph].
Halzen, F., Hooper, D., 2002. Rept. Prog. Phys. 65, 1025. arXiv:astro-ph/0204527.
Halzen, F., Hooper, D., 2006. Phys. Rev. D 73, 123507. arXiv:hep-ph/0510048.
Halzen, F., Learned, J.G., UH-511-659-88, MAD/PH/428.
Halzen, F., Saltzberg, D., 1998. Phys. Rev. Lett. 81, 4305. arXiv:hep-ph/9804354.
Halzen, F., Stelzer, T., Kamionkowski, M., 1992. Phys. Rev. D 45, 4439.
He, H.-N., Liu, R.-Y., Wang, X.-Y., Nagataki, S., Murase, K., Dai, Z.-G., 2012. Astrophys. J. 752, 29. arXiv:1204.0857 [astro-ph.HE].
He, H.-N., Wang, T., Fan, Y.-Z., Liu, S.-M., Wei, D.-M., 2013a. arXiv:1303.1253 [astro-ph.HE].
He, H.-N., Yang, R.-Z., Fan, Y.-Z., Wei, D.-M., 2013b. arXiv:1307.1450 [astro-ph.HE].
Hill, C.T., Schramm, D.N., 1983. Phys. Lett. B 131, 247.
Hillas, A.M., 2005. J. Phys. G 31, R95.
Hillas, A.M., 2006. J. Phys. Conf. Ser. 47, 168.
Hirata, K., et al., Kamiokande-II Collaboration, 1987. Phys. Rev. Lett. 58, 1490.
Hooper, D., Morgan, D., Winstanley, E., 2005a. Phys. Rev. D 72, 065009. arXiv:hep-ph/0506091.
Hooper, D., Morgan, D., Winstanley, E., 2005b. Phys. Lett. B 609, 206. arXiv:hep-ph/0410094.
Hooper, D., Taylor, A., Sarkar, S., 2005c. Astropart. Phys. 23, 11. arXiv:astro-ph/0407618.
Hooper, D., Taylor, A.M., Sarkar, S., 2011. Astropart. Phys. 34, 340. arXiv:1007.1306 [astro-ph.HE].
Hörandel, J.R., 2003. Astropart. Phys. 19, 193. arXiv:astro-ph/0210453.
Horns, D., Meyer, M., 2012. JCAP 1202, 033. arXiv:1201.4711 [astro-ph.CO].
Horns, D., Maccione, L., Meyer, M., Mirizzi, A., Montanino, D., Roncadelli, M., 2012. Phys. Rev. D 86, 075024. arXiv:1207.0776 [astro-ph.HE].
Hummer, S., Baerwald, P., Winter, W., 2012. Phys. Rev. Lett. 108, 231101. arXiv:1112.1076 [astro-ph.HE].
Hung, P.Q., Pas, H., 2005. Mod. Phys. Lett. A 20, 1209. arXiv:astro-ph/0311131.
Illarionov, A.Y., Kniehl, B.A., Kotikov, A.V., 2011. Phys. Rev. Lett. 106, 231802. arXiv:1105.2829 [hep-ph].
Inoue, Y., Inoue, S., Kobayashi, M.A.R., Makiya, R., Niino, Y., Totani, T., 2013a. Astrophys. J. 768, 197. arXiv:1212.1683 [astro-ph.CO].
Inoue, Y., Kalashev, O.E., Kusenko, A., 2013b. arXiv:1308.5710 [astro-ph.HE].
Jansson, R., Farrar, G.R., 2012. Astrophys. J. 761, L11. arXiv:1210.7820 [astro-ph.GA].
Jeong, Y.S., Reno, M.H., 2010. Phys. Rev. D 81, 114012. arXiv:1001.4175 [hep-ph].
Joshi, J.C., Winter, W., Gupta, N., 2013. arXiv:1310.5123 [astro-ph.HE].
Kalashev, O.E., Kusenko, A., Essey, W., 2013. Phys. Rev. Lett. 111, 041103. arXiv:1303.0300 [astro-ph.HE].
Kappes, A., Hinton, J., Stegmann, C., Aharonian, F.A., 2007. Astrophys. J. 656, 870. arXiv:astro-ph/0607286;
Kappes, A., Hinton, J., Stegmann, C., Aharonian, F.A.. Astrophys. J. 661 (2007) 1348 (Erratum).
Karakula, S., Osborne, J.L., Wdowczyk, J., 1974. J. Phys. A 7, 437.
Kazanas, D., Ellison, D.C., 1986. Astrophys. J. 304, 178.
Kifune, T., 1999. Astrophys. J. 518, L21. arXiv:astro-ph/9904164.
King, S.F., Luhn, C., 2013. Rept. Prog. Phys. 76, 056201. arXiv:1301.1340 [hep-ph].
Kistler, M.D., Beacom, J.F., 2006. Phys. Rev. D 74, 063007. arXiv:astro-ph/0607082.
Kistler, M.D., Stanev, T., Yuksel, H., 2013. arXiv:1301.1703.
Klein, S.R., for the IceCube Collaboration, 2013. arXiv:1311.6519 [astro-ph.HE].
Kneiske, T.M., Bretz, T., Mannheim, K., Hartmann, D.H., 2004. Astron. Astrophys. 413, 807. arXiv:astro-ph/0309141.
Kobayakawa, K., Honda, Y.S., Samura, T., 2002. Phys. Rev. D 66, 083004. arXiv:astro-ph/0008209.
Kolmogorov, A., 1941. Dokl. Akad. Nauk SSSR 30, 299. Reprinted in Proc. R. Soc. London A 434 (1941) 9.
Kopper, C., for the IceCube Collabotration, 2013. Observation of PeV neutrinos in IceCube, talk given at the IceCube Particle Astrophysics Symposium (IPA-2013). Madison, Wisconsin, 13–15 May 2013, http://wipac.wisc.edu/meetings/home/IPA2013.
Kotera, K., Allard, D., Olinto, A.V., 2010. JCAP 1010, 013. arXiv:1009.1382 [astro-ph.HE].
Kraichnan, R.H., 1965. Phys. Fluids 8, 1385.
Kurahashi-Neilson, N., for the IceCube Collaboration, 2013. Spatial clustering analysis of the very high energy neutrinos in IceCube, talk given at the IceCube Particle Astrophysics Symposium (IPA-2013). Madison, Wisconsin, 13–15 May 2013.
L'Abbate, A., Montaruli, T., Sokalski, I.A., 2005. Astropart. Phys. 23, 57. arXiv:hep-ph/0406133.
Lacki, B.C., Thompson, T.A., Quataert, E., 2010. Astrophys. J. 717, 1. arXiv:0907.4161 [astro-ph.CO].
Lacki, B.C., Thompson, T.A., Quataert, E., Loeb, A., Waxman, E., 2011. Astrophys. J. 734, 107. arXiv:1003.3257 [astro-ph.HE].
Laha, R., Beacom, J.F., Dasgupta, B., Horiuchi, S., Murase, K., 2013. Phys. Rev. D 88, 043009. arXiv:1306.2309 [astro-ph.HE].
Lai, H.-L., Guzzi, M., Huston, J., Li, Z., Nadolsky, P.M., Pumplin, J., Yuan, C.-P., 2010. Phys. Rev. D 82, 074024. arXiv:1007.2241 [hep-ph].
Learned, J.G., Mannheim, K., 2000. Ann. Rev. Nucl. Part. Sci. 50, 679.
Learned, J.G., Pakvasa, S., 1995. Astropart. Phys. 3, 267. arXiv:hep-ph/9405296, arXiv:hep-ph/9408296.
Learned, J.G., Pakvasa, S., Zee, A., 2009. Phys. Lett. B 671, 15. arXiv:0805.2429 [physics.pop-ph].
Lefa, E., Rieger, F.M., Aharonian, F., 2011. Astrophys. J. 740, 64. arXiv:1106.4201 [astro-ph.HE].
Levinson, A., Waxman, E., 2001. Phys. Rev. Lett. 87, 171101. arXiv:hep-ph/0106102.
Li, Z., 2012. Phys. Rev. D 85, 027301. arXiv:1112.2240 [astro-ph.HE].
Li, Z., 2013. Astrophys. J. 770, L40. arXiv:1210.6594 [astro-ph.HE].
Liang, E., Zhang, B., Dai, Z.G., 2007. Astrophys. J. 662, 1111. arXiv:astro-ph/0605200.
Liberati, S., Maccione, L., 2013. arXiv:1309.7296 [gr-qc].
Linsley, J., 1975. Phys. Rev. Lett. 34, 1530.
Lipari, P., 1993. Astropart. Phys. 1, 195.
Lipari, P., 2013. arXiv:1308.2086 [astro-ph.HE].
Lipari, P., Lusignoli, M., Meloni, D., 2007. Phys. Rev. D 75, 123005. arXiv:0704.0718 [astro-ph].
Liu, R.-Y., Wang, X.-Y., 2013. Astrophys. J. 766, 73. arXiv:1212.1260 [astro-ph.HE].
Liu, R.-Y., Wang, X.-Y., Inoue, S., Crocker, R., Aharonian, F., 2013. arXiv:1310.1263 [astro-ph.HE].
Loeb, A., Waxman, E., 2006. JCAP 0605, 003. arXiv:astro-ph/0601695.
Lowder, D.M., Miller, T., Price, P.B., Westphal, A., Barwick, S.W., Halzen, F., Morse, R., 1991. Nature 353, 331.
Lunardini, C., Razzaque, S., 2012. Phys. Rev. Lett. 108, 221102. arXiv:1112.4799 [astro-ph.HE].
Lunardini, C., Razzaque, S., Theodoseau, K.T., Yang, L., 2013. arXiv:1311.7188 [astro-ph.HE].
Lv, H., Liang, E., Zhang, B., Zhang, B., 2010. Astrophys. J. 725, 1965. arXiv:1001.0598.
Maki, Z., Nakagawa, M., Sakata, S., 1962. Prog. Theor. Phys. 28, 870.
Mannheim, K., 1993. Astron. Astrophys. 269, 67. arXiv:astro-ph/9302006.
Mannheim, K., 1998. Science 279, 684. arXiv:astro-ph/9803241.
Mannheim, K., Protheroe, R.J., Rachen, J.P., 2001. Phys. Rev. D 63, 023003. arXiv:astro-ph/9812398.
Matthews, J., et al., 1991. Astrophys. J. 375, 202.
Meszaros, P., 2006. Rept. Prog. Phys. 69, 2259. arXiv:astro-ph/0605208.
Milgrom, M., Usov, V., 1995. Astrophys. J. 449, L37. arXiv:astro-ph/9505009.
Minakata, H., Smirnov, A.Y., 1996. Phys. Rev. D 54, 3698. arXiv:hep-ph/9601311.
Murase, K., Ioka, K., 2013. Phys. Rev. Lett. 111, 121102. arXiv:1306.2274 [astro-ph.HE].
Murase, K., Ioka, K., Nagataki, S., Nakamura, T., 2006. Astrophys. J. 651, L5. arXiv:astro-ph/0607104.
Murase, K., Dermer, C.D., Takami, H., Migliori, G., 2012. Astrophys. J. 749, 63. arXiv:1107.5576 [astro-ph.HE].
Murase, K., Ahlers, M., Lacki, B.C., 2013. Phys. Rev. D 88, 121301. arXiv:1306.3417 [astro-ph.HE].
Neronov, A., Semikoz, D.V., Tchernin, C., 2013. arXiv:1307.2158 [astro-ph.HE].
Paciesas, W.S., et al., 2012. Astrophys. J. Suppl. 199, 18. arXiv:1201.3099.
Pakvasa, S., 1981. Lett. Nuovo Cim. 31, 497.
Pakvasa, S., 2008. Mod. Phys. Lett. A 23, 1313. arXiv:0803.1701 [hep-ph].
Pakvasa, S., Rodejohann, W., Weiler, T.J., 2008. JHEP 0802, 005. arXiv:0711.4517 [hep-ph].
Pakvasa, S., Joshipura, A., Mohanty, S., 2013. Phys. Rev. Lett. 110, 171802. arXiv:1209.5630 [hep-ph].
Parizot, E., 2004. Nucl. Phys. Proc. Suppl. 136, 169. arXiv:astro-ph/0409191.
Persic, M., Rephaeli, Y., Arieli, Y., 2008. Astron. Astrophys. 486, 143. arXiv:0802.0818 [astro-ph].
Petcov, S.T., 1982. Phys. Lett. B 110, 245.

Pian, E., et al., 2006. Nature 442, 1011. arXiv:astro-ph/0603530.
Pontecorvo, B., 1957. Sov. Phys. JETP 6, 429. Zh. Eksp. Teor. Fiz. 33 (1957) 549.
Pontecorvo, B., 1968. Sov. Phys. JETP 26, 984. Zh. Eksp. Teor. Fiz. 53 (1967) 1717.
Porciani, C., Madau, P., 2001. Astrophys. J. 548, 522. arXiv:astro-ph/0008294.
Prosekin, A., Essey, W., Kusenko, A., Aharonian, F., 2012. Astrophys. J. 757, 183. arXiv:1203.3787 [astro-ph.HE].
Ptuskin, V., 2006. J. Phys. Conf. Ser. 47, 113.
Ptuskin, V.S., Rogovaya, S.I., Zirakashvili, V.N., Chuvilgin, L.G., Khristiansen, G.B., Klepach, E.G., Kulikov, G.V., 1993. Astron. Astrophys. 268, 726.
Puget, J.L., Stecker, F.W., Bredekamp, J.H., 1976. Astrophys. J. 205, 638.
Quigg, C., Reno, M.H., Walker, T.P., 1986. Phys. Rev. Lett. 57, 774.
Racusin, J.L., 2011. Astrophys. J. 738, 138. arXiv:1106.2469.
Razzaque, S., 2013. Phys. Rev. D 88, 081302. arXiv:1309.2756 [astro-ph.HE].
Razzaque, S., Dermer, C.D., Finke, J.D., 2012. Astrophys. J. 745, 196. arXiv:1110.0853 [astro-ph.HE].
Rees, M.J., Meszaros, P., 1994. Astrophys. J. 430, L93. arXiv:astro-ph/9404038.
Reno, M.H., Quigg, C., 1988. Phys. Rev. D 37, 657.
Rephaeli, Y., Arieli, Y., Persic, M., 2010. Mon. Not. Roy. Astron. Soc. 401, 423. arXiv:0906.1921 [astro-ph.HE].
Rolli, S., Tanabashi, M., Beringer, J., et al., Particle Data Group Collaboration, 2012. Leptoquarks. Phys. Rev. D 86, 010001.
Roulet, E., Sigl, G., van Vliet, A., Mollerach, S., 2013. JCAP 1301, 028. arXiv:1209.4033 [astro-ph.HE].
Sanuki, T., Honda, M., Kajita, T., Kasahara, K., Midorikawa, S., 2007. Phys. Rev. D 75, 043005. arXiv:astro-ph/0611201.
Schatz, G., et al., KASCADE Collaboration, 2003. In: Proceedings of the 28th International Cosmic Ray Conference, Tsukuba, Japan, FZKA-6890I.
Schonert, S., Gaisser, T.K., Resconi, E., Schulz, O., 2009. Phys. Rev. D 79, 043009. arXiv:0812.4308.
Schwetz, T., et al., 2012. Review of Global fits presented at "What's ν-Invisibles", GGI Workshop, Florence.
Sigl, G., Torres, D.F., Anchordoqui, L.A., Romero, G.E., 2001. Phys. Rev. D 63, 081302. arXiv:astro-ph/0008363.
Silk, J., Olive, K.A., Srednicki, M., 1985. Phys. Rev. Lett. 55, 257.
Simet, M., Hooper, D., Serpico, P.D., 2008. Phys. Rev. D 77, 063001. arXiv:0712.2825 [astro-ph].
Sironi, L., Spitkovsky, A., 2011. Astrophys. J. 726, 75. arXiv:1009.0024 [astro-ph.HE].
Sironi, L., Spitkovsky, A., Arons, J., 2013. arXiv:1301.5333 [astro-ph.HE].
Soderberg, A.M., Kulkarni, S.R., Nakar, E., Berger, E., Fox, D.B., Frail, D.A., Gal-Yam, A., Sari, R., et al., 2006a. Nature 442, 1014. arXiv:astro-ph/0604389.
Soderberg, A.M., Nakar, E., Kulkarni, S.R., 2006b. Astrophys. J. 638, 930. arXiv:astro-ph/0507147.
Sommers, P., 2001. Astropart. Phys. 14, 271. arXiv:astro-ph/0004016.
Spiering, C., 2012. Eur. Phys. J. H 37, 515. arXiv:1207.4952 [astro-ph.IM].
Srednicki, M., Olive, K.A., Silk, J., 1987. Nucl. Phys. B 279, 804.
Stanev, T., 1997. Astrophys. J. 479, 290. arXiv:astro-ph/9607086.
Stecker, F.W., 1968. Phys. Rev. Lett. 21, 1016.
Stecker, F.W., 1979. Astrophys. J. 228, 919.
Stecker, F.W., 2005. Phys. Rev. D 72, 107301. arXiv:astro-ph/0510537.
Stecker, F.W., 2007. Astropart. Phys. 26, 398. arXiv:astro-ph/0607197.
Stecker, F.W., 2013a. Phys. Rev. D 88, 047301. arXiv:1305.7404.
Stecker, F.W., 2013b. arXiv:1306.6095 [hep-ph].
Stecker, F.W., Salamon, M.H., 1999. Astrophys. J. 512, 521. arXiv:astro-ph/9808110.
Stecker, F.W., Done, C., Salamon, M.H., Sommers, P., 1991. Phys. Rev. Lett. 66, 2697. Phys. Rev. Lett. 69 (1992) 2738 (Erratum).
Stecker, F.W., Malkan, M.A., Scully, S.T., 2006. Astrophys. J. 648, 774. arXiv:astro-ph/0510449.
Stecker, F.W., Baring, M.G., Summerlin, E.J., 2007. Astrophys. J. 667, L29. arXiv:0707.4676 [astro-ph].
Stecker, F.W., Malkan, M.A., Scully, S.T., 2012. Astrophys. J. 761, 128. arXiv:1205.5168 [astro-ph.HE].
Stumpert, M., 2008. PhD Thesis, FZKA-7380.
Su, M., Slatyer, T.R., Finkbeiner, D.P., 2010. Astrophys. J. 724, 1044. arXiv:1005.5480 [astro-ph.HE].
Swordy, S.P., L'Heureux, J., Meyer, P., Muller, D., 1993. Astrophys. J. 403, 658.
Syrovatskii, S.I., 1971. Comment. Astrophys. Space Phys. 3, 155.
Takami, H., Murase, K., Dermer, C.D., 2013. Astrophys. J. 771, L32. arXiv:1305.2138 [astro-ph.HE].
Taylor, A.M., Aharonian, F.A., 2009. Phys. Rev. D 79, 083010. arXiv:0811.0396 [astro-ph].
Taylor, A.M., Ahlers, M., Aharonian, F.A., 2011. Phys. Rev. D 84, 105007. arXiv:1107.2055 [astro-ph.HE].
Thompson, T.A., Quataert, E., Waxman, E., Loeb, A., 2006. arXiv:astro-ph/0608699.
Torres, D.F., 2004. Astrophys. J. 617, 966. arXiv:astro-ph/0407240.
Torres, D.F., Halzen, F., 2007. Astropart. Phys. 27, 500. arXiv:astro-ph/0607368.
Torres, D.F., Reucroft, S., Reimer, O., Anchordoqui, L.A., 2003. Astrophys. J. 595, L13. arXiv:astro-ph/0307079.
Torres, D.F., Cillis, A., Lacki, B., Rephaeli, Y., 2012. Mon. Not. Roy. Astron. Soc. 423, 822. arXiv:1203.2798 [astro-ph.HE].
Treister, E., Urry, C.M., Virani, S., 2009. Astrophys. J. 696, 110. arXiv:0902.0608 [astro-ph.CO].
Vietri, M., 1997. Phys. Rev. Lett. 78, 4328. arXiv:astro-ph/9705061.
Vieyro, F.L., Romero, G.E., Peres, O.L.G., 2013. Astron. Astrophys. 558, A142. arXiv:1309.6043 [astro-ph.HE].
Wanderman, D., Piran, T., 2010. Mon. Not. Roy. Astron. Soc. 406, 1944. arXiv:0912.0709.
Waxman, E., 1995. Phys. Rev. Lett. 75, 386. arXiv:astro-ph/9505082.
Waxman, E., Bahcall, J.N., 1997. Phys. Rev. Lett. 78, 2292. arXiv:astro-ph/9701231.
Waxman, E., Bahcall, J.N., 1999. Phys. Rev. D 59, 023002. arXiv:hep-ph/9807282.
Weiler, T.J., 2013. arXiv:1308.1715 [hep-ph].
Whitehorn, N., for the IceCube Collaboration, 2013. Results from IceCube, talk given at the IceCube Particle Astrophysics Symposium (IPA-2013). Madison, Wisconsin, 13–15 May 2013.
Wick, S.D., Dermer, C.D., Atoyan, A., 2004. Astropart. Phys. 21, 125. arXiv:astro-ph/0310667.
Winter, W., 2013. Phys. Rev. D 88, 083007. arXiv:1307.2793 [astro-ph.HE].
Wolfenstein, L., 1981. Nucl. Phys. B 186, 147.
Zas, E., Halzen, F., Vazquez, R.A., 1993. Astropart. Phys. 1, 297.
Zatsepin, G.T., Kuzmin, V.A., 1966. JETP Lett. 4, 78. Pisma Zh. Eksp. Teor. Fiz. 4 (1966) 114.
Zhang, B., 2007. Astrophys. J. 655, 989. arXiv:astro-ph/0610177.
Zhang, F.W., Shao, L., Yan, J.Z., Wei, D.M., 2012. Astrophys. J. 750, 88. arXiv:1201.1549.
Zheng, Y.G., Kang, T., 2013. Astrophys. J. 764, 113.